

Editor-in-Chief B.E. Paton

*Editorial Board:*

D.İ . Dyachenko  
exec. secr. (Ukraine)  
J. Focf (France)  
Ö. El Gammäl (Germany)  
İ .I. Gasik (Ukraine)  
G.İ . Grigorenko  
vice-chief ed. (Ukraine)  
B. Eoroushich (Slovenia)  
V.I. Lakomsky (Ukraine)  
V.É. Lebedev (Ukraine)  
S.F. İ edina (Spain)  
L.B. İ ädi vär (Ukraine)  
Ä. İ itchel (Canada)  
B.Ä. İ i vchan (Ukraine)  
Ä.N. Petrunko (Ukraine)  
V. Ramakrishna Rao (India)  
Ts.V. Râshâv (Bulgaria)  
N.P. Örigub (Ukraine)  
Ä.Ä. Troyansky (Ukraine)  
İ .L. Zhadkevich (Ukraine)

*Executive director*

A.T. Zelnichenko

*Translator*

V.F. Örets

*Editor*

N.A. Dmitrieva

*Electron galley*

I.S. Batasheva,

T.Yu. Snegiryova

*Editorial and advertising offices  
are located at PWI:*

International Association «Welding»,  
E.O. Paton Electric

Welding Institute of the NASU,  
11, Bozhenko str., 03680,  
Kiev, Ukraine

Tel.: (38044) 287 67 57,  
529 26 23,

Fax: (38044) 528 04 86

E-mail: journal@paton.kiev.ua

http://www.nas.gov.ua/pwj

*Subscriptions:*

4 issue per year;

**184\$** — regular, **150\$** — for subscription  
agencies, **100\$** — for students;  
postage and packaging included.  
Back issues available.

All rights reserved.

This publication and each of the articles  
contained herein are protected by copyright.  
Permission to reproduce material contained in  
this journal must be obtained in writing from  
the Publisher.

Copies of individual articles may be obtained  
from the Publisher.

## CONTENTS

### ELECTROSLAG TECHNOLOGY

**Lakomsky V.V., Pomarin Yu.M., Ryabtsev A.D. and  
Grigorenko G.M.** Metal nitriding from gas phase in ESR ..... 2

### ELECTRON BEAM PROCESSES

**Trigub N.P., Akhonin S.V., Zhuk G.V., Telin V.V. and  
Davydov S.V.** Electron beam melting of uncrushed spongy  
titanium blocks ..... 5

**Nerodenko L.M., Onoprienko E.V. and Movchan B.A.**  
Structure and mechanical properties of  
dispersion-strengthened titanium-base materials deposited  
from gas phase ..... 8

**Nakonechny N.F., Fyodorov V.N. and  
Shchekin-Krotov V.A.** Investigation of heat exchange  
processes in mould of electron beam installation ..... 12

### PLASMA-ARC TECHNOLOGY

**Koleda V.N., Shapovalov V.A., Torkhov G.F. and  
Aksinichenko A.V.** Application of plasma-arc remelting of  
technogenic waste in movable horizontal mould for producing  
quality ferroalloys and master alloys ..... 17

**Shapovalov V.A., Vislobokov O.M., Melnik G.A. and  
Tsykulenko K.A.** Geometric shape and erosion resistance of  
copper water-cooled anode of arc heat source ..... 21

### GENERAL PROBLEMS OF METALLURGY

**Malashenko I.S., Kurenkova V.V., Belyavin A.F. and  
Trokhimchenko V.V.** Short-term strength and microstructure  
of brazed joints of alloy VJL12U produced using  
boron-containing brazing alloy with addition of silicon ..... 23

**Sidorov V.A. and Sotnikov A.L.** Determination of swinging  
radius of the MCCB mould ..... 39

**Borisov Yu.S., Borisova A.L., Karpets M.V.,  
Lotsko D.V., Milman Yu.V., Adeeva L.I., Gordan G.N. and  
Doroshenko L.K.** Investigation of phase transformations in  
powders of multi-component AlCuFe-base alloy with  
quasi-crystalline structure ..... 43

### ELECTROMETALLURGY OF STEEL AND FERROALLOYS

**Kostyakov V.N., Poletaev E.B., Grigorenko G.M. and  
Medved S.N.** Behavior of vanadium in liquid-phase melting of  
vanadium-containing concentrate ..... 49

Developed at PWI ..... 4, 11, 42, 51

Index of articles for AEM'2006, Nos. 1-4 ..... 52

List of authors ..... 54



## METAL NITRIDING FROM GAS PHASE IN ESR

V.V. LAKOMSKY<sup>1</sup>, Yu.M. POMARIN<sup>1</sup>, A.D. RYABTSEV<sup>2</sup> and G.M. GRIGORENKO<sup>1</sup>

<sup>1</sup>E.O. Paton Electric Welding Institute, NASU, Kiev, Ukraine

<sup>2</sup>Donetsk State Technical University, Donetsk, Ukraine

Feasibility of metal nitriding in electroslag remelting directly from gas phase is considered. The earlier assumption about nitriding process dependence upon degree of oxidizing of slag and gas phases is confirmed. It is shown that nitriding from gas phase is possible, provided the slag is deoxidized by metal calcium and aluminium.

*Keywords:* nitrogen, gas permeability, electroslag remelting, solubility

Due to development of a great variety of nitrogen-containing steels the need occurred in developing technology of their production both in primary manufacturing of the metal and in secondary remelting. This problem is successfully solved by application of plasma-arc remelting (PAR), in which metal nitriding occurs from gas phase due to direct contact of a metal melt with gas, ionized by the plasma flame [1, 2]. However, PAR is rather expensive method of remelting, which is not fit for all kinds of steel. That's why application of a cheaper electroslag remelting (ESR) is advisable.

In opinion of many researchers slag is impermeable for nitrogen. In case of presence of molten slag, used in ESR process, alloying of a metal by nitrogen directly from gas phase is impossible. That's why a metal has to be nitrated by introduction into a metal melt of nitrated ferroalloys or nitrides of alloying elements [3, 4]. However, certain investigations prove possibility of nitriding in ESR, depending upon conditions of melting [5].

So, for establishing possibility of nitriding of a metal, covered by a layer of molten slag, directly from gas phase it is necessary to consider process of the metal melting with determination of conditions of nitrogen transfer through slag.

Transport of nitrogen through slag is called gas permeability, which is determined as product of limit solubility of nitrogen in slag  $C_N$  and coefficient of nitrogen diffusion in slag  $D_N$  [6–8]:

$$P_N = C_N D_N.$$

All researchers established solubility of nitrogen in slag in the cause of study of the dual system gas–slag. Nitrogen permeability assumes transfer of the gas phase nitrogen through slag to the metal in the triple system gas–slag–metal. Study of the triple system proves that transport properties of slag are determined by thermodynamic conditions, created not just on interface of phases gas–slag, but also on the interface slag–metal [9–11]. That's why one has to take into account not just solubility of nitrogen in

slag, but what is more important motive force of the whole process of nitrogen transfer from gas to metal, which consists in difference of values of chemical potential of nitrogen in different areas of the system gas–slag–metal [12].

In our opinion, permeability of a system is connected to a smaller degree with some component in it, because solubility is ability to absorb a component into volume of a phase, while permeability is ability to transfer a component from one phase interface to another.

For the purpose of confirming theoretical assumptions of other authors, we have carried out comparative experiments (two series of meltings in nitrogen atmosphere in a resistance furnace with application of graphite crucibles). In the first series slag was molten, while in the second series --- a metal, submerged in slag. Fluoride-oxide ESR slags and (for comparison) oxide mixtures from pure components were used. Amount of nitrogen in the slag and the metal was determined by Kjeldahl method. It is established that content of nitrogen in the slag is higher in case of interaction of gas phase nitrogen with the slag without participation of the metal than in presence of the metal. So, for example, in contacting of gas phase with the slag in absence of the metal solubility of nitrogen in slag CaO–Al<sub>2</sub>O<sub>3</sub>–15 % TiO<sub>2</sub> constitutes 0.13 %, in flux AN-295 (16 % CaF<sub>2</sub>–51 % Al<sub>2</sub>O<sub>3</sub>–31 % CaO) --- 0.119 %, while in presence of the metal these indices are 0.026 and 0.052 %, respectively, content of nitrogen in the metal in the amount of 0.035 % (slag CaO–Al<sub>2</sub>O<sub>3</sub>–15 % TiO<sub>2</sub>) and 0.026 % (slag AN-295) being below the equilibrium one (0.17 %), calculated for conditions of molten metal interaction with nitrogen.

In all evidence, in order to find out the reason of such behavior of nitrogen in the triple system gas–slag–metal, one has to determine, in which form (atom, ion or a compound) the component migrates. For this purpose it is necessary to imagine on the basis of literature data mechanism of nitrogen transport through slag melt, having preliminary considered structure of the latter.

Slags are solutions of ions [13] with free electrons in them [12]. Structurally slag melt represents a set



Weight share of nitrogen and oxygen in metal Kh6VF after ESR, %

Kind of slag	Place of sample cutting-out	[N]	[O]
ANF-1P with 7 % Ca	Lower part:		
	edge	0.032; 0.032	0.058; 0.062
	center	0.033; 0.035	0.056; 0.066
	Middle part:		
	edge	0.033; 0.032	0.049; 0.068
	center	0.032; 0.033	0.091; 0.063
	Upper part:		
	edge	0.033; 0.033	0.109; 0.161
	center	0.033; 0.034	0.072; 0.076
ANF-1P with 7 % Al	Lower part:		
	edge	0.017; 0.019	0.058; 0.066
	center	0.016	0.079; 0.064
	Middle part:		
	edge	0.028; 0.028	0.053; 0.058
	center	0.031	0.063; 0.077
	Upper part:		
	edge	0.024; 0.030	0.099; 0.061
	center	0.028; 0.031	0.061; 0.110
ANF-6	Lower part:		
	edge	0.018; 0.018	0.064; 0.070
	center	0.018; 0.018	0.068; 0.070
	Middle part:		
	edge	0.021; 0.021	0.093; 0.095
	center	0.020; 0.021	0.070; 0.079
	Upper part:		
	edge	0.019; 0.020	0.087; 0.100
	center	0.020; 0.021	0.070; 0.073

of closely packed spheres, consisting of single or complex ions [14, 15], among which there are cavities (holes) according to Frenkel's «hole» model of liquid [16]. Dissolved in slag single or complex ion may be located in them. Number of «holes» determines value of such structurally sensitive properties of slag melts as density and surface tension.

Solubility of nitrogen in slag follows Sieverts law, and according to the theory of structure of slags as mediums with collectivized electrons it depends upon oxidation degree of the slag and gas phase above the slag melt [11, 12]:

$$\lg(N) = kP_{N_2}^{1/2}P_{O_2}^{-3/4}.$$

This explains good solubility of nitrogen in slags, molten in graphite crucibles.

Dissolved in slag nitrogen may transfer to the interface slag-metal and than dissolve in the metal melt or remain in the slag without transition into the other phase. Condition for transition of nitrogen from slag into the metal will be difference of its chemical po-

tential in these melts. By establishing necessary thermodynamic conditions in contacting phases one may regulate migration of nitrogen in the triple system gas-slag-metal [17], whereby the conditions are ensured by deoxidation of slag and the metal by strong deoxidizers as it was registered in the process of our meltings in graphite crucibles.

But carbon may be used not always as deoxidizer, because its presence is desirable not in all metals. In addition to carbon, active deoxidizers are calcium and aluminium, application of which in ESR allows not just deoxidizing the metal, but enables removal of other harmful impurities (sulfur, phosphorus, etc.). Metal calcium, in contrast to aluminium, has been already tested in ESR for activation of metal nitriding [18, 19]. That's why we decided to use metal calcium and aluminium as additives into fluoride slag in ESR for comparison of their action on the triple system gas-slag-metal.

ESR with solid start was performed in the compartment furnace, designed on the basis of the A-550 unit, in nitrogen under pressure  $1.5 \cdot 10^4$  Pa. Steel Kh6VF was subjected to remelting. Flux ANF-1P with addition of 7 % of metal calcium or aluminium and standard flux ANF-6 (70 %  $CaF_2$ -30 %  $Al_2O_3$ ) were used as flux. The latter one was used for producing a reference comparative ingot. Flux ANF-1P (practically pure calcium fluoride) was chosen because of impermeability of fluorides for nitrogen. From produced ingots samples were cut out for determining content of nitrogen and oxygen using the LECO instruments. Initial content of the gases in the electrode metal was  $[N]_{init} = 0.02$  % and  $[O]_{init} = 0.09$  %.

Equilibrium content of nitrogen in steel Kh6VF, calculated on the basis of direct contact of the molten metal with gas atmosphere and parameters of our meltings ( $T = 1600$  °N and  $P = 1.5 \cdot 10^4$  Pa), is  $[N]_{eq} = 0.109$  %.

Results of performed investigations (Table) prove that in ESR under flux ANF-6 layer without addition of active metals, absorption of the gas phase nitrogen by the metal does not take place and concentration of oxygen does not change. Additives of calcium and aluminium in slag ANF-1 (practically pure calcium fluoride) cause deoxidation of the metal and, as a result, its nitriding.

As one can see from the Table, calcium exerts the strongest action in comparison with aluminium on processes of oxygen removal and nitriding of the metal from gas phase. It is, evidently, connected with high vapor pressure of calcium, which deoxidizes not just slag and the metal, but also gas phase, while aluminium deoxidizes only slag and metal melts.

So, metal may be nitrated in the process of ESR, provided certain conditions are achieved.

1. Lakomsky, V.I. (1974) *Plasma-arc remelting*. Kiev: Tekhnika.
2. Grigorenko, G.M., Pomarin, Yu.M. (1989) *Hydrogen and nitrogen in metals in plasma melting*. Kiev: Naukova Dumka.



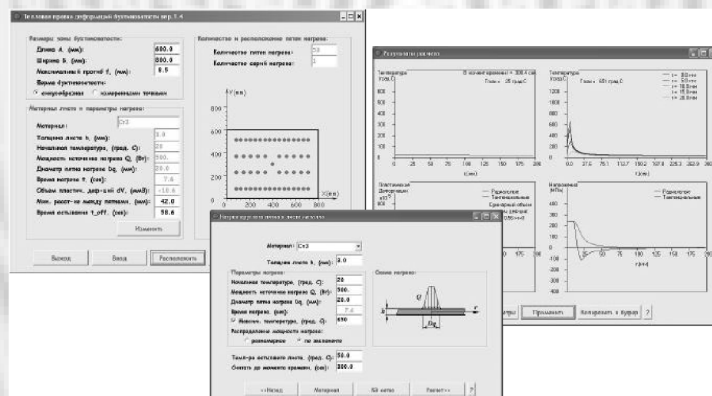
- Paton, B.E., Medovar, B.I., Saenko, V.Ya. et al. (1975) Examination of possibilities for improvement of high-strength building steel of 16G2AF grade. In: *Problems of special electrometallurgy*, Issue 1, 34–40.
- Stein, G., Menzel, I., Dorr, H. (1987) Industrial manufacture of massively nitrogen-alloyed steels. *Steel Research*, **1**, 32–38.
- Paton, B.E., Medovar, B.I., Grigorenko, G.M. et al. (1991) Nitriding processes in arc slag refining. *Problemy Spets. Elektrometallurgii*, **3**, 14–16.
- Popel, S.I., Sotnikov, A.I., Boronenkov, V.N. (1986) *Theory of metallurgical processes*. Moscow: Metallurgiya.
- Kamyshov, V.M., Esin, O.A., Chuchmarev, S.K. (1965) Nitrogen permeability of liquid slags. *Izvestiya Vuzov. Chyorn. Metallurgiya*, **2**, 57–61.
- Novokhatsky, I.A. (1975) *Gases in oxide melts*. Moscow: Metallurgiya.
- Ponomarenko, A.G., Kozlov, Yu.E. (1975) About some specifics of transfer in oxide phases. *Izvestiya Vuzov. Chyorn. Metallurgiya*, **5**, 20–25.
- Ponomarenko, A.G., Karshin, V.P., Morozov, A.N. (1968) Stoichiometric disordering and properties of liquid slags formed by stable oxides. In: *Physico-chemical principles of steel making*. Moscow: Nauka.
- Utchkin, Yu.I., Pavlov, A.V., Frojde, T. et al. (1993) Effect of oxidizing potential on solubility of nitrogen in slag melts. *Izvestiya Vuzov. Chyorn. Metallurgiya*, **3**, 10–15.
- Grigoryan, V.A., Belyanchikov, L.N., Stomakhin, A.Ya. (1986) *Theoretical principles of electric steelmaking processes*. Moscow: Metallurgiya.
- Esin, O.A., Geld, P.V. (1966) *Physical chemistry of pyrometallurgical processes*. Part 1. Moscow: Metallurgiya.
- Zhmojdin, G.I., Chatterdzhi, A.K. (1986) *Slags for metal refining. Dynamics of properties of system CaO–Al<sub>2</sub>O<sub>3</sub>–CaF<sub>2</sub>*. Moscow: Metallurgiya.
- Sokolsky, V.E., Kazimirov, V.P., Kuzmenko, V.G. (2000) Model of structure of oxide-fluoride melts based on close packing of oxygen atoms. *Problemy Spets. Elektrometallurgii*, **4**, 63–73.
- Frenkel, Ya.I. (1975) *Kinetic theory of fluids*. Leningrad: Nauka.
- Korzun, E.L., Ponomarenko, A.G., Galchenko, A.V. et al. (2001) Decrease of nitrogen content during steel melting in superpowerful arc furnace. *Elektrometallurgiya*, **11**, 3–8.
- Tokumitsu, N., Nakamura, I., Kajioaka, K. et al. (1983) Austenite stainless high-pure steelmaking by ESR method using the flux Ca–CaF<sub>2</sub>. In: *Electroslag refining*, Issue 6. Kiev: Naukova Dumka, 233–245.
- Grigorenko, G.M., Lakomsky, V.V., Ryabtsev, A.D. et al. (2003) About the feasibility of nitrogen transport through fluoride slags, containing metal calcium, in ESR. *Advances in Elektrometallurgy*, **4**, 11–13.

## COMPUTER PROGRAM

### «THERMAL STRAIGHTENING OF BUCKLING DISTORTIONS»

Software «Thermal Straightening of Buckling Distortions» allows determination of parameters of a round heat spot for a definite material and thickness of metal sheet, optimum from the point of view of producing maximum residual plastic shrinkage deformations and prevention of a local buckling of the sheet during heating. The software allows also in-process estimation and arrangement of necessary amounts of such heat spots at the area of buckling zone depending on definite sizes of the zone and value of deformation. The software has been developed to automate the process of thermal straightening of thin-sheet structures with buckling distortions and contains appropriate interface for input of data by sizes of the zone and value of deformation with an automatic system of measurement. To control the process of a manual shock-free thermal straightening, the program envisages the feasibility of a quick input of data to preset the length and width of a rectangular zone of buckling distortion and value of maximum buckling in the zone center. Software gives the opportunity of selection of interface support and reference in two languages (Russian, English).

**Purpose.** Control of process of manual or automatic thermal straightening of buckling deformations of thin-sheet structures.



View of main window of software, window of data input and representation of results of simulation of a round heat spot

**Application.** Manufacture of welded thin-sheet structures in ship-, railway car building and other branches. Cost of license for a permanent use of the program is 4900 UAH.

Contacts: Prof. Lobanov L.M.  
E-mail: office@paton.kiev.ua



# ELECTRON BEAM MELTING OF UNCRUSHED SPONGY TITANIUM BLOCKS

N.P. TRIGUB, S.V. AKHONIN, G.V. ZHUK, V.V. TELIN and S.V. DAVYDOV  
E.O. Paton Electric Welding Institute, NASU, Kiev, Ukraine

Technology of electron beam melting of uncrushed spongy titanium blocks is considered. Distribution of impurity elements over volume of spongy titanium blocks, produced at Zaporozhie Titanium-Magnesium Works, is investigated. High level of quality of ingots-slabs and technical-economic efficiency of developed technology has been achieved.

*Keywords:* electron beam melting, spongy titanium block, ingots-slabs, quality, production cost

High values of specific strength and corrosion resistance of items from titanium alloys stipulate their use on ever growing scale in aircraft- and missile-building, chemical, power production engineering and ship-building industries, and in manufacture of medical equipment and sport items.

An important criterion in selection of structural materials for manufacturing new items is the ratio price/quality. That's why reduction of production cost of titanium ingots as initial material for production of semi-finished products and improvement of their quality is urgent task [1].

The most promising is application of new technological processes, which allow excluding from the production chain certain technological stages and due to this significant reducing production cost.

In recent years electron-beam cold hearth melting (EBCHM) [2, 3] is used on ever growing scale in production of titanium ingots, which has a number of following advantages in comparison with traditional technology of vacuum-arc remelting:

- manufacturing of pressed electrode from lumpy spongy titanium is not needed, up to 100 % of titanium charge may be used as initial charge [4, 5];
- guaranteed removal of refractory inclusions, consisting of saturated with nitrogen inclusions of  $\alpha$ -titanium and carbides of refractory metals, is ensured [6];
- melting of square ingots and ingots-slabs is possible [7].

For the purpose of further reduction of production cost and labor input it was proposed at the E.O. Paton EWI to melt titanium ingots, using EBCHM method, from uncrushed spongy titanium blocks, which allows excluding from technological process of ingot production not just the process of a consumable electrode pressing for subsequent remelting, but also operation of crushing of spongy titanium blocks into pieces up to 70 mm.

Spongy titanium is produced by reduction of titanium tetrachloride by magnesium [8]. At present in Ukraine at Zaporozhie Titanium-Manganese Works

reduction units are mainly used, having productivity 0.8 t of titanium per a cycle. The process is performed in the heated up to 1073–1123 K air-tight retort by supplying at constant or variable rate titanium tetrachloride on surface of molten magnesium. Formed in the process of reduction block of spongy titanium occupies almost the whole volume of the reactor and represents a monolithic mass of porous titanium, contaminated with magnesium and magnesium chloride (Figure 1). After termination of the reduction process the retort is transferred to the next process stage, where produced spongy titanium is separated from the residual magnesium and magnesium chloride by the vacuum separation method.

In electron beam remelting of uncrushed block quality of a produced ingot depends to a great degree upon heterogeneity of distribution of impurity elements over the block volume. For determining their content local samples were taken from the bloom part of spongy titanium block in the center and at a distance of 100 mm from the block edges at three levels (upper, medium and bottom part). In addition, samples were taken from the near-surface layer of the block at the depth 5–10 mm. The samples were prepared according to GOST 23780–96. In each sample content of iron, nickel, carbon, silicon, chlorine, nitrogen and oxygen was determined.



Figure 1. Appearance of spongy titanium blocks



Distribution of impurities over volume of bloom part of spongy titanium block

Place of sampling	Mean weight share of elements, %						
	Fe	Ni	Si	C	Cl	N	O
<b>Upper part:</b>							
edge	0.020	0.012	0.002	0.012	0.063	0.015	0.025
center	0.038	0.038	0.002	0.015	0.086	0.011	0.020
edge	0.020	0.080	0.002	0.009	0.063	0.010	0.018
<b>Middle part:</b>							
edge	0.022	0.025	0.002	0.013	0.060	0.012	0.020
center	0.036	0.026	0.002	0.013	0.062	0.017	0.023
edge	0.020	0.033	0.002	0.008	0.061	0.016	0.022
<b>Bottom part:</b>							
edge	0.042	0.038	0.002	0.015	0.033	0.010	0.021
center	0.071	0.039	0.002	0.010	0.060	0.012	0.020
edge	0.062	0.036	0.003	0.010	0.033	0.011	0.023
Near-surface layer	0.220	0.160	0.003	0.018	0.065	0.024	0.031

Note. Content of impurity elements in near-surface layer is averaged according to results of 6 samplings.

Analysis of the results obtained (Table) showed that weight share of iron in the block constituted 0.020–0.071 % and in the near-surface layer it increased up to 0.22 %. In similar way nickel is distributed over the block volume --- 0.012–0.080 %, and in the near-surface layer it increases up to 0.16 %. Increased content of iron and nickel impurities in the near-surface layer is stipulated by diffusion of these elements from the retort walls, manufactured from stainless steel 12Kh18N10T.

Weight share of nitrogen in the spongy titanium, including the near-surface layer, changes within 0.005–0.015 %. Distribution of oxygen in the block is sufficiently homogeneous (0.020–0.025 %), whereby its certain increase in the bottom part is noted. In the near-surface layer content of oxygen insignificantly increases (up to 0.025 %).

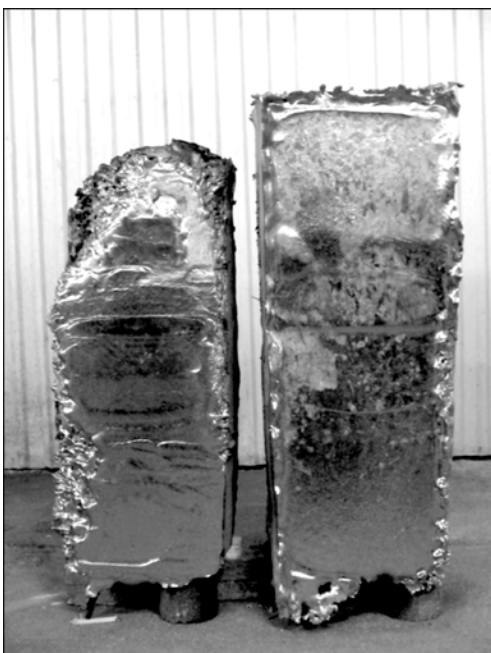


Figure 2. Appearance of spongy titanium blocks with molten surface

Content of carbon in the block makes up 0.008–0.015 % with certain increase in the near-surface layer up to 0.018 %. Silicon is characterized by uniform distribution all over the block volume (0.002–0.003 %).

Weight share of chlorine in the block, including the near-surface layer, is 0.033–0.086 %. As far as distribution of chlorine is concerned, a certain trend of its content increase from lower to upper part of the block should be noted. Its maximum content is registered in upper central part of the block.

As one can see from results of the investigations, surface layer of the bloom block has increased content of iron, nickel and partially carbon. According to traditional technology, removal of such defective layer from surface of the bloom block takes place during its cropping by means of mechanical cutting-out, which is a laborious process that causes irreversible loss of metal.

Proposed EBCHM technology for uncrushed spongy titanium blocks includes stage of electron beam melting of the block surface that allows removing the defective surface layer directly in the electron beam unit. Melting of surface of spongy titanium

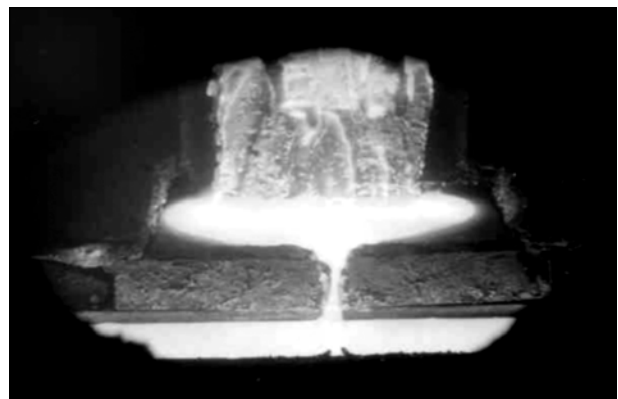
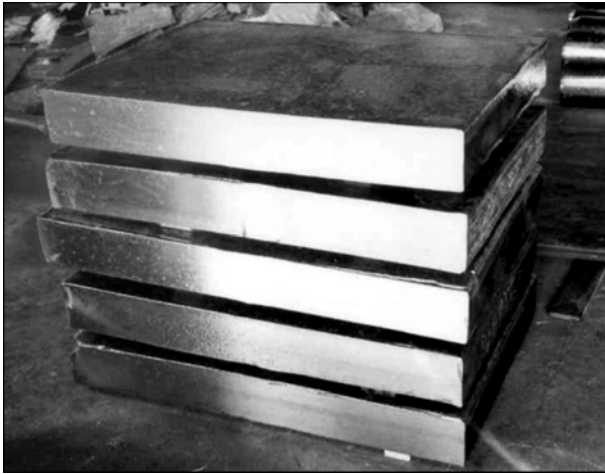


Figure 3. Process of electron beam melting of uncrushed spongy titanium block



**Figure 4.** Appearance of non-alloyed titanium slabs, produced by EMCHM of uncrushed spongy titanium block

blocks of 0.8 t mass (Figure 2) was performed in a specialized electron beam unit UE185. The process proceeded in stable manner, electron beam guns operated without discharges.

Cleaned of defective surface layer bloom blocks were remelted in electron beam cold hearth unit, forming ingots of necessary form and size.

In the process of melting of uncrushed spongy titanium block (Figure 3) formation of molten metal splashes and solid particles from the molten surface of the consumable ingot (which is characteristic of the crushed sponge melting) were not detected. It is stipulated by absence of absorbed moisture inside the block and preliminary degassing of the block surface in its electron beam melting. Remelting of spongy titanium blocks was performed at the rate of melting of lumpy titanium waste.

Produced titanium ingots-slabs, having cross-section  $165 \times 950$  mm and length 1200–1800 mm (Figure 4), were investigated in order to estimate homogeneity of impurity distribution. For this purpose 15 samples were taken from the experimental ingot-slab over its length and cross-section in the form of chips for spectral analysis and in the form of pieces for gas analysis. Samples were taken in three places (edge, center, edge) from upper end of the slab and at the distance 400, 800, 1200 and 1600 mm from the slab top (Figure 5). Before sampling mentioned places of side surface were fettled.

Results of determining content of nitrogen, oxygen, hydrogen, iron and carbon in the experimental ingot-slab from non-alloyed titanium (Figure 5) showed that distribution of impurity elements over length and cross-section of the ingots-slabs was uniform, and their content was within requirements of standards for non-alloyed titanium.

Investigation of macrostructure of transverse templates of ingots-slabs showed that the metal is characterized by high density and homogeneity without crystalline and zonal inhomogeneity. Ultrasonic non-destructive check of the quality showed that defects

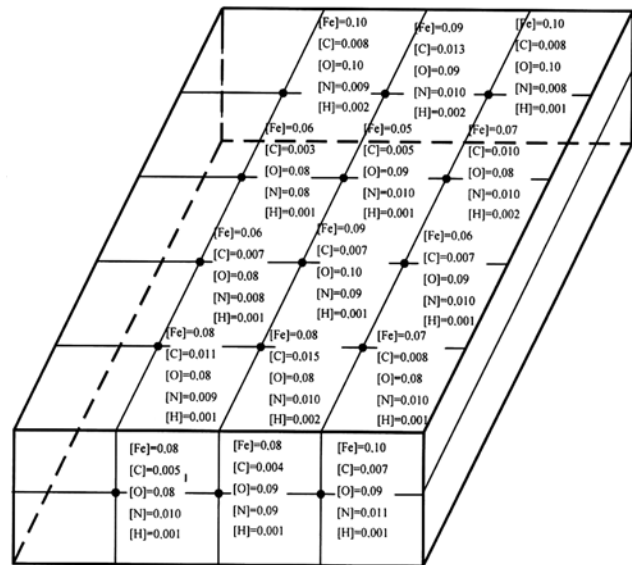


**Figure 5.** Scheme of taking samples from slab of non-alloyed titanium ( $165 \times 950 \times 1800$  mm) and results of chemical and gas analyses

in the form of pores, cavities, cracks and non-metal inclusions in titanium ingots-slabs were absent.

Comparison of efficient metal yield showed that in melting of bloom and lumpy waste evaporation losses of titanium were actually the same and by 30–40 % lower than in melting of sponge crushed into 12–70 mm fractions.

For implementing developed technology of electron beam melting of uncrushed spongy titanium blocks electron beam unit was developed at the E.O. Paton EWI, which has no analogs in the world. It allows combining processes of the block side surface melting at the stage of preliminary heating and full-scale melting in the same vacuum chamber.

Developed at the E.O. Paton EWI of NASU technology of electron beam melting of uncrushed spongy titanium blocks for producing high-quality ingots and ingots-slabs and specialized equipment for implementation of mentioned technology under conditions of industrial enterprises allowed organizing in Ukraine competitive at the world market production of high-quality titanium ingots of round and rectangular section.

1. Trigub, N.P., Akhonor, S.V. (1998) Market of titanium: state-of-the-art and prospects. *Problemy Spets. Elektrometallurgii*, **4**, 74–77.
2. Paton, B.E., Trigub, N.P., Akhonor, S.V. (1999) Electron beam melting of titanium. In: *Proc. of 9th World Conf. on Titanium* (St-Petersburg, Russia, June 7–11, 1999). St-Petersburg: CRISN Prometej.
3. Paton, B.E., Trigub, N.P., Akhonor, S.V. et al. (1996) Some tendencies of development of metallurgical processing of titanium. *Problemy Spets. Elektrometallurgii*, **1**, 25–31.
4. Paton, B.E., Trigub, N.P., Akhonor, S.V. (2003) Prospective technologies of titanium electron beam melting. *Titan*, **2**, 20–25.
5. Paton, B.E., Trigub, N.P., Zamkov, V.N. et al. (2000) Development of technology of titanium electron beam melting. *Problemy Spets. Elektrometallurgii*, **2**, 34–40.
6. Akhonor, S.V. (2001) Mathematical modeling of dissolution process of TiN inclusions in titanium melt during EBM. *Ibid.*, **1**, 20–24.
7. Paton, B.E., Trigub, N.P., Kozlitsin, D.A. et al. (1997) *Electron beam melting*. Kiev: Naukova Dumka.
8. Garmata, V.A., Petrunko, A.N., Galitsky, N.V. et al. (1983) *Titanium*. Moscow: Metallurgiya.



# STRUCTURE AND MECHANICAL PROPERTIES OF DISPERSION-STRENGTHENED TITANIUM-BASE MATERIALS DEPOSITED FROM GAS PHASE

L.M. NERODENKO, E.V. ONOPRIENKO and B.A. MOVCHAN  
E.O. Paton Electric Welding Institute, NASU, Kiev, Ukraine

Structure and mechanical properties (tensile strength, relative elongation, high-temperature creep rate) of deposited from gas phase materials Ti-Si (2–18 % Si) were investigated. It is shown that condensates, strengthened by intermetallic phases, have good prospects for development of titanium-base refractory materials.

*Keywords:* electron beam evaporation, condensates Ti-Si, microstructure, mechanical properties

Titanium-base high-strength and refractory materials relate to the most distributed structural materials. Requirements to their operation characteristics, especially at temperatures up to 800 °C, continuously get more and more stringent. Traditional method of strength increase is dispersion strengthening by formation in the alloy structure of particles of high degree of dispersity (oxides, borides, nitrides). In particular, application of the technology of rapid solidification ensured production of titanium alloys with high volume ratio of non-coherent particles, characterized by high level of resistance to coagulation at the temperature 600–800 °C and significant creep resistance [1].

Electron beam evaporation and condensation in vacuum relate to precision methods of production of dispersion-strengthened materials with regulated parameters of the strengthening phase [2].

It is shown in [3] that titanium-base dispersion-strengthened materials, produced by electron beam

evaporation with subsequent deposition in vacuum, may compete concerning their mechanical properties at 20 °C and high-temperature strength with dispersion-strengthened titanium alloys, produced by the method of rapid solidification, that is confirmed by data of Figures 1, 2, in which concentration dependence of strength and ductility parameters and rate of steady-state creep at 600 °C of condensates and alloys, produced by means of rapid solidification, are shown [4–6].

One of possible methods of dispersion strengthening of titanium alloys is application of titanium intermetallics as refractory particles. The most preferential for this purpose are aluminides TiAl, Ti<sub>3</sub>Al, Ti<sub>2</sub>AlNb, and silicides Ti<sub>5</sub>Si<sub>3</sub> and TiSi<sub>2</sub>. Titanium silicides are characterized by the whole number of positive qualities --- low density, high modulus of elasticity, and high creep and oxidation resistance. However, they have insufficient ductility at room temperature, because temperature of their brittle-ductile transition is within the range 800–1050 °C. Positive qualities of silicides may be used in case of their

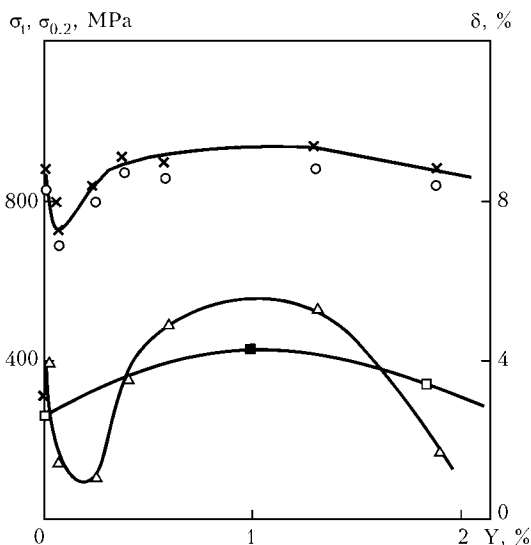


**Figure 1.** Influence of yttrium content on yield strength (O), tensile strength (X), relative elongation ( $\Delta$ ) of condensates Ti-Y and yield strength of alloys Ti-Y, Ti-Er ( $\square$ ,  $\blacksquare$ ) [4, 5] at temperature 20 °C

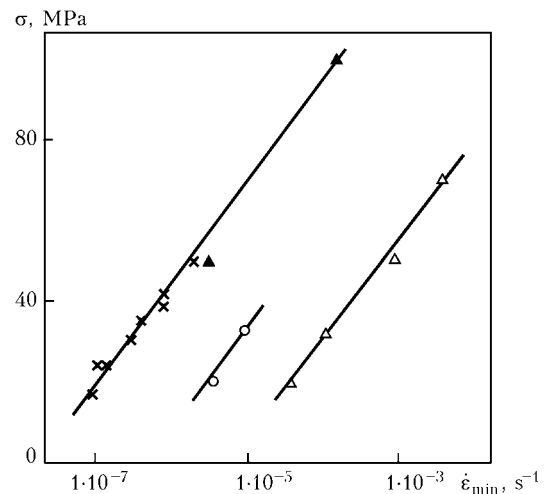


**Figure 2.** Dependence of rate of steady-state creep upon stress of Ti (O) and alloy Ti-Y (X) produced by method of rapid solidification [4, 6], as well as condensates Ti ( $\Delta$ ) and Ti-Y ( $\blacktriangle$ ) [3] ( $T_{evap} = 600$  °C)



introduction into ductile matrix of titanium in the form of finely dispersed particles (mainly  $Ti_5Si_3$ ) or in production of eutectic alloys, strengthened by  $Ti_5Si_3$  fibers. Positive influence of silicon, which forms intermetallic compounds with titanium, on high-temperature strength and refractoriness of titanium was noted for the first time in [7]. It was shown in [8] that additives of silicon were successfully used for increasing strength and high-temperature strength of cast titanium alloys.

Achievement of increased creep resistance of directionally solidified eutectic alloys Ti- $Ti_5Si_3$ , containing 8.5 % Si (approximately 30 vol.%  $Ti_5Si_3$ ), is described in [9].

In the works, carried out within the last years, materials Ti-Al-Si, produced by two methods --- directed solidification of alloys Ti-Si for the purpose of formation in the matrix  $\alpha$ -Ti of fibers  $Ti_5Si_3$  and production of fine-grain structures of pre-eutectic or eutectic composition, representing  $\alpha$ -Ti matrix with particles  $Ti_5Si_3$ , having size of several microns, were investigated [10-12]. Authors of these investigations have drawn conclusion that application of mentioned composite materials as the basis for development of new titanium materials with operation temperature up to 800 °C has good prospects.

Subject of this article are results of investigation of the structure and properties of dispersion-strengthened materials on the basis of the system Ti-Si, produced by means of electron beam evaporation and

condensation, which represent interest for application at high temperatures.

**Materials and methods of investigation.** Ingots of titanium, produced by the method of electron beam remelting in vacuum, and ingots of silicon, produced from a cylindrical specimen of a single crystal, grown according to Chokhralsky method, were used as initial materials for evaporation. Prior to the process of evaporation and condensation of initial materials anti-adhesion layer of  $CaF_2$  of 1.0-1.5  $\mu m$  thickness was deposited on surface of a disk substrate. Thickness of produced condensate was about 1 mm. For the purpose of achieving high rates materials were evaporated through molten pools of refractory materials: titanium --- through niobium pool, silicon --- through hafnium pool.

Structure of the condensates was investigated on scanning electron microscope Camscan. For analysis of element composition EDS system of microscope Camscan and Philips X-ray spectrometer X'Unique 2 were used.

Mechanical properties were determined by tensile of flat specimens with working part  $1 \times 3 \times 12$  mm at deformation rate  $1.7 \cdot 10^{-3} s^{-1}$  in vacuum. Tensile tests were also carried out under creep conditions at temperature 700 °C in vacuum with determination of minimum creep rate. Condensates with high content of silicon (8 and 18 %) were tested for three-point bend. Before mechanical tests the specimens were annealed at 750 (condensation temperature), 1000 and 1200 °C within 1 h.

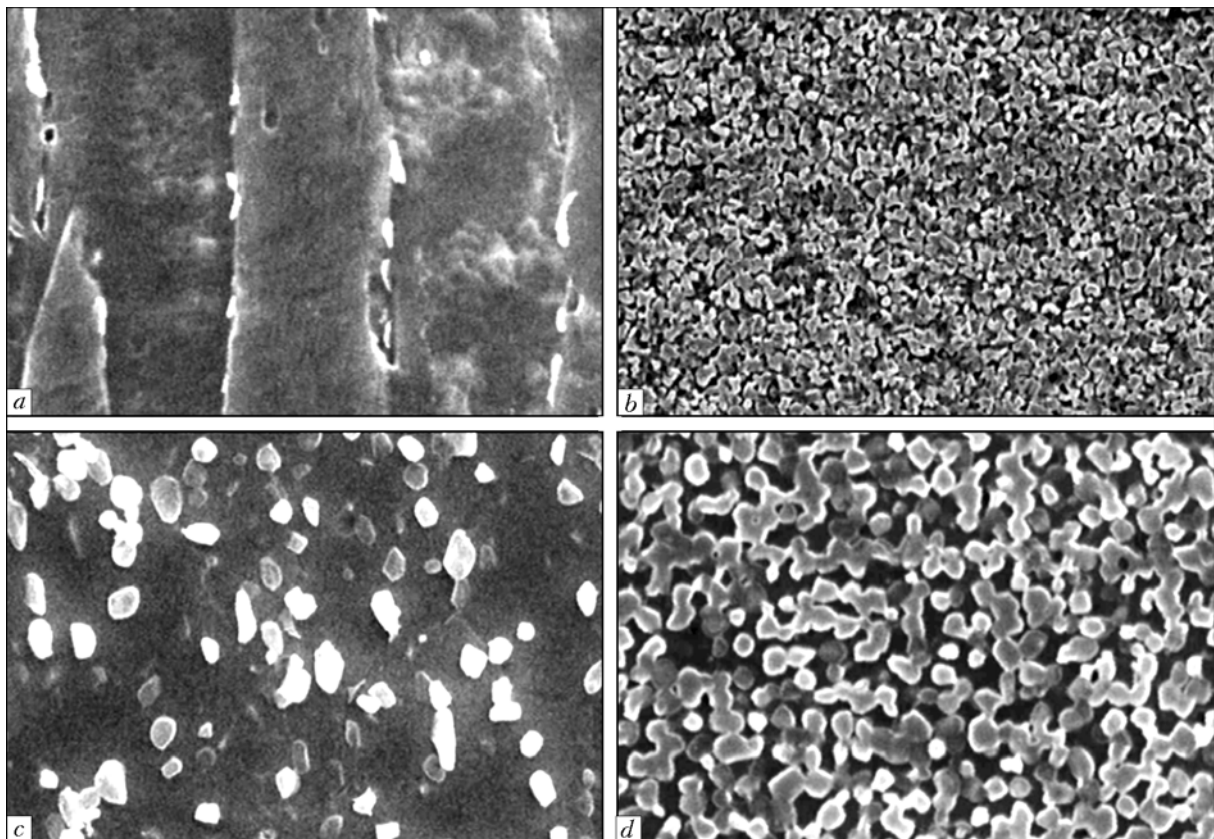


**Figure 3.** Microstructure of condensed materials Ti-Si after heat treatment: a, c --- Ti-2Si; b, d --- Ti-8Si; a, b ---  $T_{ann} = 750$  °C, 1 h, vacuum; c, d ---  $T_{ann} = 1000$  °C, 1 h, vacuum ( $\times 1000$ )

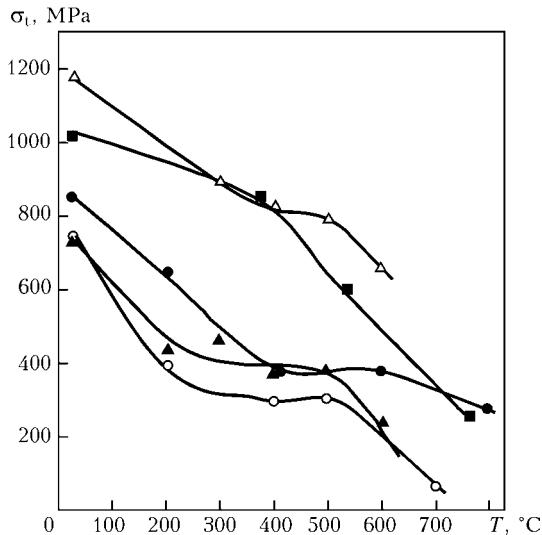


**Figure 4.** Dependence of tensile strength of materials Ti-(TiAl)-Si upon annealing temperature:  $\Delta$  — Ti-6Al-2.5 Si [5];  $\blacksquare$  — Ti-8Si [9];  $\bullet$  — Ti-3Al-2Si [11];  $\blacktriangle$  — Ti-2.5Si [5];  $\circ$  — condensate Ti-2Si

**Results of investigation.** Produced condensates contained 2, 8 and 18 % Si. Volume share of silicide phase constituted 7, 29 and 63 %, respectively (calculation).

Used technology ensures production of condensates with dense structure and sufficiently uniform distribution of elements over the condensate thickness.

Typical microstructures of investigated materials are shown in Figure 3.

For condensates with 2 % Si in initial state presence of crystallites, stretched in the direction of vapor flow fall, is characteristic; silicide phase is mainly located over boundaries of crystallites. Structure of failure zones of the specimens, subjected to tensile tests at 20 and especially 700 °C, becomes more uniform; in addition to coarse inclusions fine particles of silicide phase are present, occurrence of which is possibly caused by eutectoid disintegration under action of stress. When content of silicon equals 8 % condensates have characteristic eutectic structure, at 18 % of silicide phase has the form of a frame.

Annealing of condensates Ti-8Si at temperatures 1000 and 1200 °C enables rounding of silicide phase particles with subsequent increase of their size. Similar evolution of structure is also characteristic of condensate Ti-18Si.

Structure of condensates Ti-2Si after annealing at 1000 and 1200 °C gets equiaxial: size of the grain increases, approximately, up to 60  $\mu\text{m}$ .

**Mechanical properties.** Introduction of 2 % Si into condensed titanium increases its ultimate strength at 20 °C from 600 to 750 MPa, whereby relative elongation reduces from 14.0 to 7.6 %. Increase of silicon content approximately to 8 % enables reduction of ductility down to zero. It should be noted that ductility of eutectic alloy Ti-8.5 % Si, produced in [9] by the method of directed solidification, is, approximately, 0.55–0.65 %.

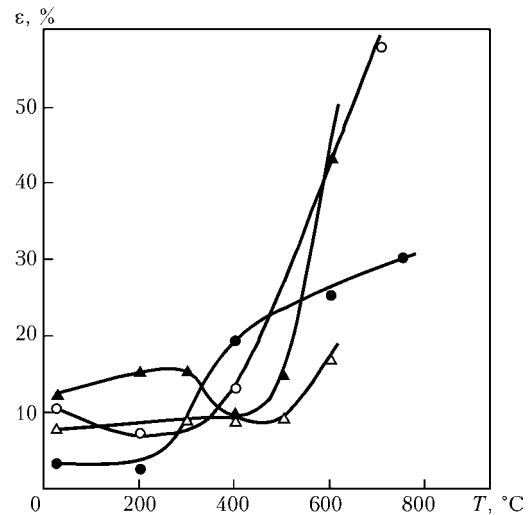


**Figure 5.** Dependence of relative elongation of materials Ti-Si and Ti-Al-Si upon annealing temperature:  $\circ$  — condensate Ti-2Si;  $\blacktriangle$  — Ti-2.5Si [3];  $\Delta$  — Ti-6Al-2.5Si [3];  $\bullet$  — Ti-3Al-2Si [8]

Temperature dependences of ultimate strength and relative elongation of condensates Ti-2 % Si after annealing at 750 °C are given in Figures 4 and 5. Here are also presented similar dependences for cast alloys Ti-2.5Si, Ti-6Al-2.5Si [8] and Ti-3Al-4.8Zr [11]. It should be noted that  $\sigma_t$  values of the condensed material and alloy Ti-2.5Si [8] are close. Naturally, presence in cast alloy of 6 % Al significantly improves its strength characteristics. On this basis further strengthening of condensate Ti-2Si by its alloying with aluminium seems having good prospects. At temperature 500 °C condensate Ti-2Si loses strength, whereby its ductility drastically increases (Figure 5). Low high-temperature strength is, evidently, stipulated by fine-crystalline structure of condensed material.

Condensates with weight share of silicon 8 and 18 %, subjected to bend test in the state after condensation, fail in resilient area; insignificant deviation, corresponding to the bend angle of approxi-

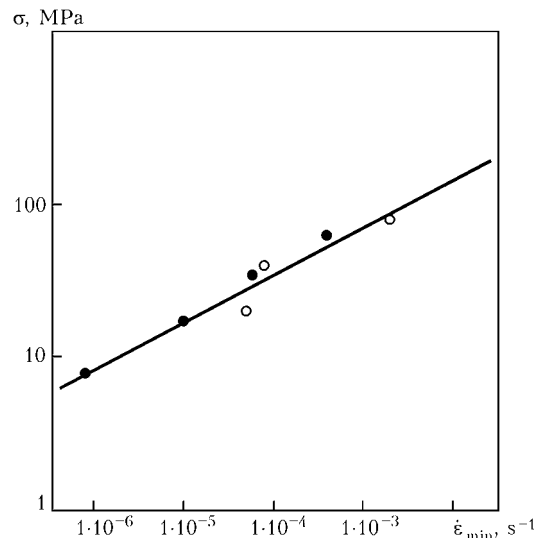


**Figure 6.** Dependence of minimum creep rate of deposited from vapor phase material Ti-2.5Si and material Ti6Al4V [13], produced by method of plasma spraying, upon stress:  $\bullet$  — Ti6Al4V ( $T_{\text{evap}} = 680$  °C);  $\circ$  — Ti-2.5Si ( $T_{\text{evap}} = 700$  °C)



mately 10', was noted in condensates Ti-8Si, annealed within temperature range 1000–1200 °C. Condensates Ti-18Si are brittle.

In Figure 6 dependence of minimum creep rate of condensate Ti-2Si upon applied stress is shown. It should be noted that  $\dot{\epsilon}_{\min}$  values of the condensate and nanocrystalline material Ti6Al14V, obtained in [13] by the method of plasma deposition of alloy Ti-6Al-4V in argon ( $d_{gr} \sim 30\text{--}100$  nm), are close.

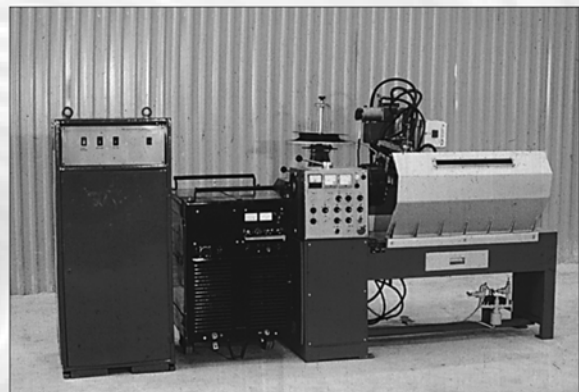
So, strengthened by intermetallic phase  $Ti_5Si_3$  (approximately 7–8 vol.%) condensed material on the basis of systems Ti-Si is a promising material for its use as the basis in development of high-temperature materials, for example Ti-Al- $Ti_5Si_3$ , with operation temperature up to 800 °C.

1. Wang Sung, H. (1986) Rapidly solidified titanium alloys for high temperature applications: Review. *J. Materials Sci.*, 21(7), 2224–2238.
2. Movchan, B.A. (1985) Production of new inorganic materials by vapor deposition in vacuum. *Vestnik AN SSSR*, 7, 21–29.
3. Korzh, A.V., Nerodenko, L.M., Molodkina, T.A. (1991) Structure and mechanical properties of dispersion-strengthened condensed materials Ti- $Y_2O_3$ . *Problemy Spets. Élektrometallurgii*, 4, 32–35.
4. Sastry, S.M.L., Peng, T.C., Beckerman, L.P. (1984) Structure and properties of rapidly solidified dispersion strengthened titanium alloys. Part 2: Tensile and creep properties. *Metal Transact. A*, 15(7), 1465–1474.
5. Naka, S., Marty, M., Octor, H. (1987) Oxide-dispersed titanium alloys Ti-Y prepared with the rotating electrode process. *J. Materials Sci.*, 22(3), 887–895.
6. Perrier, C., Naka, S., Kubin, L.P. (1989) Plastic deformation behaviour of rapidly solidified Ti-Y alloys below 700 °C. *Str. Metals*, 23(4), 477–482.
7. Sutcliffe, D.A. (1954) In: *Revue de Metal*, 51(8), 524.
8. Glazunov, S.G., Elagina, L.A., Kotova, V.I. (1961) Alloys of system titanium-silicon and titanium-aluminum-silicon. In: *Titanium in industry*. Moscow: Oborongiz.
9. Crossman, F.W., Sue, A.S. (1971) Unidirectionally solidified Ti-TiB and  $Ti_5Si_3$  eutectic composites. *Metal Transact.*, 2(6), 1545–1555.
10. Fronimeyer, G., Rosenkranz, R. (2004) Structures and properties of the refractory silicides  $Ti_5Si_3$  and  $TiSi_2$  and T-S-(Al) eutectic alloy. In: *Metallic materials with high structural efficiency*: Nato Sci. Series, 146/II, 287–308.
11. Bankovsky, O.I., Kulak, L.D., Kuzmenko, N.N. et al. (2000) Structure and mechanical properties of powder materials of Ti-Al-Si system. *Poroshk. Metallurgiya*, 5/6, 108–116.
12. Gornaya, I., Bankovsky, O., Kulak, L. et al. (2004) Effect of Zr on structure and mechanical behaviour of Ti-Al-Si alloys. In: *Metallic materials with high structural efficiency*: Nato Sci. Series, 146/II, 229–235.
13. Warren, J., Hsiung, L.M., Wadley, H.N.G. (1995) High temperature deformation behaviour of physical vapor deposited Ti-6Al-4V. *Acta Met.*, 43(7), 2773–2787.

## PLASMA HARDFACING OF PARTS OF PIPELINE STOP VALVES AND PUMPS

At the Engineering Center of Wear-Resistant Coatings of the E.O. Paton Electric Welding Institute the technology, equipment and electrode materials have been developed for plasma hardfacing of shafts, rods, slide valves, piping stop valves, bushings and pump shafts and other components of the petrochemical equipment.

Installation of UD-417M type has been designed for plasma hardfacing allowing deposition of parts of type of a shaft of 30–300 mm diameter and 50–800 mm length using filler wire of 1.2–3.6 mm diameter. Dimensions of the installation: 1680×350×1750 mm. Mass – 600 kg. Power source – VDU-506.



As electrode materials, the flux-cored wires PP-AN133, PP-AN157, PP-AN177, etc. are used. Technology of hardfacing provides: small share of parent metal in deposited layer; negligible welding deformations; good formation and high quality of deposited layer; required composition and properties of metal in the first deposited layer.

**Proposals for co-operation.** The Engineering Center of Wear-Resistant Coatings is fulfilling works on the contract base for the development of electrode materials and technological procedures of hardfacing; provides delivery, setting-up, putting into operation and implementation of installations UD-417M.

Contacts: Dr. Eremeev V.B.  
Tel.: (38044) 287 89 48, 289 15 56



# INVESTIGATION OF HEAT EXCHANGE PROCESSES IN MOULD OF ELECTRON BEAM INSTALLATION

N.F. NAKONECHNY, V.N. FYODOROV and V.A. SHCHEKIN-KROTOV  
FIKO Ltd., Kiev, Ukraine

It is shown that application of copper moulds in EBCHM of titanium alloys is not efficient. Replacement of copper by alloys, which ensure  $B_f \leq 1$  allows increasing efficiency factor of remelting from 20 to 35 % and producing ingots with smooth defect-free surface.

*Keywords:* electron beam melting, heat exchange, mould, ingot, alloy, titanium

Copper water-cooled moulds of metallurgical installations are designed for giving to a molten metal a certain assigned beforehand form and fixing it during transition of the melt from liquid to solid state. Transition of the melt into solid state is performed when part of its heat energy gets into system of the mould cooling. In this case the mould operates as a special heat exchange apparatus and should ensure the best quality of an ingot at minimum power consumption.

As far as analysis of efficiency of the moulds, used in EBCHM, is absent in literature, the purpose of this work consisted in investigation of heat exchange processes and determination of functioning efficiency of copper water-cooled moulds in EBCHM of titanium alloys.

The investigation was carried out on electron beam installation (EBI) of the FIKO electron beam metallurgy plant in the course of production of ingots of alloy VT1-0 with application of an intermediate unit (cold hearth) and copper water-cooled mould 0.655 m diameter and 0.385 m height. The ingot was molten using four electron guns of high-voltage glow discharge, the first and the second of which melted consumable billet, and the third and the fourth ones

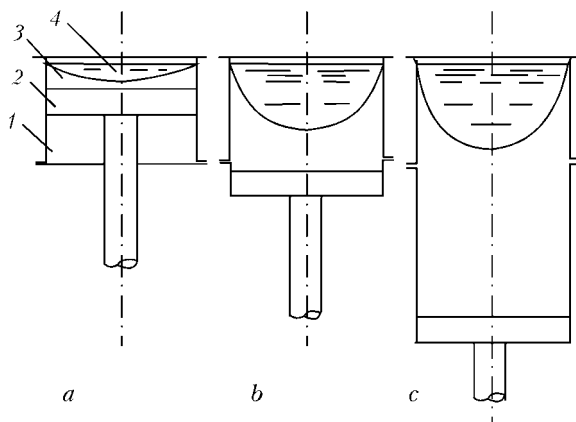


**Figure 1.** Position of tray and inoculation relative mould in EBCHM process: *a* — inoculation heating-up; *b* — exit of tray from mould; *c* — drawing of ingot; 1 — mould; 2 — tray; 3 — inoculation; 4 — molten metal

heated melt surface in the mould. Technological process of the ingot melting in the EBI mould consists of three stages:

- heating-up of inoculation (Figure 1, *a*);
- melting of the consumable billet and stretching of the ingot (Figure 1, *b, c*);
- withdrawal of a sink hole.

Inoculation, which represents a disk from alloy VT1-0 of 100 mm thickness, is located on water-cooled bottom plate (tray) and is connected by its stem with the ingot stretching mechanism.

At the beginning of melting there is clearance between cold inoculation, installed in upper part of the mould, and wall of the latter. For the metal, which gets into the mould, not to pour out through the clearance into the ingot chamber and not to solidify till complete filling of the mould, the inoculation is heated by beams of two electron guns from center to periphery, due to which the molten pool is created in center and gradually expands till the inoculation touches the mould. Then melting of the consumable billet starts, the ingot is stretched, and the guns are brought to maximum power.

Surface of melt in the mould is constantly heated by two electron guns, one of which describes spiral and the other one — spiral and circle near surface of the mould. In addition, one of the guns melts the web and heats metal in channel of the spout during pouring of the metal into the mould.

After termination of the melting process, pouring of the metal into the mould, and stretching of the ingot one gets down to withdrawal of sink hole, gradually reducing power of electron beams and bringing spirals of the guns to axis of the ingot. As a result of performance of mentioned operations an ingot is produced with high-quality dense macrostructure and wavy surface with flashes, which is subjected to complete roughing.

In this investigation at mentioned stages of the ingot production power, consumed by electron guns, rate of the consumable billet melting, water temperature at inlet and outlet from the mould, the tray and the intermediate unit, as well as its flow, were checked. After termination of melting formed condensate was collected and weighed.



Than metal temperature at slope of the consumable billet, in intermediate unit and in the mould, energy loss on radiation and evaporation of metal and energy loss, connected with heat conductivity into cooling system of the mould and the tray, were calculated. On the basis of calculation results energy balance of the mould and the remelting process was determined and efficiency of the mould operation was analyzed.

In Figure 1 different positions of the tray and the inoculation in relation to the mould in the process of remelting are shown. As one can see from the Figure, as the ingot builds up, the area of its heat exchange with the mould increases and achieves maximum when the tray exits the mould. In addition, heat resistance to heat flow along the ingot axis to the tray increases due to increase of distance between the latter and the pool surface. As showed investigations, during heating-up of the inoculation growth of heat flow into cooling system of the mould does not follow any regularity. However, in all cases, when the inoculation gets in full contact with the mould, heat flow achieves approximately the same value --- 58-61 kW (Figure 2).

As follows from Figure 3, change of the ingot length  $L$  in the course of one of investigated meltings was uniform, which is connected with stable consumption of power  $W$  for melting of the consumable billet (448 kW) and heating of metal in the mould and the spout (300 kW). Mean rate of the consumable billet melting and the ingot stretching (ratio of the ingot length change  $\Delta L$  to a respective time interval  $\Delta\tau$ ) equaled

$$v_l = \frac{\Delta L}{\Delta\tau} = \frac{1.56}{(7.27 - 1.07) \cdot 3600} = 7.01 \cdot 10^{-5} \text{ [m/s]},$$

that corresponds to mass rate of melting ( $m = 0.0998 \text{ kg/s} \approx 0.1 \text{ kg/s}$ ).

In Figure 3 change of heat flows into cooling systems of the mould and the tray is shown. As one can

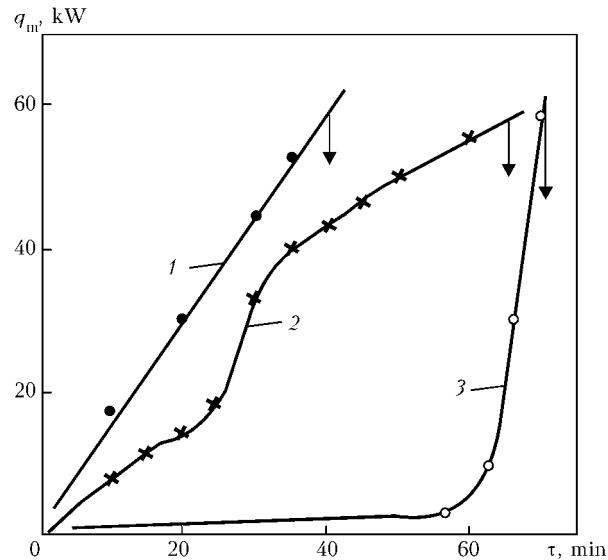


Figure 2. Growth of heat flow from inoculation to mould during its heating-up in process of meltings 1-3; arrows indicate instant of first pouring of metal

see from the Figure, heat flow to the tray increased by means of the inoculation heating-up, but reduced after its getting into contact with the mould and subsequent drawing of the ingot. Because of the same reasons heat flow into the mould cooling system started to rapidly grow. After exit of the tray from the mould heat flow into cooling system of the latter stabilized at the level 148 kW, and process of the ingot heat exchange with the mould transited into quasi-stationary stage, although heat flow reduced in direction of the tray in the process of the whole melting.

For drawing energy balance of the mould in stage of quasi-stationary heat exchange temperature of the metal, which drains from the consumable billet slope, and its overheating in the intermediate unit, were determined, and on the basis of these data heat content of the metal, which gets into the mould, was found.

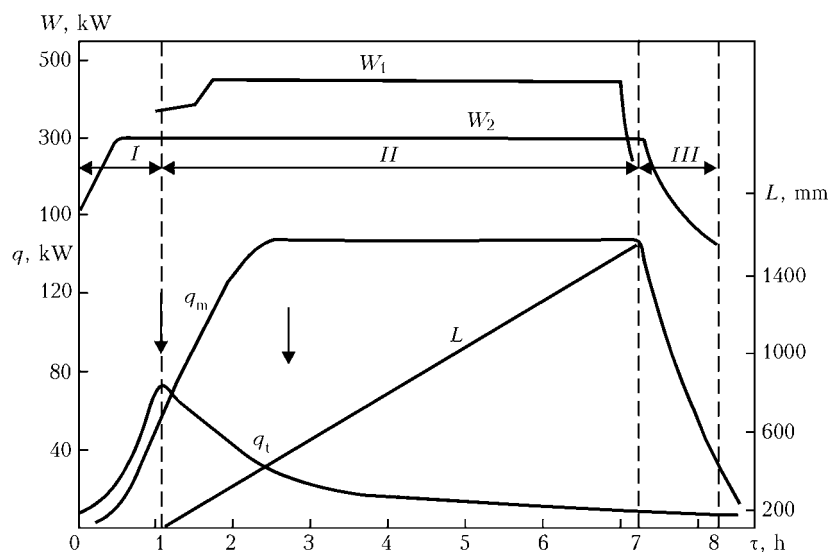


Figure 3. Change in EBCHM process of power consumption for melting of consumable billet  $W_1$  and heating-up of melt surface  $W_2$ , ingot length  $L$  and heat flows in mould cooling system  $q_m$  and tray  $q_t$ : I-III --- EBCHM stages; arrows indicate instants of first pouring and exit of tray from mould



Temperature of overheating of the metal that drains from the consumable billet slope was determined by the calculation method, described in [1], according to formula

$$t_{ov} = \frac{16200m\delta}{S - 13.94m\delta} + t_{melt},$$

where  $\delta$  is the thickness of drops or trickles on the consumable billet slope ( $8.66 \cdot 10^{-3}$  and  $5.0 \cdot 10^{-3}$  m, respectively);  $S$  is the slope surface area ( $0.208 \text{ m}^2$ );  $t_{melt}$  is the melting point of alloy VT1-0 ( $1668 \text{ }^\circ\text{C}$ ).

Mean temperature of overheating of the metal, which drains from the consumable billet slope into the intermediate unit, may be presented in the form

$$t_{mean} = \frac{t_{ov}^{dr} + t_{ov}^{tr}}{2} = \frac{1740 + 1708}{2} = 1724 \text{ }^\circ\text{N},$$

where  $t_{ov}^{dr}$  and  $t_{ov}^{tr}$  are the overheating temperatures of drops and trickles, respectively.

Overheating of melt in the intermediate unit was determined according to formula

$$\Delta t_{ov} = \frac{kW}{C_m} = \frac{0.03 \cdot 448000}{989.2 \cdot 0.1} = 135.86 \text{ }^\circ\text{N},$$

where  $k$  is the coefficient that takes into account share of power of melting guns, spent for overheating of metal in the intermediate unit. According to data of [2], in mentioned technology of melting  $k = 0.03$ ;  $C_l$  is the heat capacity of liquid titanium ( $989.2 \text{ J}/(\text{kg} \cdot ^\circ\text{C})$ ).

So, temperature of metal, which got from the intermediate unit into the mould, was

$$t_{ov} = t_{mean} + \Delta t_{ov} = 1724 + 135.86 = 1859.86 \approx 1860 \text{ }^\circ\text{C}.$$

Amount of heat energy that gets into the mould together with molten metal, was calculated, using expression

$$q_l = m[C_t(t_{melt} - t_i) + C_l(t_{ov} - t_{melt}) + q_s] = \\ = 0.1 [654.9 (1668 - 11) + 989.2 (1860 - 1668) + \\ + 295000] = 157009.57 \text{ J} \approx 157 \text{ kW},$$

where  $C_t$  is the mean heat capacity of titanium within temperature range  $20-1668 \text{ }^\circ\text{C}$ ,  $\text{J}/(\text{kg} \cdot ^\circ\text{C})$ ;  $q_s$  is the specific heat of titanium melting,  $\text{J}/\text{kg}$ ;  $t_i$  is the initial temperature of the consumable billet,  $^\circ\text{C}$ .

In calculation of the amount of energy, supplied into the mould with electron beams, it was taken into account that  $21.7 \text{ kW}$  power of the guns is consumed for heating of metal in the spout channel of the intermediate unit, 9 % of the power is consumed by the anode and cathode cooling system, and 3 % are lost on the way to the mould. That's why from  $300 \text{ kW}$  energy, consumed by the guns, into the mould get  $q_e = (300 - 21.7)[1 - (0.03 + 0.09)] = 244.93 \text{ kW}$ .

All together the following energy gets into the mould with molten metal and electron beams:

$$q_m = q_l + q_e = 157 + 244.93 = 401.93 \text{ kW}.$$

This energy is spent in the mould for radiation, evaporation, is transferred due to heat conductivity into the system of its cooling, is lost with back scattered electrons, is spent for secondary emission of electrons and X-ray radiation, and leaves the mould together with the ingot.

Energy loss, connected with radiation, was calculated taking into account Stefan-Boltzmann's law:

$$q_{rad} = C \left[ \left( \frac{T_{m.s}}{100} \right)^4 - \left( \frac{T_s}{100} \right)^4 \right] S_{surf}, \quad (1)$$

where  $S_{surf}$  is the area of melt surface in the mould ( $0.337 \text{ m}^2$ );  $T_{m.s}$ ,  $T_s$  are the temperatures of melt surface and screens ( $2173$  and  $673 \text{ K}$ , respectively);  $C$  is the reduced coefficient of radiation ( $1.729$ ).

$$C = \sigma_0 \left/ \left( \frac{1}{\epsilon_{m.s}} + \frac{S_{surf}}{S_s} \left( \frac{1}{\epsilon_s} - 1 \right) \right) \right\}$$

where  $\sigma_0$  is the Stefan-Boltzmann's constant ( $5.67$ );  $\epsilon_{m.s}$ ,  $\epsilon_s$  are the degree of blackness of melt surface and screens ( $0.3633$  and  $0.2$ , respectively), which were calculated from equation

$$e_{Ti} = 1.15 \cdot 10^{-4} T + 0.1135,$$

where  $T$  is the absolute temperature of surface, which participates in heat exchange,  $\text{K}$ ;  $S_a$ ,  $S_s$  are the areas of radiation surfaces (surface of metal in the mould and in the intermediate unit, and the consumable billet slope) and screens ( $0.784$  and  $5.9 \text{ m}^2$ ).

At mentioned values, included into formula (1), radiation losses in the mould constituted  $128.73 \text{ kW}$ .

Amount of energy, spent for evaporation of titanium from melt surface in the mould, was determined from equation

$$q_{evap} = \frac{M_c K_m q_e}{\tau},$$

where  $M_c$  is the mass of formed during the period of melting condensate ( $27 \text{ kg}$ );  $K_m$  is the share of titanium, which evaporates in this technology of melting from the mould ( $0.545$ ) according to data of [2];  $q_e$  is the specific heat of evaporation of titanium ( $9090 \text{ kJ}/\text{kg}$ );  $\tau$  is the duration of melting ( $6.25 \text{ h} = 22500 \text{ s}$ ).

Energy, needed for evaporation of titanium according to presented data, constituted  $5.944 \text{ kW}$ .

Amount of heat energy, transferred by heat conductivity into the mould cooling system  $q_h$ , equals, according to measurements in quasi-stationary heat exchange stage,  $148 \text{ kW}$  (Figure 3).

Energy losses with back scattered electrons in commercial EBIs [3] may be determined from the equation

$$q_{b.s} = 0.5 \eta_{b.s} W,$$

where  $\eta_{b.s}$  is the back scatter factor, equal for titanium  $0.215$ ;  $W$  is the power of energy of electron beams,  $\text{kW}$ .



In our case  $W = q_s$ , so  $q_{b,s} = 0.5 \times 0.215 \times 244.93 = 26.33$  kW. Insignificant part of energy of electron beams (totally  $\leq 0.01$ ) is spent for secondary emission of electrons and X-ray radiation, which constitutes

$$q_{m,s} = 0.01W = 0.01 \cdot 244.93 \approx 2.45 \text{ kW.}$$

So, power consumption in the mould according to mentioned positions constitutes

$$Sq_m = q_{rad} + q_{ev} + q_h + q_{b,s} + q_{m,s} = 128.73 + 5.944 + 148 + 26.33 + 2.45 = 311.454 \text{ kW.}$$

Non-consumed in the mould energy leaves it together with the ingot. Its amount equals difference of supplied into the mould energy and energy, spent on mentioned items, i.e.

$$q_i = q_m - \Sigma_m = 401.93 - 311.454 = 90.476 \text{ kW.}$$

On the basis of carried out investigations and calculations energy balance of the mould was drawn (Table).

Proceeding from data of the Table, it is possible to calculate amount of energy, transferred to the mould by molten metal, which is a measure of fulfilled by it useful work and equals difference between energy, brought into the mould by molten metal, and energy, which left it together with the ingot:

$$q_{l,m} = q_l - q_m = 157 - 90.476 = 66.524 \text{ kW.}$$

Energy efficiency of the mould may be represented as ratio of amount of energy, transferred to the mould by molten metal  $q_{l,m}$  to amount of whole energy  $q_e$ , spent in it. It will equal

$$\eta_m = \frac{q_{l,m}}{q_m} \cdot 100 = \frac{66.524}{401.93} \cdot 100 = 16.55 \text{ \%}.$$

Energy efficiency of EBR process equals ratio of energy, spent for heating, melting and overheating of alloy VT1-0, to the whole spent for its melting and solidification energy:

$$\eta_{ov} = \frac{q_l}{W_{1-2} + W_{3-4}} \cdot 100 = \frac{157}{448 \cdot 300} \cdot 100 = 20.9 \text{ \%}.$$

So, at efficiency factor of the mould 16.55 % and EBCHM 20.9 % a dense, physically macro-homogeneous ingot with poor-quality surface, which has to be completely roughened, is produced.

In [4] thermal efficiency of EBR process of different metals is given. Under optimum conditions of remelting efficiency values reduce when passing from iron and nickel to more refractory niobium and tungsten from 20–35 to 4.0–0.5 % because of energy loss on radiation and need to replace it by the energy of electron beams.

At the same time when using as material for moulds metals, which ensure criterion  $B_i$  (ratio of heat resistance of the ingot to heat resistance of the environment) less or equal to one, in upper part of the mould a zone is formed, the height of which is several dozen millimeters, in which melt, when it contacts with the mould, remains in liquid state without additional heating [5]. It follows from this that in this case there is not need to heat up in EBCHM meniscus by electron beams, keep the mould open, lose energy on radiation, and compensate this loss by energy of electron beams.

Criterion  $B_i$  in formation of an ingot in the investigated melting of alloy VT1-0 may be determined from the expression

$$B_i = \frac{\alpha_{env} R_{ing}}{\lambda_{ing}}, \quad (2)$$

where  $\alpha_{env}$  is the heat transfer coefficient from an ingot surface into environment;  $R_{ing}$  and  $\lambda_{ing}$  are the radius of the ingot and heat conductivity of molten metal of the ingot, respectively;

$$\alpha_{env} = \frac{1}{R_{env}},$$

where  $R_{env}$  is the heat resistance to heat flow from the ingot surface to water, which cools the mould. In

Mould energy balance

Parameter No.	Supply and consumption of energy	Amount of energy	
		kW	%
<i>Supply</i>			
	Supplied with electron beams	244.93	60.93
	Supplied with molten metal	157.00	39.06
	Total supply	401.93	99.99
<i>Consumption</i>			
1	Lost on radiation	128.73	32.02
2	Spent for evaporation of titanium	5.94	1.47
3	Transferred by heat conductivity into mould cooling system	148.00	36.82
4	Lost with back scattered electrons	26.33	6.55
5	Spent for secondary emission of electrons and X-ray radiation	2.45	0.60
6	Lost with ingot	90.47	22.51
	Total consumption	401.92	99.97



the meniscus zone molten metal wets the mould. That's why here transitional contact resistance equals zero.

So,

$$R_{\text{env}} = \frac{1}{\alpha_w} + \frac{\delta_c}{\lambda_c}, \quad (3)$$

where  $\alpha_w$  is the heat transfer coefficient from the cooling channel to water;  $\delta_c$  and  $\lambda_c$  are the thickness and the heat conductivity of copper wall, respectively.

In the course of investigated melting values, which enter into formulas (2)–(3), and parameters were as follows:

$$\begin{aligned} R_{\text{ing}} &= 0.3275 \text{ m}; \lambda_{\text{ing}} = 33.1 \text{ W}/(\text{m}\cdot^\circ\text{C}); \\ \alpha_w &= 6000 \text{ W}/(\text{m}^2\cdot^\circ\text{C}), \delta_c = 0.035 \text{ m}; \\ \lambda_c &= 380 \text{ W}/(\text{m}\cdot^\circ\text{C}). \end{aligned}$$

At mentioned values of parameters  $R_{\text{env}} = 2.456 \cdot 10^{-4} (\text{m}^2\cdot^\circ\text{C})/\text{W}$ ,  $\alpha_{\text{env}} = 4071.4 \text{ W}/(\text{m}^2\cdot^\circ\text{C})$ .

So, in direct contact of molten titanium with the copper mould surface criterion  $B_i$  equals

$$B_i = \frac{\alpha_{\text{env}} R_{\text{ing}}}{\lambda_c} = 4071.4 \cdot \frac{0.3275}{33.1} = 40.28.$$

It means that outflow of heat energy from the ingot surface proceeded 40 times quicker than inflow and, therefore, for maintaining meniscus in molten state this disbalance had to be compensated by energy of electron beams. The data obtained allow determining amount of heat energy, transferred into the mould cooling system by electron beams for compensation of mentioned disbalance. It equals difference between the whole energy, supplied into the cooling system, and energy transferred by molten metal, i.e.

$$q_{t.e} = q_t - q_{l.m} = 148 - 66.524 = 81.476 \text{ kW}.$$

It was also necessary to compensate all other losses of energy, connected with heating of the metal surface. For this kind of compensation the energy of electron beams, equal to 244.93 kW, was necessary. Despite intensive heating, meniscus of the melt at distance 3–5 mm from the mould surface is in solid state, which is the reason of waviness of the ingot surface and presence of flashes [6–8]. Ingots with mentioned defects of surface are subjected to roughening or electron beam melting, which requires for additional expenses.

When using mould, manufactured from metals with  $B_i \leq 1$ , there is no need in constant heating of the melt surface in the mould. In this case electron guns may be used only for heating of inoculation and withdrawal of the sink hole. In the course of melting

radiation surface of melt should be isolated in order to prevent energy loss according to items 1–5 (see the Table), whereby efficiency of the mould may be increased up to  $\eta_m = \frac{q_{l.m}}{q_l} \cdot 100 = \frac{66.524}{157} \cdot 100 = 42.34 \%$

and of the remelting up to  $\eta_{\text{ov}} = \frac{q_l}{W_{1-2}} \cdot 100 = \frac{157}{448} \times 100 = 35.04 \%$ .

Presence of a zone of molten metal, which contacts with surface of the mould in its upper part, allows, in addition to saving energy, producing even and smooth surface of the ingot without waviness and flashes [9].

Titanium alloys are remolten into copper moulds of 0.4 m diameter and more (criterion  $B_i > 24$ ). For saving energy and producing ingots with smooth defect-free surface in such moulds it is necessary to develop alloys, which ensure criterion  $B_i < 1$ .

So, performed investigations showed that application of copper water-cooled moulds in EBCHM process of titanium alloys is (from the viewpoint of energy losses) inefficient. Withdrawal of heat from the melt meniscus in them occurs dozen times quicker than heat supply, which causes solidification of the melt near the mould walls, formation of waviness and flashes, and requires for additional significant energy consumption for maintaining ingot surface in the mould in liquid state. Application of alloys with  $B_i < 1$  for manufacturing of moulds allows (theoretically) refusing from heating melt in the mould, increasing efficiency of remelting from 20 to 35 % and producing ingots with smooth defect-free surface. At the same time it is necessary to carry out additional investigation for practical application of such moulds.

1. Nakonechny, N.F., Fyodorov, V.N., Shchekin-Krotov, V.A. (2004) Metal temperature at consumable billet downward slope in EBCHM of titanium alloys. *Advances in Electrometallurgy*, **2**, 19–22.
2. Nakonechny, N.F., Fyodorov, V.N., Shchekin-Krotov, V.A. (2003) About functioning of intermediate crucible in EBCHM of titanium alloys. *Ibid.*, **4**, 22–27.
3. Smelyansky, M.Ya., Elyutin, A.V. (1971) *Electron beam melting furnaces*. Moscow: Energiya.
4. Schiller, S., Gajzig, U., Pantzer, S. (1980) *Electron beam technology*. Moscow: Energiya.
5. Vejnik, A.I. (1958) *Theory of specific types of castings*. Moscow: Mashgiz.
6. Galatskaya, I.K. (1973) *Metallography of metallurgical defects in extruded aluminium alloy semi-finished products*. Kujbyshev.
7. Elisov, V.S., Stepanov, Yu.A. (1971) Influence of operation of continuous casting machine assembly units on aluminium alloy ingot quality. *Tsv. Metally*, **5**, 71–75.
8. Nakonechny, N.F., Fyodorov, V.N., Shchekin-Krotov, V.A. (2005) Formation of ingot surface in electron beam melting of titanium ingots. *Protsessy Litia*, **1**, 39–48.
9. Getselev, Z.N., Balakhontsev, G.A., Cherepok, G.V. (1980) Development and improvement of machines and technology for aluminium alloy casting in electromagnetic moulds. *Tsv. Metally*, **2**, 59–63.



# APPLICATION OF PLASMA-ARC REMELTING OF TECHNOGENIC WASTE IN MOVABLE HORIZONTAL MOULD FOR PRODUCING QUALITY FERROALLOYS AND MASTER ALLOYS

V.N. KOLEDA, V.A. SHAPOVALOV, G.F. TORKHOV and A.V. AKSINICHENKO  
E.O. Paton Electric Welding Institute, NASU, Kiev, Ukraine

Expediency of using plasma-arc remelting of technogenic waste in movable mould for producing high-quality ferroalloys and master alloys is shown. Conditions of achieving plasma arc stability and high quality of ingot are considered. Chemical compositions of produced ferroalloys and master alloys and values of specific consumption of electric power and argon in their melting are given.

*Keywords:* ferroalloys, master alloys, plasma-arc remelting, movable mould

In the course of conversion of defense facilities nomenclature of alloys, used in the industry, reduces, that's why application of many kinds of waste for metallurgical conversion into ingots of required composition requires, is connected at present with certain difficulties.

Processing of technological waste into different alloys and master alloys is anyway expedient because of many reasons. Firstly, single-stage processing of complex alloyed alloys into ready product is possible. Secondly, in production of ferroalloys and master alloys key parameters of the process may be reduced [1], for example, melting point, activity of highly reactionary metals, heat conductivity, etc.

Increased interest was noted to processing of the wastes of chemically active metals, for example, titanium into high-percentage ferrotitanium.

New technologies of titanium melting in electron-beam and plasma-arc furnaces with intermediate skull unit and pouring metal over into the mould, in which an ingot is formed, provide for producers of titanium products additional possibilities for more full and efficient use of titanium waste, and this enables significant reduction of the amount of titanium waste, which is traditionally used in production of 70 % ferrotitanium.

Increasing demand for 70 % ferrotitanium, on one hand, and reducing amount of titanium waste, on the other hand, stimulate development of new technologies for melting 70 % ferrotitanium. One of the options of such technologies is melting of 30–40 % ferrotitanium from ilmenite or rutile with its subsequent fusion with titanium scrap in the proportions, which ensure production of 70 % ferrotitanium [2].

One more problem exists. For 70 % ferrotitanium, used in melting of special-purpose stainless steels, increased requirements are established concerning

content of harmful impurities (carbon, oxygen, and nitrogen). Such ferrotitanium may be produced only by the method of skull melting (without contact of molten metal with lining) by means of fusion of titanium waste with iron, using «clean» sources of heating — electron beam or plasma [3].

Developed in the E.O. Paton EWI plasma-arc method of charge remelting in movable mould allows avoiding such shortcomings, inherent to commercial methods of melting of ferroalloys [4, 5] as contamination of the metal with carbon, components, which enter into composition of lining, slag inclusions, nitrogen, and oxygen. This makes it possible to significantly improve quality of ferroalloys and alloyed steels [6, 7].

Purpose of this work is study of possibility of producing ferroalloys and master alloys from waste of highly reactionary and refractory metals, and determination of main technological parameters of the process of plasma-arc remelting in a flat cooled mould.

The experiments were carried out on experimental plasma-arc installation OB1957 of the E.O. Paton



Figure 1. Appearance of installation OB1957

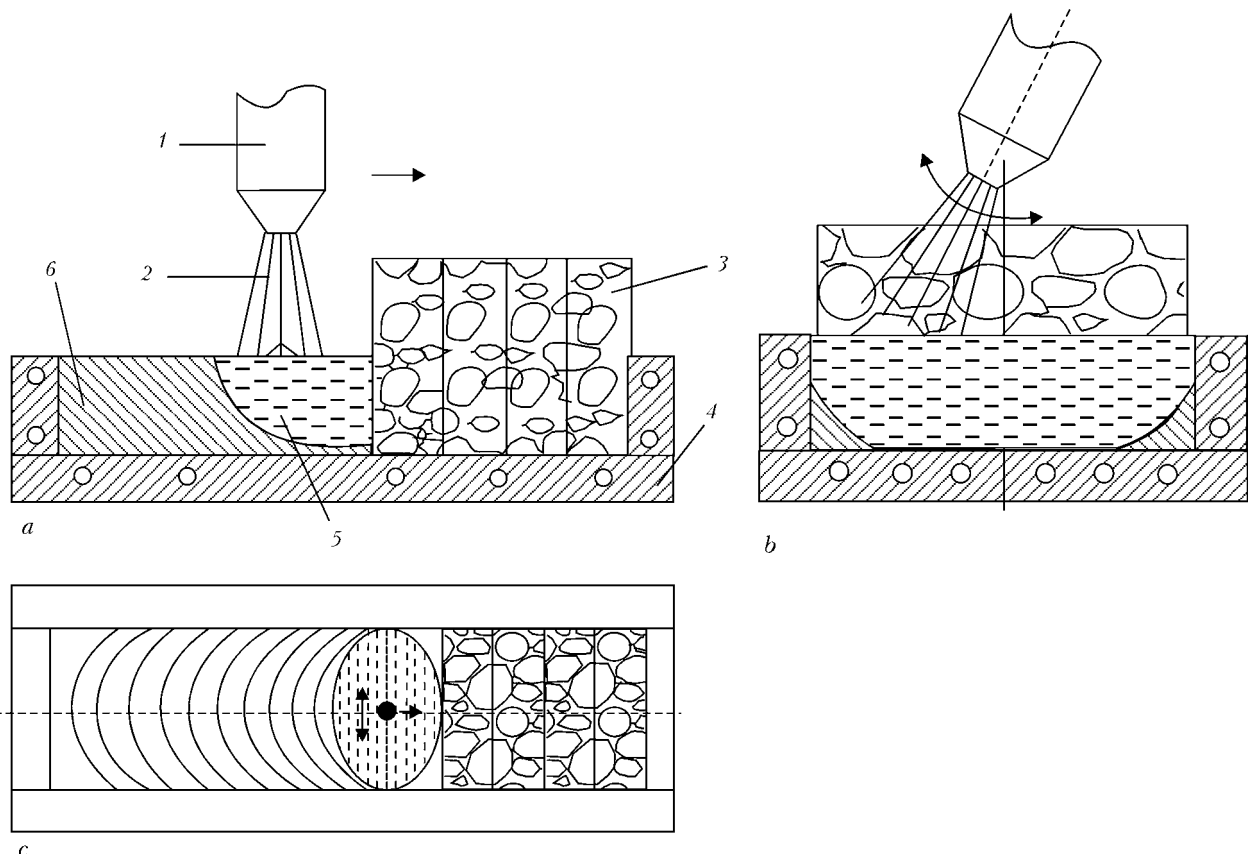


**Figure 2.** Scheme of remelting: *a* — side view; *b* — end view; *c* — top view; 1 — plasmatron; 2 — arc; 3 — charge; 4 — mould; 5 — molten metal pool; 6 — ingot

EWI (Figure 1), additionally equipped with copper water-cooled mould (internal dimensions  $600 \times 300 \times 70$  mm), mounted on a movable bogie. The installation includes a melting chamber, a movable bogie, a group of plasmatrons located above the bogie, and mechanisms for moving the bogie and oscillation of plasmatrons. Power sources of the PD-110 plasmatrons are transformers A-1458 complete with rectifying units A-1557.

Waste of steel St3 and metal titanium, vanadium, niobium, molybdenum or alloys thereof with weight share of the main element not less than 95 %, were used as the charge.

The charge was loaded directly into the flat mould, and iron and alloying elements were uniformly distributed over the mould area. Then the movable bogie with the mould was placed under the plasmatrons, the chamber was vacuumized and filled with argon, and a small excessive pressure was created.

Principle diagram of the process is shown in Figure 2. In the experiments one plasmatron, located in center of the mould, was used. Remelting was started in extreme point of the charge location and due to transverse oscillations of the arc molten metal pool was induced all over the width of the mould. After formation of general pool the bogie with the mould and the ingot was moved at assigned speed.

Level of current in the experiments varied from 900 to 1100 A, frequency of transverse oscillations of the plasmatron — from 0.5 to 2.5 oscillations per minute, speed of the mould movement — from 5 to

15 mm/min, arc length — from 70 to 210 mm, thickness of the charge layer — from 60 to 180 mm. Amplitude of the arc oscillation corresponded to the mould width.

In the process of remelting voltage in the arc and stability of its burning were registered. After termination of remelting, depth of penetration and length of the pool were measured, and quality of produced ingot was studied. Using chemical and spectral analysis of taken samples distribution of alloying elements and harmful impurities over length, width and depth of ingots was measured.

Carried out investigations allowed choosing optimal parameters of melting and technological parameters, which ensure guaranteed penetration all over the ingot at depth 20–50 mm, depending upon chemical composition of ferroalloys and master alloys, whereby, as one had to expect, the higher is melting point of the alloying element, which enters into composition of the ferroalloy, the lower is thickness of an ingot, which ensures its full penetration.

Width of an ingot is determined by dimensions of the mould and, taking into account shrinkage of the metal, varies within 293–296 mm.

It is confirmed that level of the plasmatron current exerts significant influence on the penetration depth, and speed of the mould movement — on length of the molten metal pool. Arc voltage depends upon its length and angle of the plasmatron inclination.

Optimization of parameters of described technology allowed producing homogeneous ingots: variation



**Table 1.** Chemical composition of alloys

Weight share of elements, %													
Ti	V	Nb	Mo	Al	Si	Mn	Cu	Sn	C	P	S	O	N
28–29	0.15	--	0.03	0.095	0.72	0.035	0.10	--	0.10	0.015	0.012	0.17	0.070
34–35	0.11	--	0.025	0.30	0.56	0.15	0.12	--	0.12	0.014	0.017	0.21	0.085
39–40	0.16	--	0.07	2.12	0.81	0.80	0.12	--	0.05	0.015	0.012	0.23	0.100
60–61	0.12	--	0.05	1.47	0.47	0.09	0.18	--	0.11	0.001	0.013	0.18	0.092
64–65	0.19	--	--	3.70	0.94	0.75	0.09	0.012	0.10	0.015	0.010	0.27	0.150
70–72	0.15	--	0.35	1.64	0.75	0.24	0.15	--	0.07	0.013	0.011	0.25	0.110
78–81	--	--	--	--	0.35	0.07	0.10	--	0.05	0.012	0.010	0.11	0.120
--	35–36	--	--	0.80	0.95	0.54	0.15	--	0.12	0.015	0.013	0.14	0.015
--	50–51	--	--	0.95	0.78	0.47	0.082	--	0.09	0.012	0.013	0.17	0.027
--	61–63	--	--	0.17	0.29	0.64	0.09	--	0.11	0.015	0.012	0.21	0.016
--	--	35–36	--	0.07	0.15	0.83	0.17	--	0.12	0.013	0.014	0.13	0.022
--	--	55–56	--	0.09	0.63	0.35	0.085	--	0.14	0.013	0.012	0.18	0.017
--	--	60–62	--	1.15	0.81	0.80	0.11	--	0.085	0.012	0.014	0.20	0.019
--	--	68–70	--	1.75	0.95	0.56	0.16	--	0.07	0.012	0.014	0.25	0.025
--	--	--	55–56	0.95	1.22	0.63	0.13	--	0.10	0.010	0.011	0.12	0.025
--	--	--	60–62	1.34	0.87	--	0.011	--	0.09	0.010	0.011	0.12	0.031
59–52	--	--	--	48–50	0.02	0.03	--	--	0.05	0.010	0.010	0.11	0.025
--	50–52	--	--	48–50	0.015	0.07	--	--	0.07	0.010	0.010	0.07	0.016
--	--	50–52	--	48–50	0.04	0.045	--	--	0.04	0.015	0.010	0.09	0.024

Note. The rest is iron.

of weight share of alloying elements over the ingot length did not exceed 4 %, width --- 1 %, depth --- 0.3 %, which is quite acceptable for ferroalloys and master alloys. Chemical composition of molten ferroalloys and master alloys is given in Table 1.

As it follows from the Table, mentioned method of melting allows producing ferroalloys and master alloys of assigned composition with low content of carbon, oxygen, nitrogen and other harmful impurities, which contributes to high quality of these ma-

terials. In all cases taken samples did not have slag inclusions and had metallic color.

In Figure 3 specimens of 70 % ferrotitanium and 60 % ferromolybdenum, produced by the method of plasma-arc remelting of charge in movable mould, are shown.

Values of specific electric power and argon consumption at optimum mass of remolten metal of different chemical composition of ferroalloys and master alloys are given in Table 2.

**Table 2.** Technological parameters of remelting process

Type of alloy	Weight share of alloying element, %	Mass of metal in one melting, kg	Electric power consumption, kW·h/kg	Consumption of argon, l/kg
FeTi	28–40	60–70	1.0–1.2	70–80
FeTi	60–70	50–55	1.2–1.5	80–90
FeTi	70–80	45–50	1.3–1.6	90–100
FeV	30–40	50–55	1.0–2.3	120–140
FeV	50–60	45–50	2.1–2.5	125–145
FeV	60–70	40–45	2.3–2.7	130–150
FeNb	30–40	45–50	2.2–2.6	120–140
FeNb	50–60	40–45	2.5–2.8	130–150
FeNb	60–70	35–40	2.8–3.1	140–160
FeMo	50–60	30–35	3.3–3.7	150–170
Al–Ti	50–52	45–50	0.8–1.0	70–80
Al–V	50–52	45–50	1.0–1.2	75–85
Al–Nb	50–52	45–50	1.2–1.4	80–90

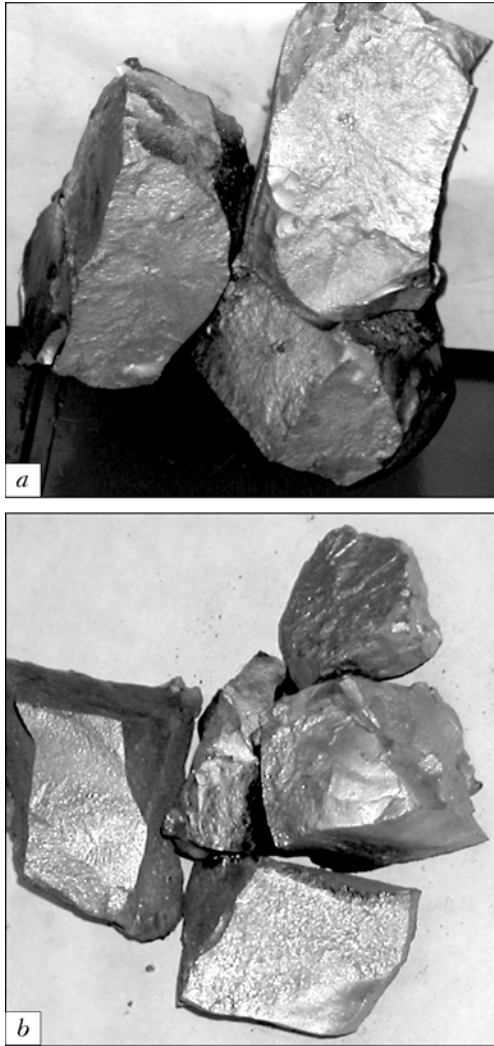


**Figure 3.** Specimens of produced ferroalloys: *a* — ferrotitanium; *b* — ferromolybdenum

As one can see from the Table, the higher is temperature of the main alloying element, the lower is optimum mass of the remolten metal and the higher is specific consumption of electric power and argon.

If increase of titanium content in ferroalloy enables reduction of its density and melting point of the alloy changes insignificantly [8], in melting of fer-

rovanadium, ferroniobium and ferromolybdenum sharp increase of temperature of alloys is observed as content of the main alloying element increases, which causes reduction of the pool dimensions and need to reduce optimum mass of the metal being remolten. For improving energy and economic indices it is necessary to increase dimensions of the mould and develop multi-plasmatron scheme of remelting, whereby dimensions of technogenic waste lumps may be commensurable with dimensions of the mould, which does not require for special preparation of the charge.

This method of remelting of bulky charge may be recommended for development of a commercial melting complex of up to 1 t capacity with acceptable energy and economic parameters of the process and high quality of produced ferroalloys and master alloys.

## CONCLUSIONS

1. It is established that plasma-arc remelting of charge in a movable mould allows producing high-quality ferroalloys and master alloys with low content of slag inclusions, carbon, oxygen, nitrogen, and other harmful impurities.

2. Values of specific consumption of electric power and argon at optimum mass of ferroalloys and master alloys of different chemical composition are determined.

1. Gasik, L.N., Ignatiev, V.S., Gasik, N.I. (1975) *Structure and quality of commercial ferroalloys and master alloys*. Kiev: Tekhnika.
2. Rozhkov, D.E. (2004) Tendencies of development of production and consumption of ferrotitanium in Russia and abroad. In: *Proc. of Int. Conf. on Ti-2004 in CIS* (St.-Petersburg, 25–26 May, 2004). St.-Petersburg.
3. Lakomsky, V.I. (1974) *Plasma-arc remelting*. Ed. by B.E. Paton. Kiev: Tekhnika.
4. Edneral, F.P. (1963) *Electrometallurgy of steel and ferroalloys*. Moscow.
5. Durrer, F., Folkert, G. (1976) *Metallurgy of ferroalloys*. Moscow: Metallurgiya.
6. Meskin, V.S. (1964) *Principles of steel alloying*. Moscow.
7. Vinograd, M.I. (1963) *Inclusions in steel and its properties*. Moscow.
8. Shank, F.A. (1973) *Structures of binary alloys*. Moscow: Metallurgiya.



# GEOMETRIC SHAPE AND EROSION RESISTANCE OF COPPER WATER-COOLED ANODE OF ARC HEAT SOURCE

V.A. SHAPOVALOV, O.M. VISLOBOKOV, G.A. MELNIK and K.A. TSYKULENKO  
E.O. Paton Electric Welding Institute, NASU, Kiev, Ukraine

Experimental investigations of three copper water-cooled anodes with different geometric shapes of tips under similar conditions of their operation in argon were carried out. Optimum shape of the tip for the purpose of minimizing erosion of electrode was experimentally determined.

*Keywords:* arc heat source, copper water-cooled anode, erosion of electrode, service life of plasmatron

Experience of operation of arc heat sources in electrometallurgy shows that their service life is mainly determined by erosion rate of electrodes. Erosion depends upon material of electrodes, their geometric dimensions and mutual position, gas composition of working environment, and values of arc current. Experimental investigations of erosion rate of copper water-cooled anode in argon at various values of arc current were carried out [1].

Purpose of this work consists in investigation of influence of geometric shape of the copper anode tip on erosion, all other conditions of operation being the same.

Specific erosion of copper anode depends upon accuracy of maintaining operation conditions, which ensure diffusion character of the arc tying to anode. Transition of diffusion conditions to constricted ones enables significant local heating-up, melting, evaporation and outburst of the anode material into the environment. Even provided issue of arc discharge stabilization and compression is solved, it is required for stable diffusion conditions of operation of water-cooled anode that such parameters as current, arc length and diameter of anode be in a certain optimal area of their interrelations. Let us consider physical processes, which proceed between electrodes, for estimation of influence of frontal diameter of anode on conditions of arc discharge.

In Figure 1 scheme of movement of electric charge carriers in discharge chamber according to based on many physical experiments model of Kimblin is shown [2].

Hot cathode emits high number of electrons into the environment. After leaving the cathode a portion of electrodes collides at once with the nearest molecules (atoms) of gas with formation of positive ions and secondary electrons.

Light electrons (primary and secondary ones) rush under action of electric field to the anode. The nearest to the cathode layer of space is filled with inertial

ions, forming around the cathode positive spatial potential barrier. Ions and ionized couples of the cathode metal, which do not enter into this barrier layer, effuse in isotropic way into the environment.

Number of positive ions in the layer near anode, immediately adjacent to its frontal diametric surface, reduces, because anode is a collector of electrons, which are always in abundance near this plane, and insignificant portion of ions is easily recombined by electron bombardment.

So, part of space adjacent to frontal diametric plane of anode is charged negatively, i.e. the anode potential barrier occurs. The smaller is frontal diameter of the anode, the lower share of positive ions gets on this plane, while greater part of electrons rushes

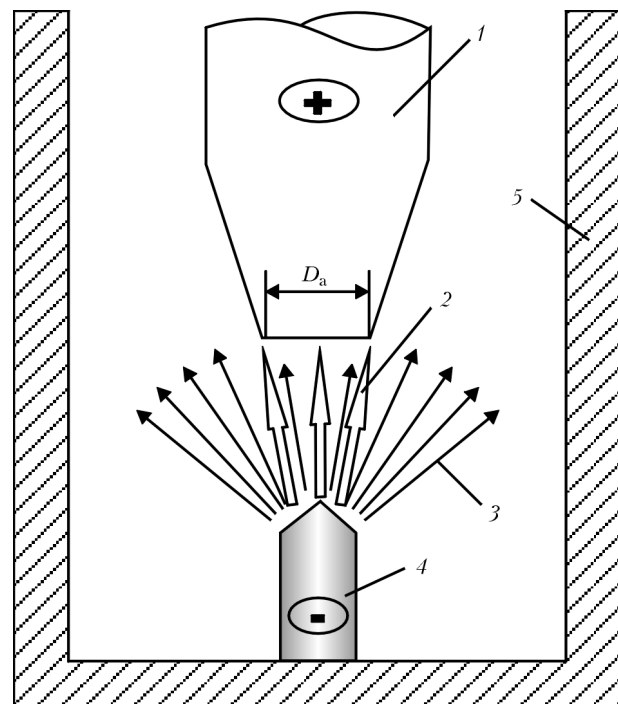


**Figure 1.** Scheme of movement of charge carriers in plasmatron discharge chamber: 1 — anode; 2, 3 — direction of movement of ions and electrons, respectively; 4 — cathode; 5 — chamber;  $D_a$  — frontal diameter of anode

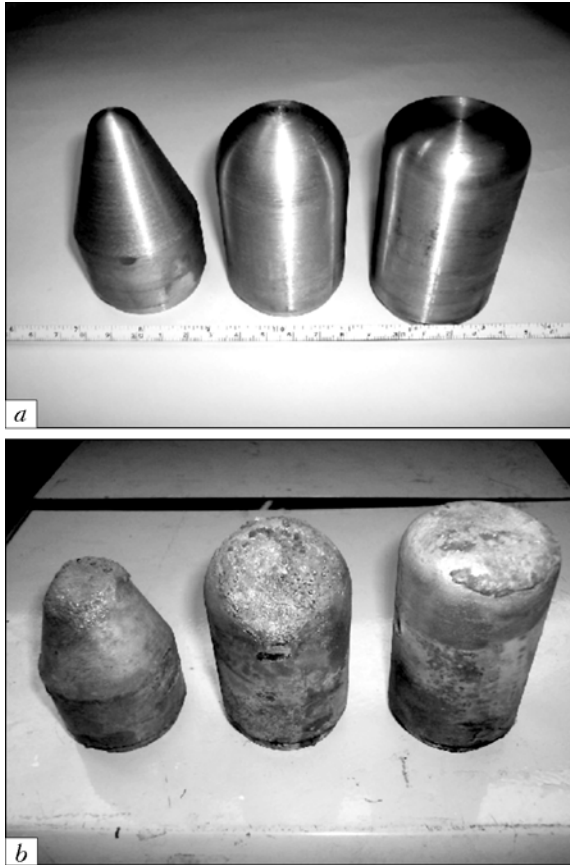


**Figure 2.** Anode tips before (a) and after (b) tests

exactly to it. So, as frontal diameter of the anode reduces, the anode fall of voltage increases, which, in its turn, causes occurrence of the conditions for constricted discharge.

For determining optimum shape of the copper anode tip three specimens of conic, semi-spherical, and cylindrical shape were sequentially subjected to comparative tests (Figure 2, a) on the same installation in commercial argon at arc current 400 A for 75 h.

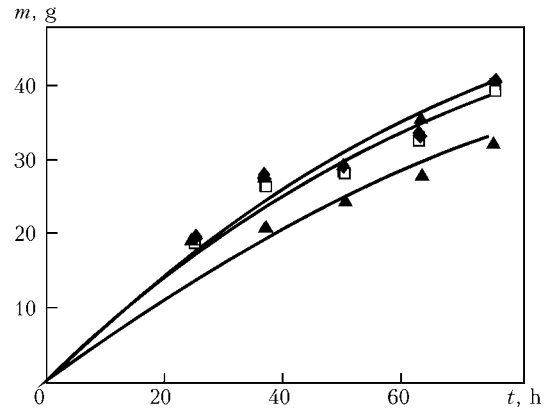


**Figure 3.** Erosion  $m$  of copper anode depending upon its shape and duration of tests  $t$ :  $\blacklozenge$  — conic shape;  $\blacksquare$  — semi-sphere;  $\blacktriangle$  — cylinder

Used methods of tests, technology and equipment are described in [1]. Appearance of the anode tip specimens after the tests is shown in Figure 2, b. Obtained diagrams of erosion dependence upon duration of the tests prove that erosion of conic and semi-spherical anodes is practically the same (Figure 3).

Erosion of anode of cylindrical shape is notably lower than in other specimens, because frontal diameter of this electrode is bigger than reduced frontal diameters of conic and semi-spherical electrodes. Specific erosion of cone-like and semi-spherical anodes constituted  $3.7 \cdot 10^{-7}$ , while of cylindrical anode —  $2.9 \cdot 10^{-7}$  g/K.

So, when developing arc heat sources for the purpose of increasing their service life, one has to use copper water-cooled anodes with tips of cylindrical shape.

1. Shapovalov, V.A., Melnik, G.A., Vislobokov, O.M. et al. (2006) Experimental investigation of erosion of copper water-cooled anodes. *Advances in Electrometallurgy*, 1, 14–16.
2. Kimblin, S.U. (1977) Erosion of electrodes and ionization processes in near-electrode zones of vacuum arcs at atmospheric pressure. In: *Experimental investigations of plasmatrons*. Novosibirsk: Nauka.



# SHORT-TERM STRENGTH AND MICROSTRUCTURE OF BRAZED JOINTS OF ALLOY VJL12U PRODUCED USING BORON-CONTAINING BRAZING ALLOY WITH ADDITION OF SILICON

I.S. MALASHENKO, V.V. KURENKOVA, A.F. BELYAVIN and V.V. TROKHIMCHENKO  
RC «Pratt and Whitney–Paton», Kiev, Ukraine

Interrelation of a seam metal microstructure and physical-mechanical properties of brazed joints of alloy VJL12U, produced with application of complex boron-containing brazing alloys, into which 15–25 % of commercial brazing alloy NS12 (Ni–12 wt.% Si) were additionally introduced in the form of additive material, is considered. Presence in the complex brazing alloy of 2.5–3.0 % Si enables reduction of heterogeneity of a brazed seam metal and changes morphology and size of precipitated carboboride phase. Strength of such brazed joints at temperature 20 °C achieves 80–95 % of strength of the base alloy, and their relative elongation equals 5–7 %.

*Keywords:* alloy VJL12U, high-temperature brazing in vacuum, boron-containing brazing alloy, silicon-containing brazing alloy NS12, filler Rene-142, heat treatment, strength, elongation, structure of seam metal

High level of strength is one of the most important requirements, established for brazed joints (BJ) of nickel high-temperature alloys (HTA). At the same time they should have satisfactory low-temperature ductility. Application of composite boron-containing brazing alloys on the basis of system Ni–Co–Cr–Al–2.5 % B (#1) together with fillers from powders of alloys Rene-142 and JS6U allowed producing BJ of alloy VJL12U, strength properties of which are rather stable. In [1] data on strength of BJ, produced from the metal of nozzle doors of aviation gas turbine engines (GTE) (alloy VJL12U) after 500 h operation of the item are given.

Failure of BJ in tensile tests of specimens occurred, as a rule, in the brazed seam metal. The main reason of brittle failure of the specimens, i.e. non-realized strength of the seam metal, became concomitant with brazing liquation and shrinkage microporosity, which could not be removed by subsequent reduction heat treatment in vacuum.

In [1, 2] composite brazing alloys are considered, in which only boron is used as a depressant. In Ni–Cr–B–C low-alloy systems of brazing alloys at different values of temperature and duration of isothermal seasoning in the process of solidification in matrix solution of seams centrally axial eutectics form, which represent, mainly, nickel (Ni<sub>3</sub>B) and chromium (CrB) borides. Composition of eutectics depends upon temperature of brazing and duration of seasoning. At brazing temperature 1100 °C the residual liquid phase is solidified in the process of cooling into nickel-base matrix solution. At a lower temperature proceed binary and triple eutectic reactions with formation of brittle boride phases.

Boron, which reduces melting point of nickel-base austenite matrix, at short seasoning, i.e. its insufficient diffusion through area of the seam to the base, is the reason of formation of liquid phase over axis of a seam. As temperature of brazing and duration of seasoning increase, number of eutectic precipitates reduces. It is expressed in diffusion migration on solid-liquid phase boundary in the process of isothermal seasoning of a brazed joint [3, 4].

Because of low solubility of boron in nickel (0.1 at.% or 0.02 wt.% at 1000 °C), in boron-containing brazing alloys form in solidification, first of all, borides, which increase brittleness of the seam metal and adjacent zone of mutual diffusion. That's why it is difficult to achieve satisfactory ductility of brazed joints, produced with application of brazing alloys, which contain only boron as a depressant. Brazing alloys with boron are characterized by inter-grain penetration of the latter into the base in the course of brazing.

For optimization of properties of brazed joints amount of boron in the brazing alloy material should completely ensure saturation of the alloy boundaries of a component being renovated, whereby formation of boride phases directly in the brazed seam metal should not be allowed.

Improvement of wettability by the melt of surfaces being brazed and contact interaction between powder particles of the brazing alloy and the base metal are achieved by introduction into the brazing alloy of second depressant — silicon. In brazing of nickel HTA with application of standard commercial VPr-24, VPr-11, NS12 and new complex brazing alloys certain peculiarities, inherent to silicon-containing brazing alloys, were noted: less reactionary behavior of mentioned brazing alloys in relation to the base metal (low chemical erosion of the base), good filling of the gap and penetration all over the depth of a cap-



illary, limited porosity, absence of shrinkage defects in the seam, etc. All this proves positive influence of silicon as a depressant in nickel-base brazing alloys [5].

After introduction of silicon into the brazing alloy melting point of a composite system reduces. Silicon, which actively dissolves in nickel matrix (up to 15 at.% or 7.5 wt.% at 1000 °C), effects reduction of melting point of alloys and at the same time improves fluidity of a melt. Contact angle of wetting at brazing temperature 1225 °C achieves, approximately, 1° for compositions Ni-12 % Si, and for Ni-4 % B --- 3° [5].

In composite brazing alloys, into composition of which enters chromium, silicon increases resistance to corrosion and oxidation. In [6] influence of variable content (0.05 and 1.00 wt.%) of silicon on high-temperature strength and mechanical properties of alloys MAR-M200 and 713C is investigated. It is established that silicon increases resistance to oxidation, whereby values of long-term strength and ductility of alloys reduce. Silicon reduces temperature of dissolution of carbides in the matrix solution. Its action does not depend upon chemical composition of the matrix and mainly consists in reduction of temperature of liquidus and solidus of the base alloy.

After introduction into a boron-containing brazing alloy of insignificant amount of silicon in the process of solidification in the matrix solution form both binary and triple eutectics. Binary eutectics represent  $\gamma$ -Ni/Ni boride;  $\gamma$ -Ni/Ni silicide;  $\gamma$ -Ni/Cr boride; triple ---  $\gamma$ -Ni/Ni boride/Cr boride and  $\gamma$ -Ni/Ni boride/Ni silicide. When dissolving in a melt as depressants, silicon and boron influence on each other (mutually exclude each other), and this has to be taken into account when selecting a system of brazing alloys. When in addition to boron, silicon is present in the brazing mixture, triple eutectic  $\gamma$ -Ni/Ni boride/Cr boride does not form, but eutectic with nickel silicide ---  $\gamma$ -Ni/Ni boride/Ni silicide forms [7]. Formation of chromium borides in the matrix is blocked. Enrichment of the matrix by residual chromium (because of suppression of formation of chromium borides) increases high-temperature strength of the solid solution, and due to high solubility of silicon in nickel (up, approximately, to 8 wt.%) fluidity of a brazing alloy melt increases.

At brazing temperature 1100-1200 °C diffusion of boron and silicon from a brazing alloy into the base is the main control factor. Silicon and chromium are usually distributed in center of a brazed seam in the form of brittle eutectic phases, and boron is uniformly distributed in the metal of a joint seam, because it penetrates easily through a brazing alloy into the base [8].

Weight share of alloying elements in the brazing alloy filler determines type of the seam metal structure. For low-alloy systems dendritic structure on the basis of  $\gamma$ -solid solution and carboboride eutectics is characteristic. At increased content of chromium, carbon and boron, dendritic-vesicular structure mani-

fest itself only near the fusion line; presence of excessive carbides, eutectics on their basis, and carboboride  $Me_{23}(C, B)_6$  surrounded by  $\gamma$ -eutectic, is characteristic of it. As number of alloying elements increases, the structure transits from hypo- to the hypereutectic one, the sign of which is presence of excessive carbides [8].

In addition to selection of composition of a brazing alloy and conditions of the brazing performance, the very process of heat treatment of produced joints is important. According to [5, 6] brazing alloy of the system Ni-19 % Cr-10.2 % Si is promising due to possibility of plastic straining of brazed joints after homogenization. Brittle silicide phases in the gap disappear because of high solubility of silicon in solid solution in vacuum annealing. When the gap is small diffusion causes change of composition of the brazed seam metal mainly with formation of a solid solution.

It is impossible to increase ductility of brazed joints by heat treatment when using only boron-containing brazing alloys because of low solubility of boron in nickel. When brazing alloys of the system Ni-Cr-B are used, the metal being brazed intensively dissolves in the brazing alloy melt, and boron diffuses over grain boundaries into depth of the metal. Heat treatment intensifies penetration of brazing alloy into the base and enables concentration of brittle phases over grain boundaries over the base/melt fusion line. Width of a gap is an important characteristic in this case. Big width of filled by a brazing alloy gap assumes presence of significant amount of boron-containing material, which participates in processes of interaction of the base and the brazing alloy and formation of brittle boride phases.

The main goal of heat treatment of the components being renovated is homogenization, which ensures leveling of the metal of brazed seams and the base.

**Materials and methodology of experiments.** Material of the investigation were plates of alloy VJL12U, cut out from nozzle door of aviation GTE after 500 h of the turbine operation. Billets for brazing were ground and annealed at 1200 °C during 1 h and refined on abrasive paper.

For preparation of the brazing mixture powders of boron-containing brazing alloy Ni-Co-Cr-Al-2.5 % B (#1), commercial brazing alloy NS12, and 60 % of filler from powder of alloy Rene-142 were used. Ready mixtures were mixed up on an imported binder (of acrylate resin type) and applied on ends of billets to be brazed, which were installed into a technological device that allowed fixing position of the plates with applied brazing alloy. Natural gap that occurred in the joints was determined by granulometric composition of the initial powder mixture. Maximum size of powder particles of the brazing alloy did not exceed 120  $\mu$ m.

Plates with applied brazing alloy were dried in thermostat at temperature 120 °C within 24 h. Assembled billets were placed into the vacuum furnace on ceramic supports in such way that line of the seam

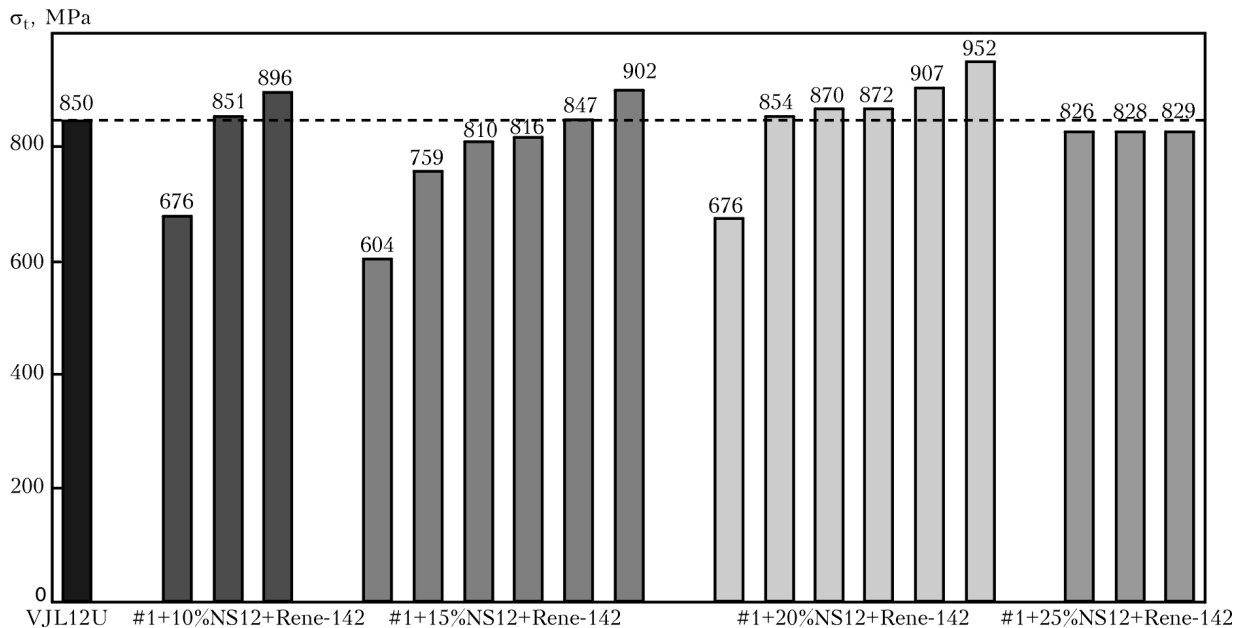


**Figure 1.** Level of short-term strength at 20 °C of brazed joints of alloy VJL12U, produced with application of complex brazing alloys consisting of #1 + Rene-142 and NS12; dash line designates tensile strength of base metal VJL12U 850 MPa regulated by specifications

not to get in contact with the support surface (in order to avoid leakage of the brazing alloy between the metal and the ceramics).

The VJL12U billets being brazed were heated stepwise [2]. Isothermal brazing was performed in vacuum of  $1.3 \cdot 10^{-2}$  Pa at temperatures 1210 (20 min) and 1220 °C (10 min). After brazing the billets were cooled down to room temperature and annealed according to two-stage mode --- 1160 °C (2 h) + 1050 °C (2 h). Cooling with the furnace after annealing was performed at the rate 15--17 °C/min within the range  $T_{br}$ –850 °C.

Specimens for tests at 20 °C, having dimensions of the working part  $(1.6-1.7) \times 3 \times 10$  mm, were cut out from the billets by electro-erosion method [1]. Length of the working part of specimens for high-temperature tests was 35 mm. Roughness  $R_a$  of surface of the specimens did not exceed 0.3 μm.

According to averaged literature data 850 MPa were used as the base value of the alloy VJL12U strength [9--11]. According to our estimation, after heat treatment, similar to two-stage heat treatment of BJ, strength of the VJL12U plates was 915--938 MPa.

**Experimental results.** First influence of the amount of brazing alloy NS12, introduced into the mixture for brazing, on mechanical properties of joints was investigated. Its weight share varied from 10 to 25 %. In Figure 1 results of tensile tests of the specimens, produced with application of brazing alloys, compositions of which are given in captions, are shown. Strength of BJ, containing Si + B in brazing alloys, achieved 850–900 MPa. Steadily high results in tests were achieved on the specimens, brazed at temperature 1220 °C within 10 min. Increase of brazing temperature from 1210 °C just by 10 degrees made it possible to get more dense structure of metal of brazed seams.

Strength values of BJ, produced with application of brazing alloys of different chemical composition, were, approximately, at the same level. Repeatability of the results was registered both within framework of one and several experiences, which is one of the main important results.

Trend of ductility (relative elongation) preservation is most pronounced in complex brazing alloy with 20 wt. % of NS12. That's why composition of the brazing alloy 20 % #1 + 20 % NS12 + 60 % Rene-142 is considered the most efficient (from the viewpoint of combination of strength and ductility of BJ) for repairing items from alloy VJL12U (Figure 2).

Data on statistical processing of tensile test results of BJ at temperature 20 °C, produced with application of boron-containing brazing alloys without silicon and with silicon, are presented in Figure 3. Noticeable difference not just in level, but also in stability of strength values was registered. More than 60 % of tested specimens, brazed by a complex brazing alloy containing silicon, had ultimate strength corresponding to that of the base metal.

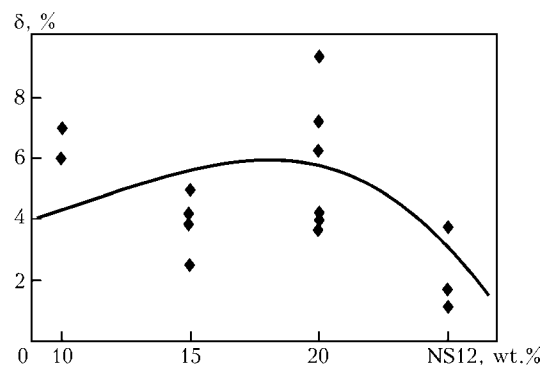


**Figure 2.** Relative elongation of brazed joints of alloy VJL12U formed at temperature values 1210–1220 °C (20–10 min) depending upon content of powder NS12 in composite brazing alloy #1 + 60 % Rene-142

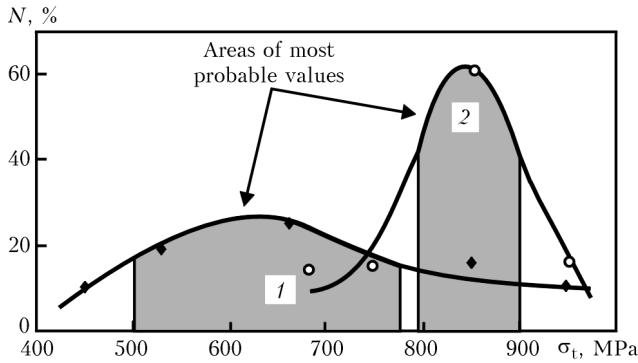


**Figure 3.** Statistical curve of strength distribution of brazed joints of alloy VJL12U produced with application of boron-containing brazing alloys: 1 — without silicon (◆); 2 — with addition of silicon (○); N — number of specimens

Curve  $N = f(\sigma)$ , which characterizes repeatability of strength property values of brazed joints, produced by complex brazing alloy, containing both silicon and boron, was located more to the right and significantly higher of the curve  $N = f(\sigma)$ , which describes properties of BJ, produced with application of standard brazing alloy #1 + 60 % Rene-142. This is confirmed by interconnection between relative elongation and level of deformation strengthening of the VJL12U BJ (Figure 4). As content of silicon-containing brazing alloy in BJ got higher, relative elongation of the specimens increased.

While relative elongation of BJ, produced with application of binary systems of boron-containing brazing alloys, constituted 1.0–2.3 %, introduction of 15–20 wt.% of brazing alloy NS12 into the brazing composition allowed achieving elongation of specimens equal to 4–7 % (Figure 4).

High strength of the seam metal and the fusion line ensured for BJ necessary reserve of ductility due to deformation of the base metal. Failure of the specimens occurred mainly in the brazed seam metal, but not in the line of fusion of a seam with the base metal.

Comparatively small amount of powder NS12, introduced into standard brazing alloy 40 % #1 + 60 %

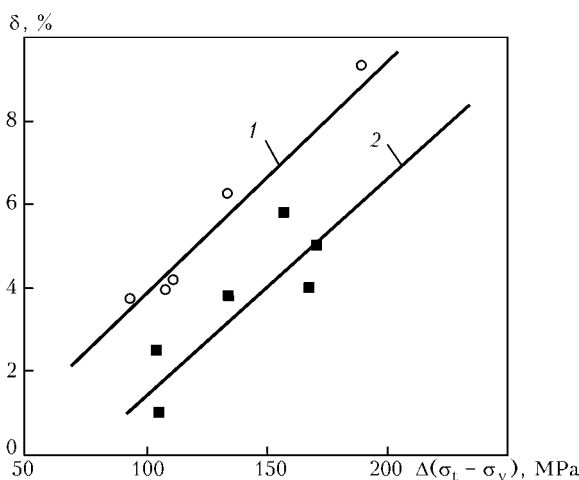


**Figure 4.** Interrelation between relative elongation and level of strain hardening of brazed joints of alloy VJL12U produced with application of complex brazing alloys on basis of #1 + Rene-142: 1 — 20 % NS12; 2 — 15 % NS12

Rene-142, ensured for brazed joints of alloy VJL12U high reliability in regard to the work necessary for their failure (it was estimated by character of the curve of deformation strengthening during tensioning of a brazed specimen).

The most stable fracture toughness had BJ, produced with the additive in the form of 15–20 wt.% of NS12 in the complex brazing alloy, whereby higher technological ductility was achieved after isothermal brazing at 1210 °C.

Complex brazing alloy, containing both boron and silicon, is characterized by ability to efficiently wet contacting surfaces and powder particles of the brazing alloy. It ensures optimal phase composition and morphology of strengthening phases, uniformly distributed in the seam metal. Silicon increases fluxing capacity of the brazing alloy melt [6], due to which improves wettability of surface of the plates being brazed and fluidity of the brazing alloy that fills the gap, density of solidified melt increases, and casting microporosity is removed.

High-temperature tensile tests of BJ of alloy VJL12U of  $3.0 \times 2.5$  mm section with length of the working part equal to 35 mm were carried out in air at temperature 900 °C on state-of-the-art installation MTS-810, equipped with electron system of reading data, obtained from the specimen being investigated, and recording of the deformation curve in coordinates  $\sigma$  (MPa)– $\varepsilon$  (%). Test results are given in Figure 5. Minimum level of Q-factor of joints at 900 °C was 72 %, maximum level was 87 %.

Significant difference in strength values of BJ, depending upon amount of introduced into the complex brazing alloy powder NS12, was not noted. Relative elongation at temperature 900 °C did not exceed 2 %; failure always occurred in the seam metal.

**Metallographic investigations.** Analysis of short-term strength of BJ was performed, depending upon

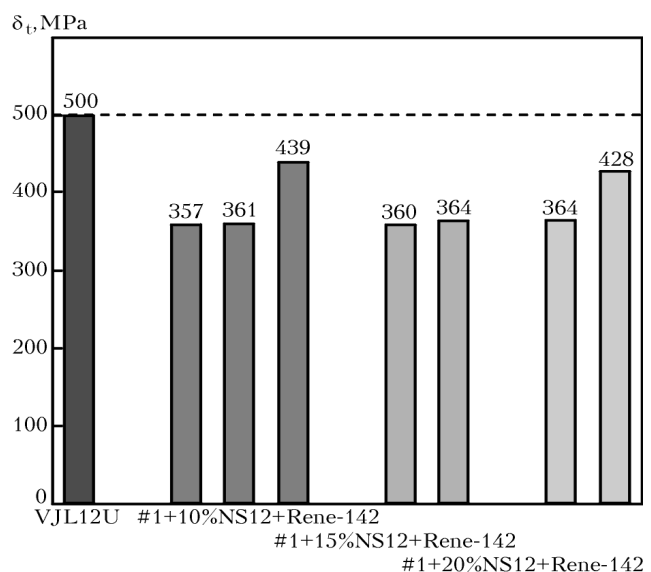


**Figure 5.** Strength of brazed joints of alloy VJL12U, produced with application of complex brazing alloys #1 + 60 % Rene-142 containing NS12, at 900 °C; dash line designates  $\sigma_t = 500$  MPa of base metal VJL12U after annealing at 1160 °C, 2 h + 1050 °C, 2

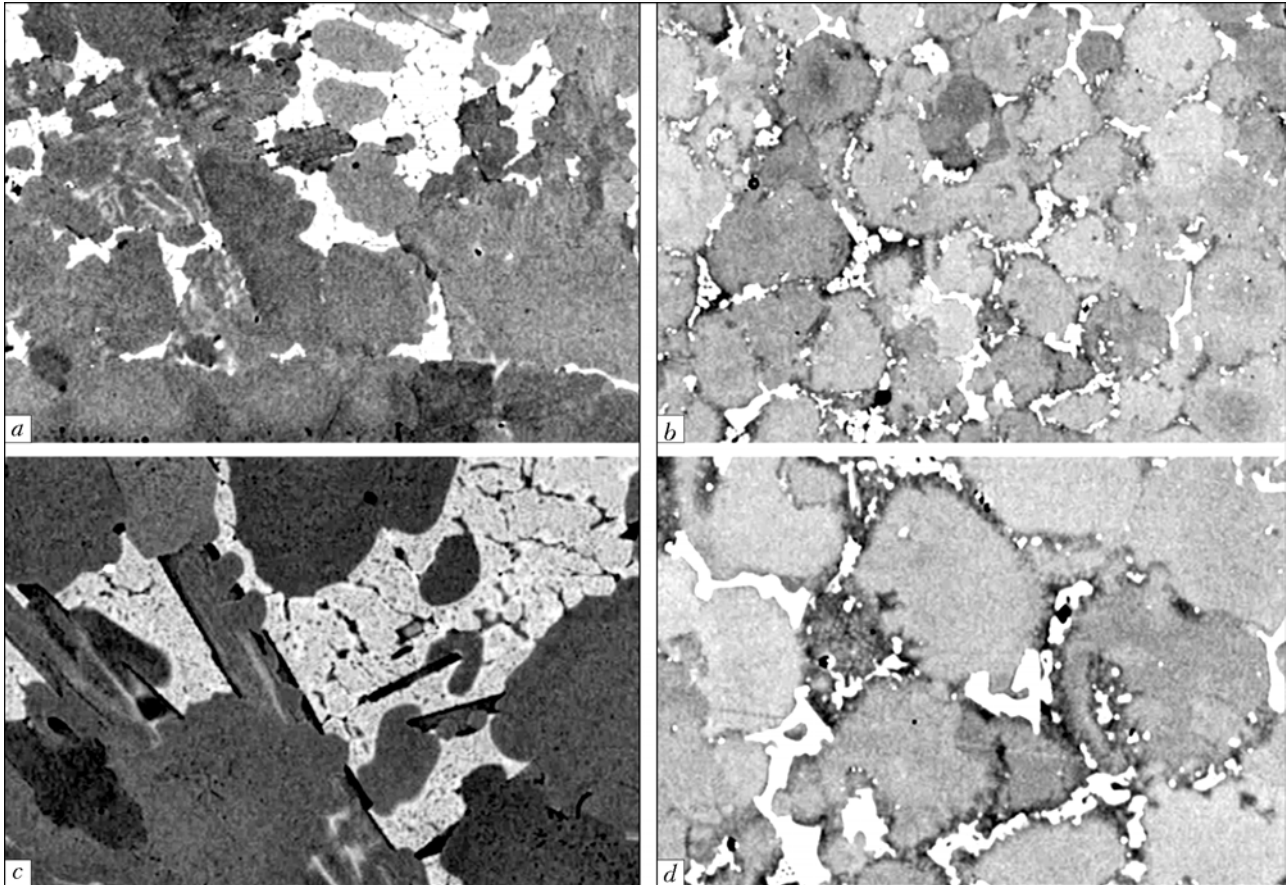


**Figure 6.** Microstructure of seams metal produced in process of solidification after isothermal brazing at 1210 °C for 20 min with application of composite brazing alloys: *a, c* — #1 + 60 % Rene-142; *b, d* — #1 + 20 % NS12 + 60 % Rene-142; *a, b* —  $\times 200$ ; *c, d* —  $\times 500$

microstructure of the seam metal. Rather large precipitates of carbide phases were detected, which enabled brittle failure in loading because of their high microhardness. Carbide phases occurred during solidification of a seam metal in the process of BJ cooling.

For substantiation of selection of the complex brazing alloy #1 + Rene-142 with addition of powder NS12 the following experiment was carried out. On nickel-chromium substrate different types of brazing alloys were applied, and isothermal brazing in vacuum at 1210 °C within 20 min was performed.

After solidification of basic brazing alloy #1 + Rene-142 coarse chromium carboborides  $\text{Cr}_{21}(\text{W}, \text{Mo}, \text{Re})_2(\text{C}, \text{B})_6$  (wt.%: 55–60 Cr, 9–10 W, 3–3.5 Mo, 7–8 Re) of eutectic type and developed boundary eutectics ( $\gamma$ - $\gamma'$ ), having in their composition mainly nickel, hafnium, and tantalum, i.e. elements, which stabilize  $\gamma$ -phase (Figure 6, *a, c*; 7, *a*; Table 1), were detected in the matrix solution. Dendritic structure in the seam metal was not registered in contrast to the brazing alloy, which additionally contained NS12.

A specimen of BJ, in which complex brazing alloy #1 + 20 % NS12 + 60 % Rene-142 was used, was produced in the same experiment without application of NS12.

After solidification metal of complex brazing alloy had dendritic equiaxial structure with size of a cell, approximately, 30–50  $\mu\text{m}$  (Figure 6, *b, d*). In the seam metal structure coarse carbide eutectic phases were absent; precipitates of secondary phases repre-

sented boundary carbides and discretely distributed particles of  $\gamma$ -eutectic phase. Carbide phases corresponded to compounds of  $\text{Me}_3\text{C}$  type, which are actually a form of cubic carbides  $\text{Me}_6\text{C}$  in the alloys, containing sufficient content of chromium, tungsten, molybdenum and rhenium (Figure 7; Table 1).

As a result of introduction into the base brazing alloy of powder NS12, about 17 wt.% Ni were brought into the seam metal in addition to silicon. So, degree of the seam alloying reduced, and in structure of the solidified brazing alloy  $\gamma$ -solution and carbide phases of cementite type mainly formed, whereby clear dendritic-vesicular structure occurred, characteristic of hypoeutectic nickel alloys [12].

When composite brazing alloy #1 + Rene-142 was used, it was impossible to completely prevent brittle failure of BJ after final two-stage heat treatment because of presence in the seam metal of coarse carbide (carboboride) phases  $\text{Me}_{23}(\text{C}, \text{B})_6$ . These phases, characterized by microhardness 12000–15000 MPa, remained rather stable at temperature of homogenization and were loci of trans-crystalline failure in loading. In the seam metal residual primary complex carbides of dash type  $\text{MeC}$ , containing chromium, nickel, molybdenum, tungsten, titanium and tantalum, preserved. Mentioned carbides are less stable because of their non-equilibrium.

Dash carbides are characterized by significant energy of interface, that's why their branches split up

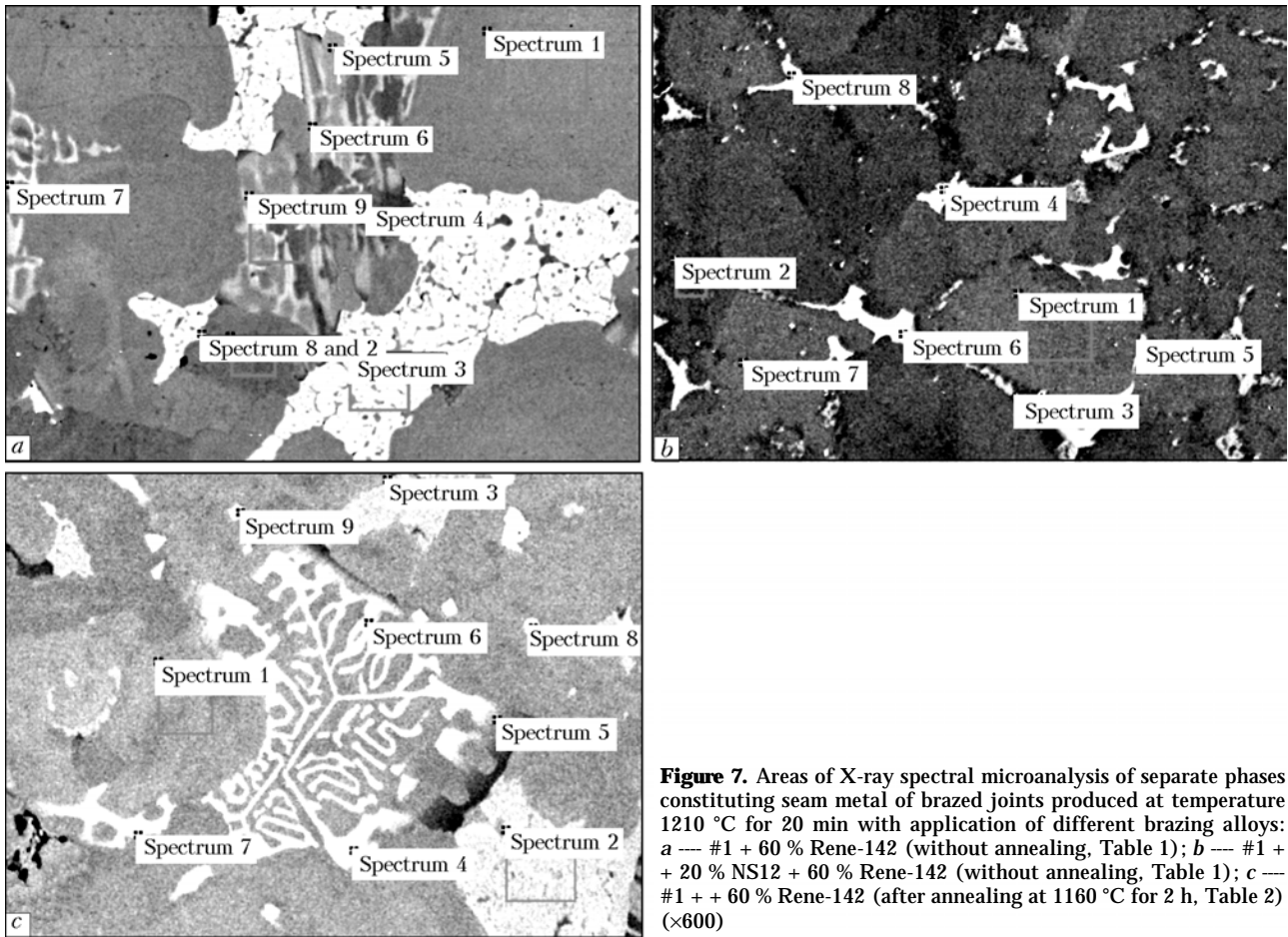


**Figure 7.** Areas of X-ray spectral microanalysis of separate phases constituting seam metal of brazed joints produced at temperature 1210 °C for 20 min with application of different brazing alloys: *a* — #1 + 60 % Rene-142 (without annealing, Table 1); *b* — #1 + 20 % NS12 + 60 % Rene-142 (without annealing, Table 1); *c* — #1 + 60 % Rene-142 (after annealing at 1160 °C for 2 h, Table 2) (×600)

**Table 1.** Chemical composition of different phases in seam metal of brazed joints produced with application of two kinds of brazing alloys in process of isothermal brazing at  $T = 1210\text{ °C}$  for 20 min (without subsequent annealing)

System of brazing alloy	Spectrum of analysis	Weight share of components, %											
		C	Al	Si	Cr	Fe	Co	Ni	Mo	Hf	Ta	W	Re
#1 + 60 % Rene-142	1	--	5.33	--	11.30	5.98	9.87	64.73	0.67	--	--	2.13	--
	2	2.02	4.93	--	10.84	8.14	9.05	62.96	0.31	--	--	1.75	--
	3	--	2.36	--	7.45	6.77	11.20	63.91	0.49	2.22	5.60	--	--
	4	--	4.65	--	8.85	7.96	9.68	65.85	--	--	1.07	1.93	--
	5	4.05	4.29	--	7.77	7.54	9.04	63.58	0.34	--	1.76	1.62	--
	6	3.61	--	--	55.10	4.40	5.57	10.98	3.37	--	--	9.90	7.08
	7	3.37	--	--	60.53	3.87	4.93	6.56	3.26	--	--	9.57	7.92
	8	3.17	1.92	--	6.26	5.49	11.04	60.72	0.41	3.54	6.62	0.83	--
	9	--	3.38	--	23.09	7.16	8.17	50.65	0.99	--	--	4.26	2.30
#1 + 20 % NS12 + + 60 % Rene-142	1	2.68	4.62	1.90	6.82	0.43	8.90	64.26	1.05	--	2.54	3.47	3.32
	2	2.15	4.46	2.19	6.90	0.55	9.14	66.07	0.76	1.52	2.06	3.34	2.39
	3	3.65	2.49	3.77	6.01	0.64	9.90	66.99	--	--	3.39	1.63	--
	4	4.45	--	--	36.62	--	3.50	5.48	7.74	--	--	16.42	25.79
	5	3.39	0.81	--	5.36	--	11.47	68.95	--	--	10.01	--	--
	6	9.47	--	--	31.01	--	4.77	8.25	11.37	--	4.48	16.89	13.77
	7	2.50	4.49	1.65	6.79	0.56	9.25	65.39	0.63	--	2.66	4.17	1.90
	8	5.03	--	--	30.34	--	2.71	6.57	8.20	--	0.44	22.41	24.30



**Table 2.** Chemical composition of metal of main phases of solidified metal of seam produced with application of brazing alloy 40 % #2 + 60 % Rene-12 after annealing at 1160 °C for 2 h

Spectrum of analysis	Weight share of components, %												
	C	Al	Ti	Cr	Fe	Co	Ni	Nb	Mo	Hf	Ta	W	Re
1	1.62	6.23	4.35	6.93	0.68	11.30	66.26	0.51	1.00	–	1.13	–	–
2	2.14	0.84	5.31	8.32	0.65	19.99	53.77	2.05	0.81	3.83	1.70	0.59	–
3	2.60	0.88	5.29	8.10	0.95	20.45	54.67	1.96	0.61	3.12	1.35	–	–
4	7.86	–	2.63	36.00	0.46	5.26	6.65	1.37	26.72	–	0.98	8.59	3.48
5	5.48	–	2.16	50.10	0.42	7.10	7.24	0.78	18.47	–	0.65	4.47	3.13
6	5.19	0.38	2.71	29.07	0.26	5.94	15.78	0.47	24.95	–	1.36	9.47	4.43
7	6.40	0.29	2.44	30.61	0.42	4.72	7.83	1.38	28.81	1.24	0.34	11.45	4.07
8	18.96	–	24.78	1.06	–	0.49	3.01	10.56	7.28	–	25.17	8.69	–
9	17.68	0.39	25.11	0.86	0.16	0.55	3.14	11.17	6.44	–	25.56	8.94	–

in high-temperature heat treatment and form carbides of another morphology. The instant of beginning of disintegration of a complex carbide of eutectic type is shown in Figure 7, c; Table 2. New carbides  $Me_{23}C_6$  were detected over periphery of the primary carbide, and disperse carbides of MeC type --- in the seam matrix.

In the base composite brazing alloy #1 + 60 % Rene-142 weight share of boron in the seam metal constitutes about 1 %. Due to introduction of NS12, when content of silicon in complex brazing alloy achieved 1.2–3.0 wt.%, content of boron reduced from 1.0 to 0.6–0.375 wt.%, and silicon dissolved in the brazed seam metal. Relatively low content of depressants in used system of brazing alloys excluded formation of pure borides, all the more silicides, in solidified metal of brazed seams.

The main factor, which characterizes favorable action of silicon on the metal of BJ seam, is reduction of penetration ability of active boron-containing brazing alloy into thermally instable base. In high-temperature brazing without a gap the seam being formed with silicon acquired more clear outlines at narrower width because of limited diffusion of boron through

the interface into the base (Table 3). Reduction of the seam width was in proportional dependence upon amount of introduced depressant, i.e. silicon (Figure 8). Size of the solidified metal grain reduced as weight share of NS12 powder increased.

Silicon changes morphology of carbide phase and suppresses precipitation of carbides of eutectic type (Figure 8, b, f). It remains mainly in the seam matrix or enters into composition of disperse carbide phases MeC. Character of precipitation of carboboride phases is shown in Figures 9 and 10.

Silicon significantly reduces temperature values of the brazing alloy liquidus and solidus and dissolution of carbide phases [13]. In absence of depressants temperature of complete dissolution of  $\gamma$ -phase of high-alloyed alloy Rene-142 is about 1260–1270 °C. However, presence of silicon enables reduction of dissolution temperature of both primary carbides of eutectic type and carbides  $Me_6C$  and dissolution temperature of metastable boundary  $\gamma$ - $\gamma'$  phase. That's why after solidification of brazing alloy #1 + 20 % NS12 + 60 % Rene-142 and subsequent heat treatment (1160 °C, 2 h + 1050 °C, 2 h) in the seam metal structure partial carbide transformations occurred.

**Table 3.** Chemical composition of metal of main zones of brazed joint formed with application of brazing alloy 20 % NS12 + 20 % #1 + 60 % Rene-142 at 1220 °C (10 min) and annealing at 1160 °C, 2 h + 1050 °C, 2 h

Investigated zones of brazed joint	Spectrum of analysis	Weight share of components, %											
		Ni	Al	Co	Ti	Cr	W	Mo	Ta	C	Nb	Re	Si
VJL12U	Composition of alloy (nominal)	Base	5.0–5.7	12.0–15.0	4.2–4.7	8.5–10.5	1.1–1.8	2.7–3.4	–	0.12–0.20	0.5–1.0	–	–
Base metal	2	61.88	5.3	14.11	4.84	9.48	1.75	2.64	–	–	–	–	–
Diffusion zone metal	3	63.0	4.8	13.6	3.70	9.11	1.42	2.56	–	–	0.8	0.32	0.64
Seam metal	4	67.98	4.0	9.36	1.44	6.33	2.74	1.08	3.06	–	–	1.25	2.76

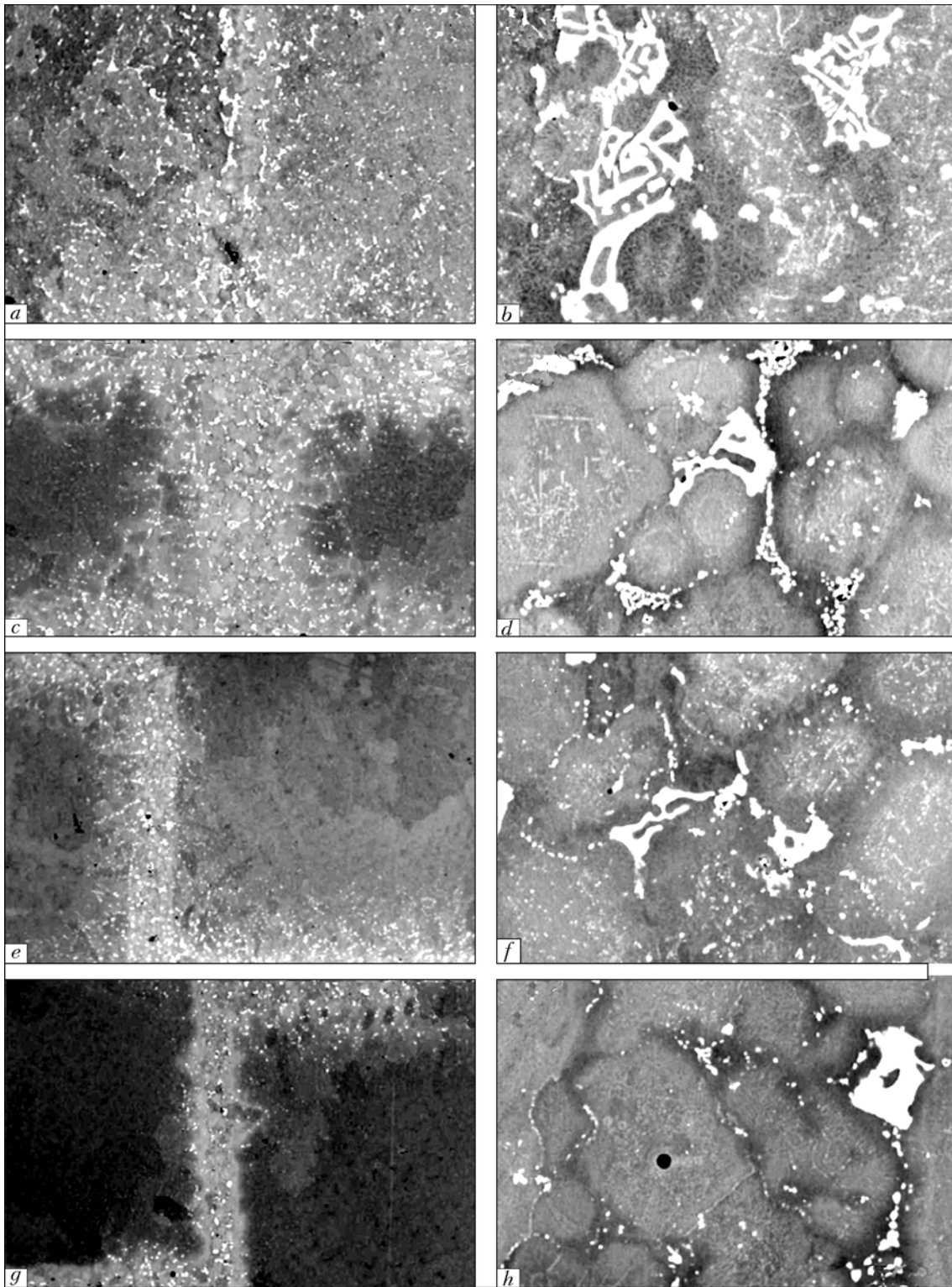


**Figure 8.** Microstructure of metal of brazed joints formed at temperature 1210–1220 °C (20–10 min) and annealed according to two-stage mode with application of complex brazing alloys of type #1 + Rene-142: *a, b* — without NS12; *c, d* — with 15 % NS12; *e, f* — with 20 % NS12; *g, h* — with 25 % NS12; *a, c, e, g* —  $\times 25$ ; *b, d, f, h* —  $\times 500$

Loose ( $\gamma$ - $\gamma$ )-eutectics and coarse carbide phases were not detected.

Presence of hafnium (from the filler powder) in the brazing alloy effects structural state of metal of seams, formed with addition of silicon. Even small amounts of hafnium effect specificity of the carbides being formed and their heat stability.

Alloying of the brazing alloy by  $\gamma$ -forming elements (titanium, niobium, hafnium) cause enrichment of inter-dendritic areas with formation of eutectic  $\gamma$ -phase.

At temperature 1100–1245 °C highly dispersive strengthening  $\gamma$ -phase actively dissolves, due to which diffusion redistribution of alloying components

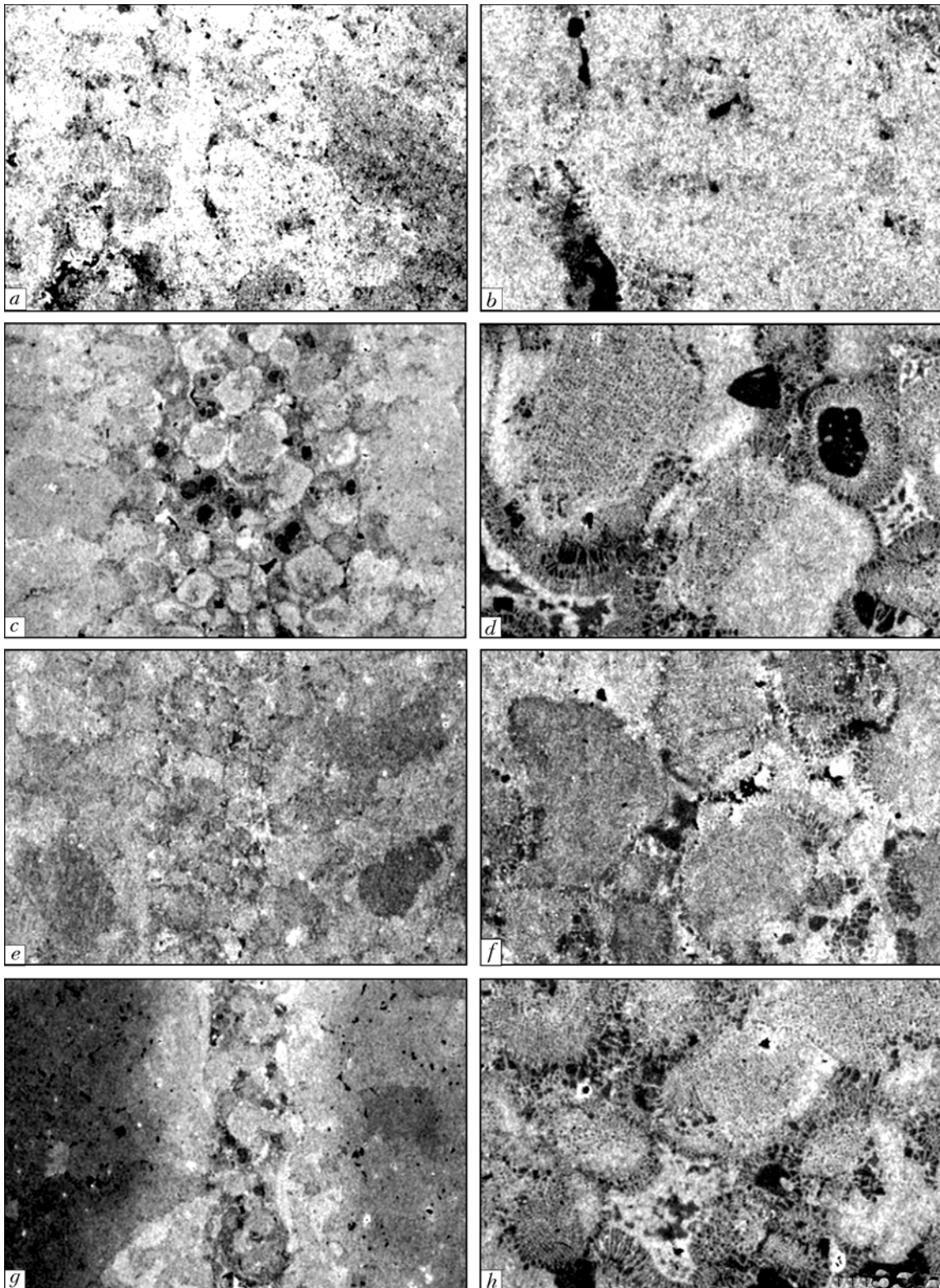


**Figure 9.** Microstructure of metal (after chemical etching) of brazed joints formed at temperature 1210—1220 °C (20–10 min) and annealed according to two-stage mode with application of complex brazing alloys of type #1 + NS12 + 60 % Rene-142 with different amount of silicon-containing brazing alloy: *a, b* — 10 % NS12; *c, d* — 15 % NS12; *e, f* — 20 % NS12; *g, h* — 25 % NS12; *a, c, e, g* —  $\times 100$ ; *b, d, f, h* —  $\times 500$

occurs. This intensifies process of carbide transformations in matrix solution.

Hafnium changes dash morphology of carbides MeC into a faceted polyhedral one. Presence of hafnium in alloys enables formation at high temperatures,

in addition to carbides (Nb, Ti)C, of  $Me_6C$  of other structural components, which represent complex eutectics in inter-axial areas, enriched with hafnium. The base of eutectics constitutes intermetallic compound  $Ni_nHf_m$  (50 % Ni–28 % Hf–0.6 % Al–6.6 %

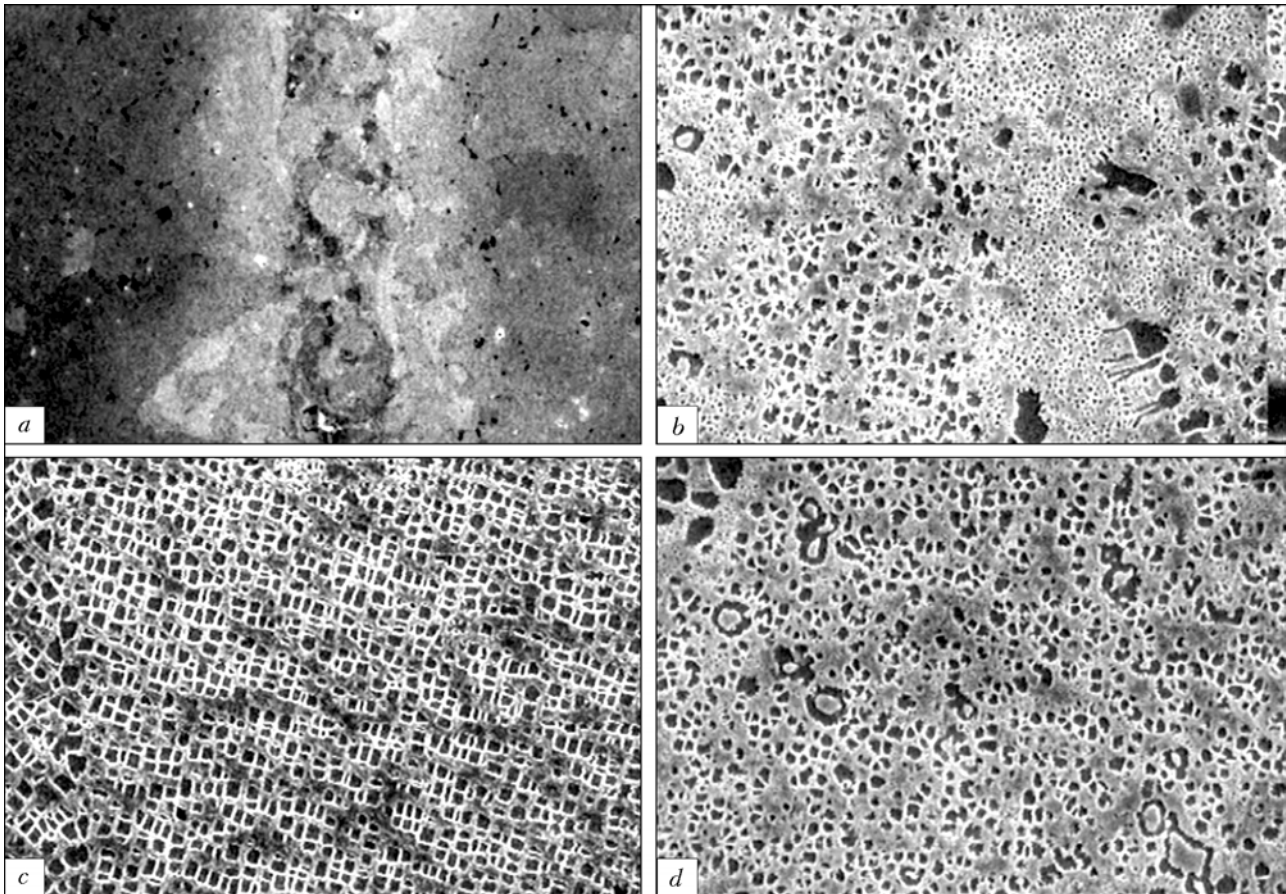


**Figure 10.** Microstructure of metal of main zones of brazed joint formed with application of composite brazing alloy #1 + NS12 + Rene-142: *a* — general view of joint; *b* — seam; *c* — base alloy; *d* — diffusion zone ( $\times 200$ )

Co–3.8 % W–5.8 % Nb–0.5 % Ti). Mentioned eutectics dissolve at high temperature, characteristic of vacuum isothermal brazing of nickel HTA.

At isothermal seasoning above 1100 °C processes of dissolution of non-equilibrium carbides of MeC–(Ti, Nb)C type (first of all of dash morphology) proceed in systems with hafnium with simultaneous formation of carbides of Me<sub>6</sub>C–(Ni<sub>3</sub>W<sub>3</sub>)C type and structurally stable carbides MeC–(Nb, Hf, Ti)C. Due to low solubility of tungsten in  $\gamma$ -phase, during disintegration of ( $\gamma$ – $\gamma'$ )-eutectics under conditions of high temperature, tungsten enriches areas adjacent to the eutectic phase and enables formation of carbides Me<sub>6</sub>C, immediately adjacent to eutectic colonies within dendrite volume. As a result of two-stage heat treatment carbides Me<sub>6</sub>C dissolve and precipitate from oversaturated solution in the form of dispersed globular particles.

Joint influence of silicon, hafnium and nickel determine microstructure of the metal of formed seams. Introduction of 17 % Ni (with powder NS12) enables reduction of relative concentration of alloying elements and amount of carbon in the seam metal; silicon — reduction of solidus temperature; hafnium — displacement from inter-phase boundaries of chromium and tungsten. That's why in seams with additive NS12 insignificant volume share of carbide phases, representing mainly twin Me<sub>6</sub>C and disperse MeC

carbides, was present. Number of carbide phases reduced as share of introduced powder NS12 increased.

After two-stage heat treatment of BJ introduction into the base brazing alloy #1 + 60 % Rene-142 of 10 wt.% of powder NS12 caused increase of silicon content in the matrix solution up to 0.66–1.33 wt.%. In the seam metal structure carbide phases were present with size of the grain 10–20  $\mu\text{m}$ . Coarse particles corresponded to the type Me<sub>6</sub>C (on the basis of tungsten, chromium, molybdenum and rhenium). Microhardness of these phases changed within 14400–21000 MPa (as tungsten content increased). Single precipitates of grey color were detected in the matrix with microhardness 6600–6800 MPa, similar to intermetallic inclusions of Hf<sub>n</sub>Hf<sub>m</sub> type.

So, small additions of silicon as a depressant into the boron-containing system enabled reduction of general number of carbide phases and suppression of formation of carboboride eutectics, whereby relatively coarse particles Me<sub>6</sub>C preserved (Figure 10; Table 4).

Matrix solution of the seam metal and zone of mutual diffusion had microhardness 4010 and 4030 MPa, respectively, microhardness of the base being 4100 MPa. This fact proves weak disperse strengthening, i.e. still insignificant processes of carbide disintegration in the brazed joint metal in heat treatment.

Formed phases had discrete character; they were detected in the form of fine needles (Me<sub>6</sub>C) or tan-



**Table 4.** Chemical composition of metal of main phases of solidified metal of seam produced with application of brazing alloy #1 + 10 % NS12 + 60 % Rene-142

Spectrum of analysis	Weight share of components, %													
	C	Al	Si	Ti	V	Cr	Co	Ni	Nb	Mo	Hf	Ta	W	Re
1	--	5.85	1.33	1.40	0.39	8.07	11.64	64.70	--	1.11	0.84	--	2.93	1.74
2	1.79	4.97	1.06	1.68	--	7.42	11.94	63.96	--	1.00	1.66	1.64	1.76	1.12
3	3.59	0.38	--	3.11	--	2.28	13.35	58.26	--	--	13.93	3.72	0.46	0.91
4	2.76	0.17	--	1.12	1.60	20.46	3.57	5.66	--	26.39	0.60	2.87	27.33	7.45
5	3.72	0.32	7.54	1.76	--	1.11	6.53	40.95	1.92	0.46	27.57	6.36	1.40	0.38
6	4.85	0.15	--	0.91	1.41	17.18	2.81	5.14	--	25.07	0.91	2.84	32.34	6.40
7	3.75	6.30	0.74	4.02	--	2.28	7.62	66.67	0.80	0.35	2.92	4.22	0.32	--
8	4.43	0.28	--	0.83	1.12	17.41	2.92	5.36	--	25.29	1.28	2.32	32.98	5.79
9	4.00	0.42	--	0.92	1.36	38.52	6.66	10.66	0.92	16.72	--	1.04	11.78	6.99

talum-, hafnium-, titanium-base discrete inclusions MeC (Figure 10; Table 5).

Dissolution and precipitation of new phases enables occurrence of stresses in the matrix and its plastic strain (phase cold hardening). That's why microhardness of matrix of BJ, formed at 1220 °C (10 min) with application of brazing alloy #1 + 20 % NS12 + 60 % Rene-142, which was subsequently annealed, increased up to 4510--4615 MPa. Microhardness of separate coagulated phases of Me<sub>6</sub>C type (on the basis of molybdenum, tungsten and chromium) achieved 28800 MPa (Figure 10, c; Table 5).

Increase of isothermal brazing duration from 10 to 20 min at temperature 1210 °C created conditions for fuller dissolution of boundary phases and carbide transformations in matrix of the brazing alloy with 20 % NS12. After heat treatment a solidified seam metal represented homogeneous solution with rare precipitates of twin carbides Me<sub>6</sub>C and disperse polyhedral carbide particles MeC (having microhardness

26600 MPa). Tantalum-base (up to 40 %) particles MeC with hafnium, titanium and niobium are products of disintegration of primary dash carbide phases and high-temperature inter-dendrite eutectics, and are structurally stable in further operation at high temperature (Figure 10, d; Table 5).

At longer duration of brazing the process of carbide formation proceeded more completely, and microhardness of the matrix solution constituted 4400 MPa. Under conditions of brazing 1210 °C for 20 min specimens of brazed joints with 20 % NS12 demonstrated at 20 °C Q-factor 102--112 % and relative elongation 6.25--7.20 %.

Increase of weight share of powder NS12 in complex brazing alloy up to 25 % gave good results in regard to BJ strength (Q-factor = 97 %), but ductility reduced down to 1.70--3.75 %.

Content of silicon in the matrix achieved 2.3 wt.%, and near grain boundaries it increased up to 3.4 wt.%. Judging from structure of the formed seam metal, in

**Table 5.** Chemical composition of different phases in metal of seam produced with application of brazing alloy #1 + NS12 + 60 % Rene-142 at different conditions of brazing

Conditions of brazing	Spectrum of analysis	Weight share of components, %													
		C	Al	Si	Ti	V	Cr	Co	Ni	Hf	Mo	Nf	Ta	W	Re
1220 °N, 10 min	1	--	4.53	0.67	2.73	--	7.74	11.62	65.59	0.58	1.56	--	2.57	2.40	--
	2	--	4.70	0.07	2.16	--	8.52	11.45	63.33	--	0.81	--	3.92	5.02	--
	3	--	4.55	1.78	2.93	--	6.68	11.83	68.68	0.63	1.46	0.48	--	0.97	--
	4	5.66	--	--	1.34	1.89	24.63	3.80	4.37	--	30.29	--	1.84	18.88	7.31
	5	6.93	--	--	4.59	1.02	15.48	3.64	11.65	1.43	19.79	0.62	15.50	14.48	4.87
	6	4.32	0.82	--	1.70	1.50	18.91	4.88	21.39	0.76	21.24	--	1.62	18.08	4.77
	7	6.12	2.16	1.27	6.08	--	9.56	10.01	41.43	2.98	1.59	2.35	15.05	1.40	--
1210 °N, 20 min	1	0.54	5.61	0.73	2.16	--	7.62	11.03	64.66	0.32	2.17	--	1.97	2.77	0.40
	2	1.06	4.76	0.92	1.85	--	9.24	13.70	63.05	0.61	1.62	--	1.26	1.94	--
	3	0.80	6.04	1.09	2.85	--	6.48	10.86	65.40	0.61	1.15	--	2.18	1.50	1.03
	4	10.90	0.47	1.11	15.20	--	1.47	2.19	13.40	4.31	1.76	1.10	45.20	2.94	--
	5	5.82	0.23	--	1.23	1.93	15.86	2.79	5.58	0.47	32.18	0.67	1.44	27.47	4.33
	6	13.73	0.26	2.84	16.99	--	1.81	1.64	9.15	5.31	2.62	1.43	40.32	3.90	--
	7	11.40	0.42	2.19	17.80	--	1.22	1.74	10.60	5.40	2.04	2.36	40.90	3.83	--

**Table 6.** Chemical composition of main phases of solidified seam metal produced with application of brazing alloy 25 % NS12 + 15 % #1 + 60 % Rene-142

Spectrum of analysis	Weight share of components, %														
	C	Al	Si	Ti	V	Cr	Fe	Co	Ni	Nb	Mo	Hf	Ta	W	Re
1	–	4.05	2.29	1.01	–	7.40	–	9.51	67.04	–	1.41	–	1.90	3.17	2.24
2	2.37	2.26	3.73	1.29	–	8.74	0.52	12.20	66.97	–	0.98	–	–	–	0.94
3	2.30	5.30	2.75	1.74	–	3.87	–	7.29	70.45	–	–	–	3.00	3.30	–
4	2.80	2.12	3.41	1.29	–	8.66	0.69	12.18	67.33	–	0.37	–	–	1.14	–
5	4.27	–	–	0.92	0.72	22.22	–	3.78	6.82	0.68	24.53	–	3.42	21.53	11.10
6	3.69	–	–	2.59	–	1.12	–	4.14	37.00	1.69	1.02	18.89	23.97	5.89	–
7	4.27	–	–	2.52	–	1.13	–	4.22	36.74	2.31	0.97	19.22	23.84	4.77	–
8	5.56	–	–	0.84	0.56	8.15	–	7.03	13.55	–	21.29	–	5.45	26.38	11.20
9	4.67	3.17	2.72	0.84	–	7.87	0.41	10.69	65.02	–	0.98	–	–	1.52	2.10

boundary areas rare coagulated particles  $Me_6C$  and precipitates of intermetallic phases of  $Ni_nHf_m$  type, containing tantalum, hafnium, nickel and titanium, preserved (Table 6; Figure 10, e). Presence of boundary  $\gamma$ -eutectic phase, which edged carbides and intermetallic compounds, proved beginning of the process of dissolution of strengthening phases, coarse carbides, and precipitation of more disperse carbides. Duration of isothermal seasoning in brazing was insufficient for complete dissolution of initial carbides and precipitation of completely dispersed phases (see Figure 10, e; Table 6).

After introduction into brazing alloy #1 + 60 % Rene-142 of powder NS12 structure of diffusion zone, which edges the seam, also changed. Silicon-containing seams had faintly developed diffusion zones because of lower amount of active depressant (boron). Silicon diffused restrictedly into nickel alloy and concentrated in the seam metal. Process of carbide transformations in the seam metal both in brazing and in the course of heat treatment enables dissolution of boundary eutectics, containing  $\gamma$ -stabilizing components (tantalum, hafnium). The latter ones due to their diffusion into the interphase base/brazing alloy boundary and binding with carbon of the base (0.12–0.20 %), form disperse carbide phases  $MeC$ , whereby their composition also includes niobium and titanium from the base. These carbide phases are stable at high

temperature and create a kind of a barrier for further diffusion of active components of the melt (boron, silicon) into the base (Figure 10, f; Table 7).

Two-stage heat treatment of BJ --- annealing at 1160 °C (2 h) and 1050 °C (2 h) --- enabled equalization of the structure in different zones of joints (Figure 11). After high-temperature homogenization in matrix of the alloy being brazed strengthening  $\gamma$ -phase with volume share up to 50 % precipitated. After annealing at 1050 °C (2 h) size of particles of  $\gamma$ -phase was 0.4–0.7  $\mu m$ . In the diffusion zone, in addition to the main strengthening phase, precipitation of carbide particles  $MeC$ , having size not more than 2–3  $\mu m$ , was detected.

In the seam metal structure, in addition to primary particles of  $\gamma$ -phase having size 0.4–0.5  $\mu m$ , in near-boundary areas of dendrites precipitation of disperse particles of  $\gamma$ -phase, having size 0.05–0.08  $\mu m$ , was registered as consequence of proceeding diffusion processes.

**Peculiarities of fracture.** Fractography of fracture allows estimating the weakest place in a specimen during its tensioning and fracture. Brazed joints of alloy VJL12U, produced with application of additives of brazing alloy NS12, failed, as a rule, over line of fusion with the base metal. Fracture of joints in the case, when relative elongation of specimens exceeded in tensioning 3.7 % (achieved 7.2 %), occurred in

**Table 7.** Chemical composition of main phases of solidified metal of diffusion zone produced with application of brazing alloy #1 + 20 % NS12 + 60 % Rene-142

Spectrum of analysis	Weight share of components, %													
	C	Al	Si	Ti	V	Cr	Co	Ni	Nb	Mo	Ta	W	Re	
1	–	4.48	1.15	1.28	0.47	7.90	11.75	65.45	–	1.89	1.97	2.52	1.13	
2	–	4.44	1.13	1.59	–	8.33	11.72	66.58	–	1.49	1.32	3.40	–	
3	–	3.99	2.63	1.30	–	7.72	11.08	68.24	–	1.40	–	2.00	1.63	
4	13.19	1.14	–	12.83	0.56	3.25	3.53	22.93	3.91	3.67	29.70	5.31	–	
5	12.11	1.75	0.77	11.17	0.56	2.65	4.05	31.97	3.53	1.46	27.75	2.23	–	
6	10.55	1.97	0.73	5.30	0.54	7.99	5.09	31.97	1.80	7.05	17.78	7.24	1.97	
7	13.86	0.78	0.90	17.42	–	1.46	1.89	16.18	6.35	2.22	34.93	4.01	–	

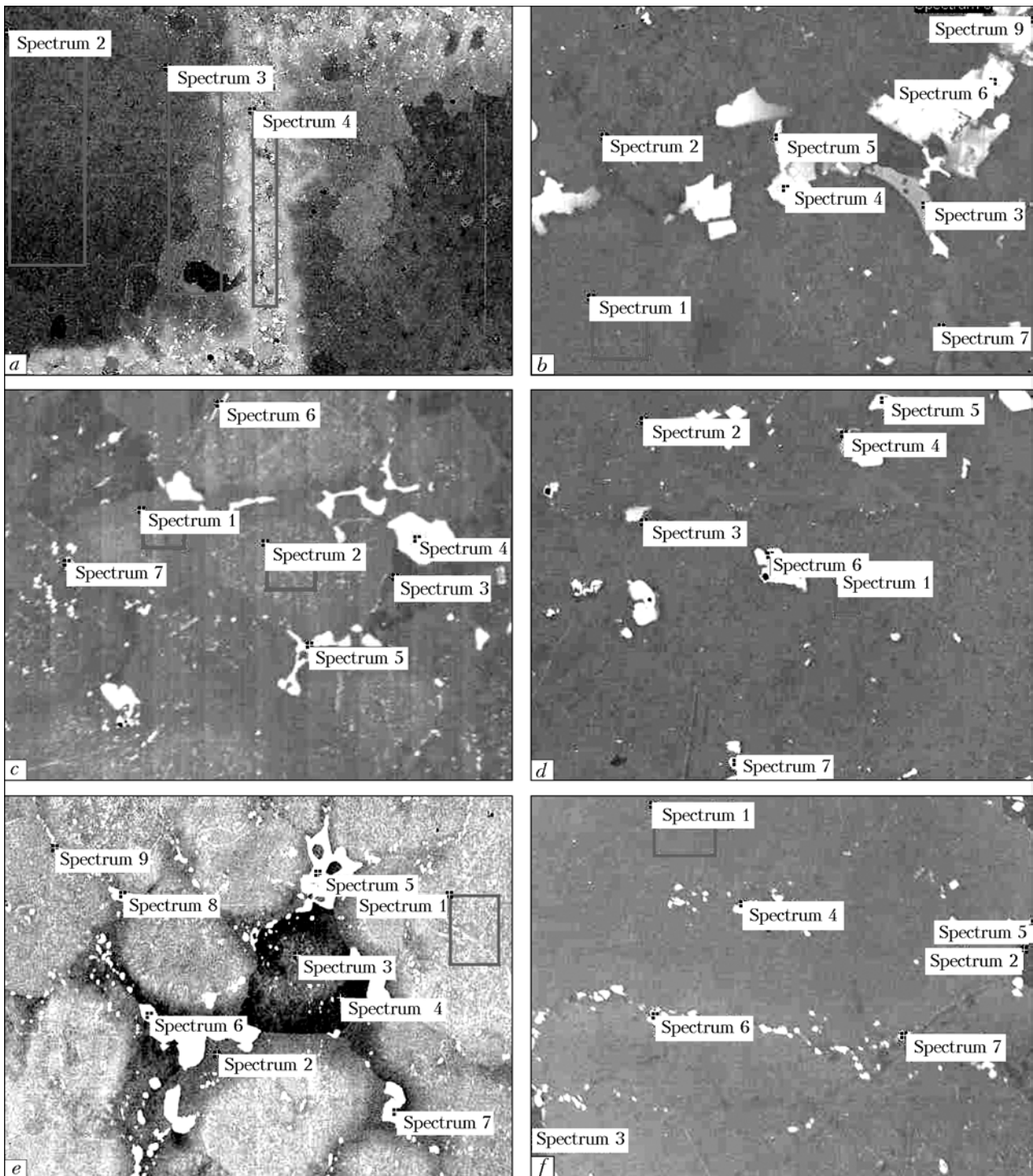


**Figure 11.** Areas of X-ray spectral microanalysis of produced zones of brazed joints: *a* — VJL12U/ #1 + 20 % NS12 + 60 % Rene-142 (Table 3,  $\times 25$ ); *b* — metal of seams produced with application of brazing alloys #1 + 10 % NS12 + 60 % Rene-142 (Table 4,  $\times 400$ ); *c* — #1 + 20 % NS12 + 60 % Rene-142 at 1220 °C for 10 min (Table 5,  $\times 400$ ); *d* — #1 + 20 % NS12 + 60 % Rene-142 at 1210 °C for 20 min (Table 5,  $\times 400$ ); *e* — #1 + 25 % NS12 + 60 % Rene-142 (Table 6); *f* — metal of diffusion zone (Table 7,  $\times 400$ )

combined way with coverage of areas of the solidified seam metal and the zone, adjacent to the base metal.

In Figure 12 picture of final fracture of BJ specimens, in which composite brazing alloy #1 + 60 % Rene-142 (*a*, *b*) and complex brazing alloys with different amount of added powder NS12 (*c*–*f*) were used, is shown. In the first case in fracture of the specimen rare areas of faulty brazing and shrinkage porosity were registered, and transcristalline character of fracture prevailed. Due to introduction into brazing alloy

of powder Ni–12 % Si fractures of destroyed specimens had fine-grain dim surface, corresponding to structure of tough brake-off.

In tensile tests in flat specimens of BJ occurred rigid three-axial stressed state, and fracture proceeded under conditions of flat strain. In joints, produced under conditions of flat strain, fracture occurred along the weakest place of a specimen — over metal of the brazed seam, in which point metallurgical defects (micro-cavities) were present.

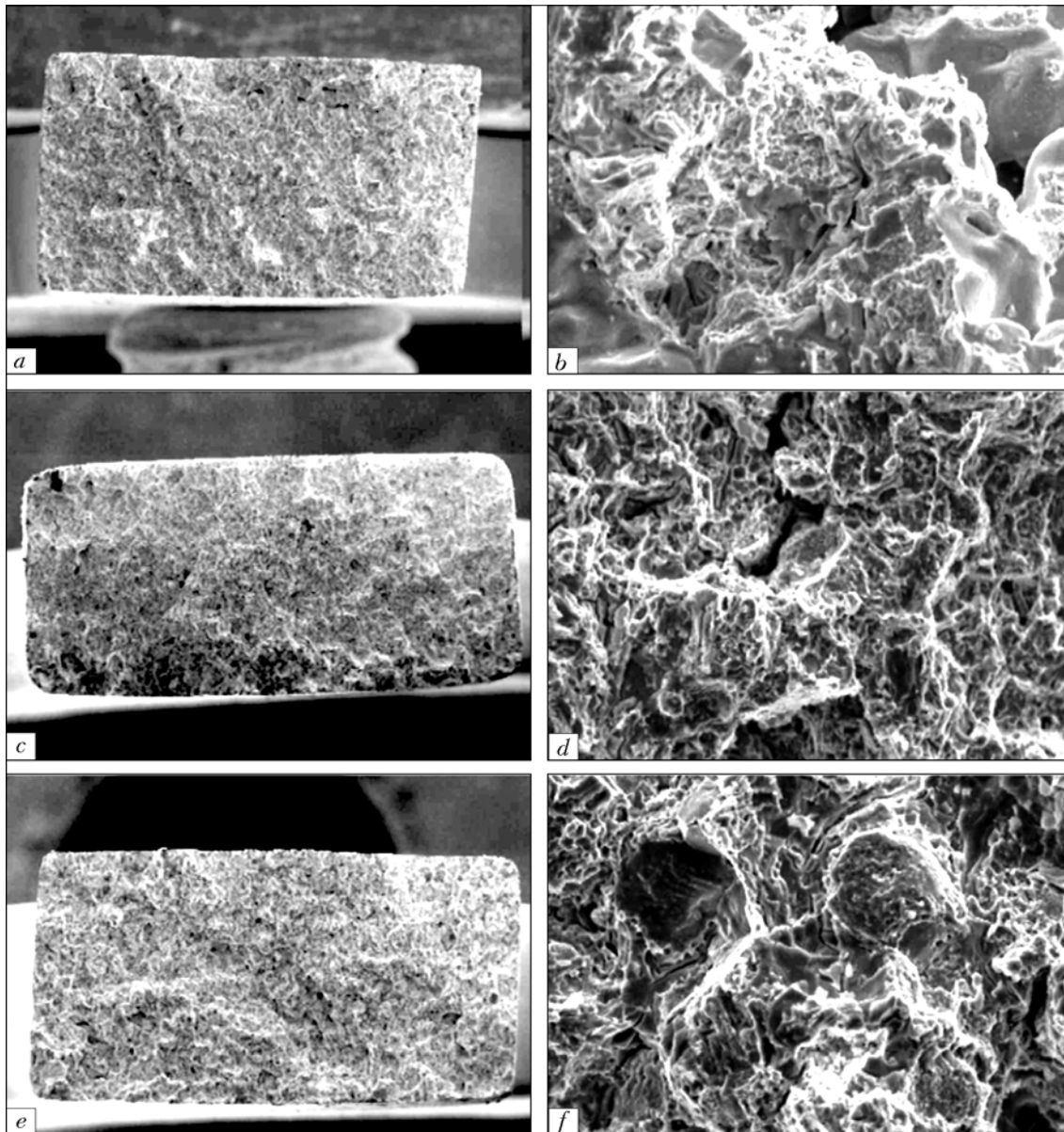


**Figure 12.** Picture of fracture of specimens of brazed joints produced with application of complex brazing alloy of type #1 + NS12 + Rene-142 at single-axis tension with different content of silicon-containing brazing alloy: *a, b* — without NS12 (Q-factor = 40 %); *c, d* — with 15 % NS12 (Q-factor = 96 %); *e, f* — with 25 % NS12 (Q-factor = 97 %): *a, c, e* —  $\times 23$ ; *b, d, f* —  $\times 500$

Characteristic peculiarity of fractures of specimens, produced with application of brazing alloys containing both boron and silicon, was change of the morphology and size of carbide phases. In case of the traditional system #1 + Rene-142 boundary carbides had size more than  $10\ \mu\text{m}$  across, and volume share of disperse carbide phases within dendrite volume was 25–30 %. Silicon increases dispersity of carboboride phases and homogeneity of their distribution. Reduction of the number of carboboride particles in interdendrite areas ensured dispersion strengthening of the matrix and higher level of short-term tensile strength of a BJ (Figure 13, *d, f*).

In back scattered electron images (BEI) (Figure 13) discrete carbide phases were uniformly distributed within a grain volume, whereby their number was significantly higher in the zone of mutual diffusion between the base and a brazed seam, i.e. in the

zone with discrete precipitates  $\text{MeC}$  over grain boundaries. High content of carbon in the alloy (0.12–0.20 %) and presence of strong carbide-forming agents, like tantalum, in the seam metal caused formation in the fusion zone of disperse carbide components like  $(\text{Ta, Nb, Ti})\text{C}$ , which in presence of hafnium in the brazing alloy were secondary components after disintegration of complex carbides, preserving stability in further operation.

Inspection of surface of the fractures showed decohesion of carbide particles  $\text{Me}_6\text{C}$  and  $\text{MeC}$  and of the matrix, which enabled formation of discontinuities in the seam metal. Material of complex brazing alloy with silicon failed because of formation of internal necks caused by shear strain, occurring in the seam matrix.

As far as distance between carbide particles in the matrix is insignificant, fracture of brazed joints was

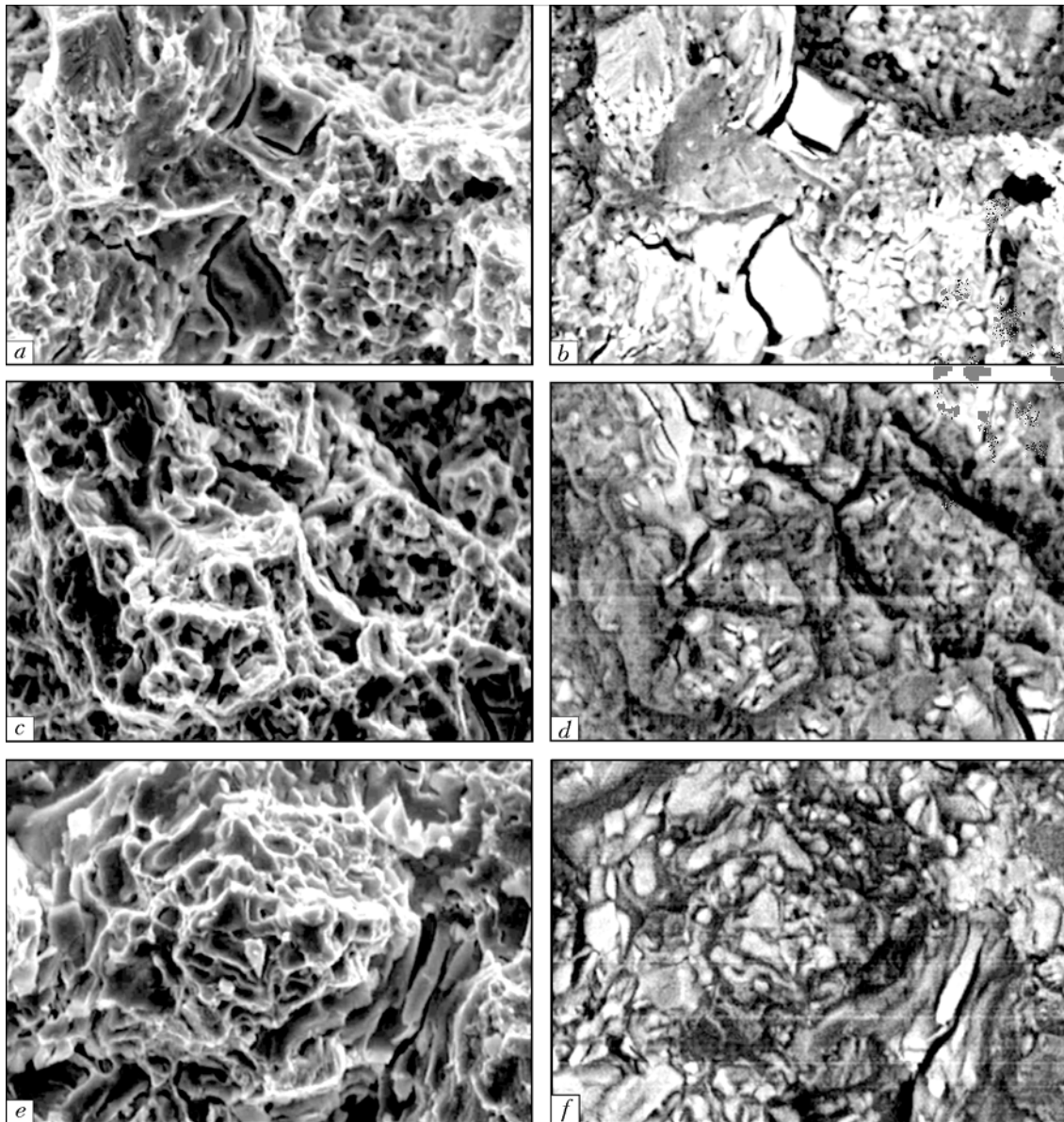


**Figure 13.** Influence of silicon on character of carbide phase precipitates in fractures of specimens after single-axis tensile test: *a, b* — seam metal (brazing alloy #1 + 60 % Rene-142); *c, d* — seam metal (brazing alloy #1 + NS12 + 60 % Rene-142); *e, f* — diffusion zone (brazing alloy #1 + NS12 + 60 % Rene-142) ( $\times 1000$ )

macroscopically brittle, although on microscopic scale failure of the seam metal was tough. Final appearance of the fracture surface was determined by ductility of the seam metal, dispersity, and volume share of strengthening phases. (In case of a brazing alloy with 20 % NS12 microhardness of the seam metal was 4100–4300 MPa.)

In Figure 14 longitudinal section of BJ specimen, produced with application of brazing alloy #1 + 20 % NS12 + 60 % Rene-142, is shown. Failure of the specimen was of combined character and occurred both over fusion line and over the seam metal. Carbide phases, located in the seam metal or in the diffusion zone, cracked under action of a load. However, discreteness of their location over grain boundaries affected character of cracks, occurring in the seam over brittle phases — they were not continuous, but had a form of ruptures.

Due to complex alloying of the seam metal and high fluxing capacity of the brazing alloy melt, containing silicon, significant strength of brazed joints was achieved, which completely excluded brittle fracture over the seam or the fusion line.

## CONCLUSIONS

1. Positive action of introduction of silicon into composition of boron-containing brazing alloy of the system Ni–Co–Cr–Al–2.5 % B, used in repair of nickel alloys by isothermal brazing in vacuum, was considered.

2. It is established that brazed joints of alloy VJL12U, produced by application of complex brazing alloy with addition of 15–20 wt.% NS12, showed high stability of strength characteristics in tensile tests. Q-factor ( $\sigma_t^{BJ} / \sigma_t^{BA}$ ) of mechanical properties at 20 °C was 72–95 %.

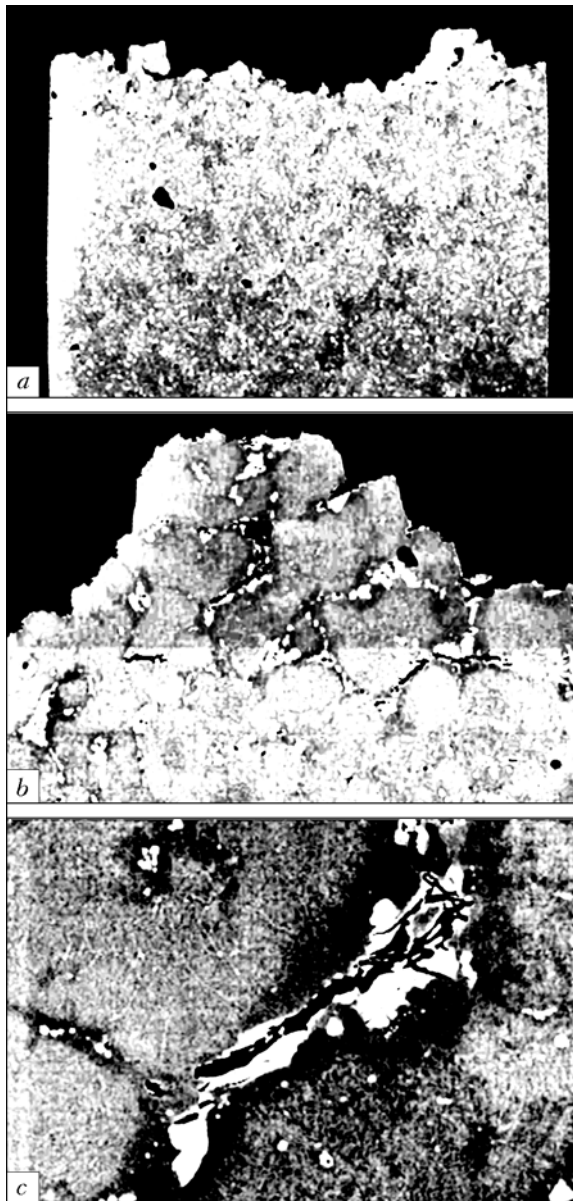


**Figure 14.** Inter-grain fracture of metal of brazed joint VJL12U/ #1 + 20 % NS12/ VJL12U in area of fusion line in tension: a — longitudinal section of specimen ( $\times 23$ ); b, c — formation of cracks in boundary carbide phases under action of applied load ( $\times 100$ ;  $\times 500$ )

3. It is shown that 2.0–2.5 wt.% Si change morphology of carbide phase, transforming it from the dash form into the globular one, uniformly distributed in the seam metal matrix and over grain boundaries.

Silicon restricts diffusion of boron from the seam metal into adjacent to the seam volumes of the alloy being brazed, due to which diffusion zone width in brazed joints gets narrower.

4. It is determined that disperse carbide phase ensures efficient strengthening of a brazed joint and possibility of occurrence of plastic strain over fusion line in the area seam metal–base alloy. Relative elongation of brazed joints of alloy VJL12U, produced with a silicon-containing brazing alloy, achieved after final heat treatment 5–7 %, while in brazing with brazing alloys, not containing silicon, elongation did not exceed 2.3 %.

5. Q-factor of brazed joints of alloy VJL12U, produced with application of mentioned brazing alloy at 900 °C, constituted 72–87 %. Fracture of BJ occurred over the seam.

1. Kurenkova, V.V., Malashenko, I.S., Trokhimchenko, V.V. et al. (2006) Short-term strength of brazed joints of nickel alloy VJL12U at temperatures 20 and 950 °C. *Advances in Electrometallurgy*, **3**, 27–37.
2. Malashenko I.S., Kurenkova, V.V., Belyavin, A.F. et al. (2006) Strength and physical metallurgy of brazed joints of cast nickel alloy ChS70 VI. *Ibid.*, **1**, 19–30.
3. Chaturvedi, M.C., Ojo, O.A., Richards, N.L. (2004) Diffusion brazing of cast Inconel 738 superalloy. *Advances in Technol. Materials & Materials Proc.*, **2**(6), 206–213.
4. Ohsasa, K., Shinimura, T., Narita, T. (1999) Numerical modeling of the transient liquid phase bonding process of Ni using Ni–B–Cr ternary filler metal. *J. Phase Equilibria*, **20**(3), 199–206.
5. Kvasnitsky, V.F. (1986) *Welding and brazing of high-temperature alloys in shipbuilding*. Leningrad: Sudostroenie.
6. Miner, R.V. (1977) Effect of C and Hf concentration on phase relations and microstructure of a wrought powder-metallurgy superalloy. *Metals Transact. A*, **8**(2), 259–263.
7. Tung, S.K., Lim, L.C., Lai, M.O. (1996) Solidification phenomena in nickel base brazes containing boron and silicon. *Scripta Materialia*, **34**(5), 763–769.
8. Blue, C.A., Blue, R.A., Lin, R.Y. et al. (2001) Joining of Hastelloy X to Inconel 718 using an infrared process. *J. Materials Proc. Technol.*, **113**(1–3), 215–221.
9. Kishkin, S.T., Pankratov, V.A., Lukovkin, A.I. et al. (1981) Nickel cast alloy for nozzle blades of gas turbine engine. *Aviats. Promyshlennost*, **12**, 37–38.
10. Pankratov, V.A., Shalygina, V.I. (1979) Influence of short-time heatings on structure and properties of VJL12U alloy. *Ibid.*, **6**, 59.
11. Shpindler, S.S., Londa, M.I., Portnoj, Ya.P. et al. (1978) Influence of technological factors on structure and properties of VJL12U alloy. *Ibid.*, **3**, 62–64.
12. Wu, X., Chandel, R.S., Li, H. et al. (2000) Induction brazing of Inconel 718 to Inconel X-750 using Ni–Cr–Si–B amorphous foil. *J. Materials Proc. Technol.*, **104**(1/2), 34–43.
13. (1987) *Heat resistance of cast nickel alloys and their protection from oxidation*. Ed. by B.E. Paton. Kiev: Naukova Dumka.



*From Editorial Board*

*Present level of development of continuous steel casting in Ukraine can not but cause concern. Key link, which determines both quality of produced continuously cast billets and stability and safety of the processes of steel casting on machines for continuous casting of billets (MCCB) is the mould that performs oscillating movements, directly in which proceed processes of formation of a continuously cast ingot.*

*By publishing this article the Editorial Board hopes to attract attention of the readers to this problem also because in remelting processes of special electrometallurgy, implemented according to the ingot drawing scheme, exist similar to MCCB problems, which wait for their final solution.*

## DETERMINATION OF SWINGING RADIUS OF THE MCCB MOULD

V.A. SIDOROV and A.L. SOTNIKOV

Donetsk National Technical University, Donetsk, Ukraine

Oscillating movement of a MCCB mould, directed along its technological axis, is ensured due to respective design of the swinging mechanism. Owing to natural processes, constant change of technical state of the swinging mechanism occurs, that effects parameters and direction of the MCCB mould movement. It is suggested for radial MCCB to check of the mould coaxiality with technological axis of the machine with the help of a swinging radius.

*Keywords: MCCB, swinging mechanism, trajectory of movement, technical state, check, swinging radius, oscillation range*

Oscillating movement of a mould of the machine for continuous casting of billets (MCCB) is ensured by the swinging mechanism. The path, along which moves the mould between two extreme positions, corresponds to technological axis of the machine. For radial MCCB technological axis represents an arc of a circle, and movement of the mould is reciprocation-rotary one relative center of the MCCB curvature.

Primary formation of a continuously cast billet (CCB) is performed in the mould. That's why its deviation from coaxiality with technological axis of the machine, as well as with other equipment of the CCB formation area, caused by various reasons, leads in combination with superimposition of oscillations to violation of symmetry and stability of movement of metal flows in the mould. This stipulates formation of external and intermediate cracks, distortion of geometric shape and dimensions of the billet, breaks of the ingot, and wear of the units and mechanisms of the MCCB equipment [1, 2].

In this connection check of correctness of installation and coaxiality of the swinging mechanism, which determines orientation of working surface of the mould sleeve relative technological axis of MCCB both in statics and in dynamics (in swinging), is an urgent task that is confirmed by the works, carried out in this direction.

Systems and methods for alignment and check of the working cavity, trajectory, and other parameters of the mould movement are proposed [3–7], which require for practical approbation for making decision on their commercial usability, because they are based on application of complex electron-measurement elements. In addition, long time is needed for performance of the check-measurement works [3, 4].

At metallurgical enterprises of foreign and CIS countries systems for check of the MCCB swinging mechanisms are being introduced, based on vibrometry methods. Systems of companies «First-Alpine Industrialangebau» (Austria) and «Technoap» (Russia), which allow determining parameters and trajectory of movement of the swinging mechanism points of the MCCB mould, are widely known.

Taking into consideration combination of the factors, which effect change of the MCCB mould parameters and direction of movement, inaccuracies, stipulated by kinematics of the swinging mechanism, wear of friction units, and wrong installation, not a single of the proposed methods allows estimating to full degree occurring deviations with indication of the reasons, which cause them. The information being obtained is insufficient for ensuring efficiency of the continuous casting process and high quality of the billets being produced. In this respect potential of vibrometry methods is not used to its utmost, because till now tasks of diagnosing swinging mechanism of a mould with their assistance are solved vary rarely.

For MCCB of radial type technological axis in the area of CCB formation (the mould–the drawing-align-

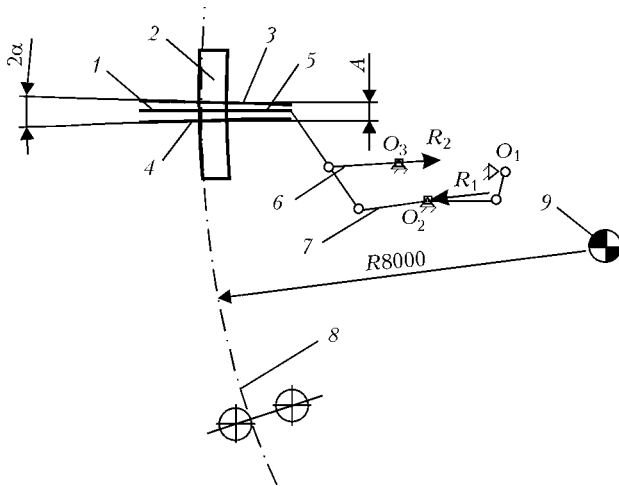


**Figure 1.** Kinematic scheme of swinging mechanism of MCCB mould: 3-5 — extreme upper and lower, as well as neutral positions of swinging table, respectively; 8 — technological axis of MCCB; 9 — center of curvature;  $\alpha$  — angle between extreme positions of swinging table (the rest designations see in the text)

ment device) represents an arc with radius of a circle equal to the base radius of MCCB. According to requirements of coaxiality of the MCCB units and equipment mechanisms, direction of oscillating movement of the mould should coincide with the technological axis. Parameter of curvilinear portion of the MCCB technological axis is the base radius. For points of working side of a mould with big radius of curvature, movement trajectories will also represent arcs with radius of a circle, equal to the base radius of MCCB. So, radius of arc of a circle, which corresponds to technological axis of the machine and represents trajectory of movement of the points of the working side of a mould, is the only parameter, determining coaxiality of the mould. For a mould that

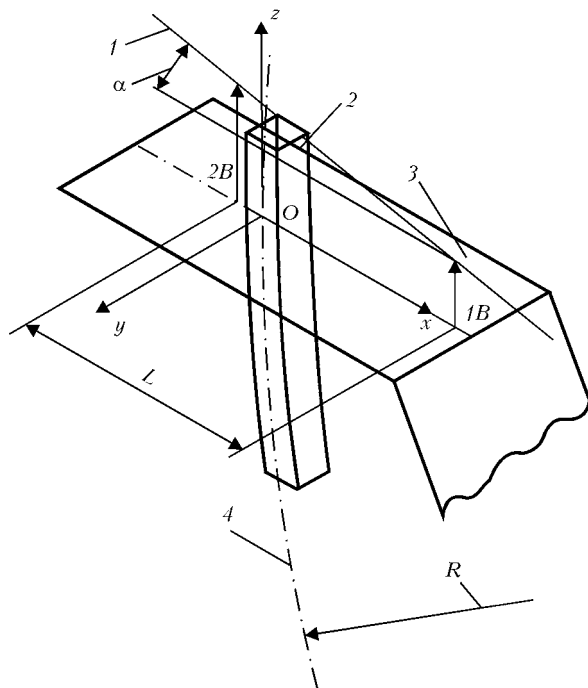


**Figure 2.** Spatial geometry of swinging table of MCCB mould: 1 — distribution of amplitudes; 2 — mould; 3 — swinging table; 4 — technological axis

performs oscillating movements this parameter will be a swinging radius.

Taking into account unused possibilities of vibrometry methods in solution of tasks of diagnosing a swinging mechanism, a comprehensive approach to check of the mould swinging mechanism was proposed, which allows preventing reasons of its deviation. For this purpose it is necessary to take readings in two check points using a portable vibration analyzer during planned and unplanned shutdowns of steel casting process on MCCB, and in case of using a stationary system — also during MCCB operation. Approbation of the method was carried out under conditions of metallurgical plants on radial bar MCCB.

The MCCB is equipped with swinging mechanism of moulds, manufactured according to the scheme of a hinge four-link mechanism (Figure 1). The swinging mechanism, consisting of a table, a lever system and a drive, is installed on foundation in such way that the drive is on the side of the curvature center of technological axis of the MCCB strand. The drive switches on an electric motor, a reduction gear, a flexible and an eccentric couplings, by means of which movement of the table according to the sine law is performed. Rolling bearings are used as hinge elements. Equilibration is performed by means of pneumatic shock absorbers.

Functions of the swinging table performed link 1 of the mechanism, on which the mould 2 was installed and fixed. The lever system represents a twin four-link mechanism with one common link 7 (see Figure 1).

Due to the fact that shoulders (links 6 and 7) of the output four-link mechanism have the same length and are directed to curvature center of the MCCB technological axes, points of the swinging table 1, which performs plane-parallel movement, move over assigned trajectory. The trajectories represent arcs of circles with the center, coinciding with the MCCB curvature center. Respectively the mould, installed and fixed on the swinging table, will perform reciprocation-rotary movement relative the MCCB curvature center. Installation of the mould is performed in such way that points of the working side of the sleeve with big radius of curvature move over the trajectory, corresponding to technological axis of MCCB — arc of a circle with the radius, equal to the base radius of MCCB.

It is necessary to consider technological axis of MCCB in two mutually perpendicular planes (Figure 2) — longitudinal and transversal ones.

Let's assume that longitudinal axis passes through curvature center of technological axis of the MCCB strand and is parallel to its profile. In horizontal plane its projection forms axis of the mould symmetry. Longitudinal plane passes through the mould side in the same way as technological axis of MCCB. Horizontal plane is located lower of the MCCB curvature center and is the plane of neutral position of the swinging table, when the table and upper end of the mould are

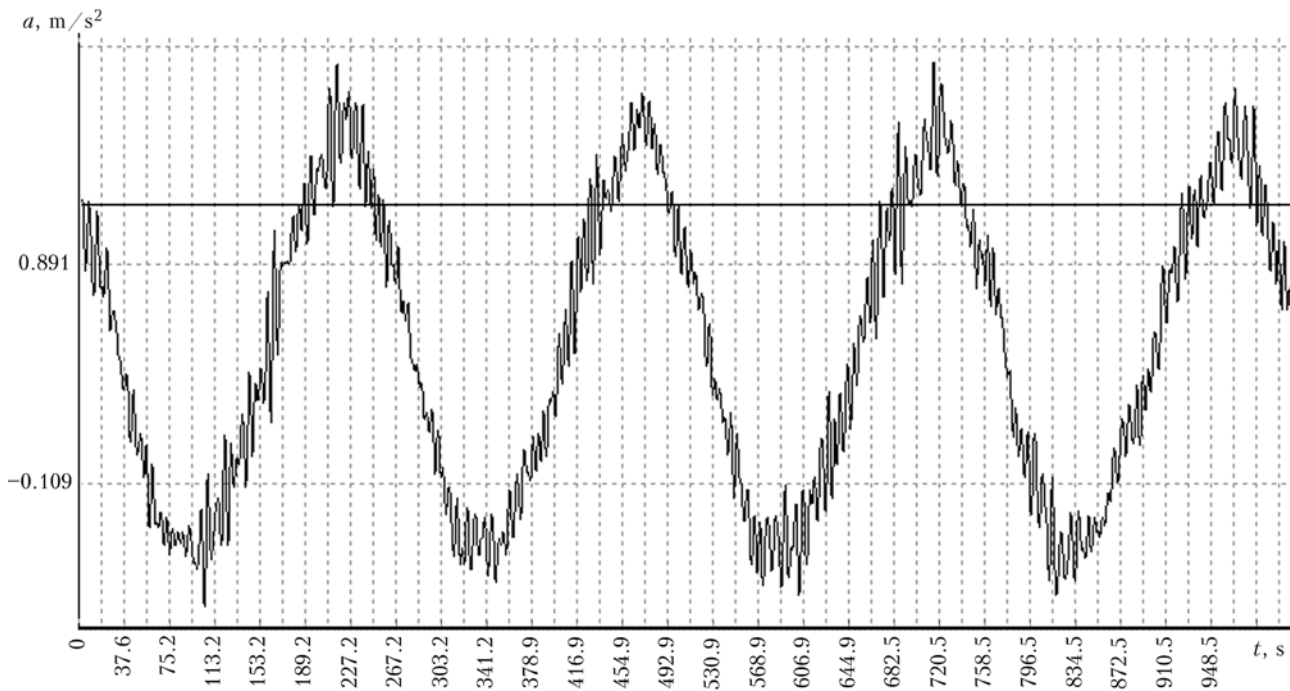


**Figure 3.** Temporal shape of vibration acceleration signal  $a$  in case of wear of hinge bearings

parallel to this plane. Intersections of all three planes form axes of three-dimensional system of coordinates with the center, coinciding with technological axis of the MCCB strand. Axis  $X$  is directed at the side of the curvature center, axis  $Y$  --- to the left, if to look from the side of the MCCB curvature center, axis  $Z$  --- upwards.

In longitudinal plane  $OXZ$  technological axis is represented in the form of an arc of a circle, and in transversal plane  $OYZ$  --- in the form of a straight line. Swinging table of the MCCB mould moves symmetrically relative horizontal plane (axis  $OX$ ) upwards and downwards. In transversal plane (along axis  $OY$ ) movements are absent (see Figure 2). Along axis  $OZ$  the swinging table moves at  $A/2$  into one direction, and total movement into other direction represents the oscillation amplitude (range of oscillations or swinging path)  $A$  (see Figure 1).

Correspondence of technological axis of the MCCB mould to the theoretical one in transversal plane is determined by deviations relative axis  $OY$ , and in longitudinal plane --- by deviations from the arc of the circle (trajectory of movement of points of the mould working side).

Small angles of movement, high loads, and operation under conditions of dustiness and increased temperature contribute to local galling in link supports of the output four-link mechanism, located oppositely to directed normal reactions  $R_1$  and  $R_2$ . In the process of operation occurs wear of the drive elements and weakening of thread connections. Under real conditions swinging mechanism of the mould also may have manufacture and installation defects.

So, position of swinging centers  $O_2$  and  $O_3$  distorts, which is manifested in deviation of the theoretical technological axis (change of the mould swing radius). As deviation increases, transversal action of

the swinging mould on an ingot, which stipulates enhanced wear of working surface of the mould, worsening of CCB surface quality, and breaks of the ingot, also increases (see Figure 1).

Shape of the vibration signal (vibration displacement), by which oscillation amplitude of the mould swinging table was determined, was measured using analyzer of vibration. Measurements were carried out in vertical direction in two points  $1B$  and  $2B$ , located on longitudinal axis of symmetry  $OX$  of the swinging table at a distance  $L$  from each other in such way that point  $2B$  to be as close as possible to technological axis of the MCCB strand (see Figure 2).

As far as in the simplest case the swinging table performs rotational movement around center of the MCCB curvature, distribution of amplitudes over the table length in longitudinal plane will follow the law of distribution. After transformation we get the final formula for determining swinging radius of the MCCB mould, for example, for point  $2B$ :

$$r_{2B} = \frac{A_{2B}L}{A_{2B} - A_{1B}},$$

where  $A_{2B}$  and  $A_{1B}$  are the oscillation amplitudes of the swinging table in respective points.

Approbation of proposed methodology for determining swinging radius of the mould showed high convergence of the results. Deviation of the radius of the circle arc of trajectory of movement of the working side points of the mould sleeve from the theoretical one is established and its reasons are determined.

Vibrometry methods allow getting, in addition to parameters of movement, information on technical state of MCCB units and mechanisms and estimating quality of repair and mounting works.



Temporal form of vibration parameters gives information on deviation of law of motion from the sine law and is the most illustrative method of presenting information on character of oscillations. In Figure 3 example of temporal shape of the vibration acceleration signal in point 2B, characterized by practically correct sine curve with small high-frequency modulation of the signal, which is characteristic of wear of the hinge bearings, is shown.

At present works are carried out, directed at enhancing possibilities of proposed methodology by check of the motion trajectory in other planes using vibrometry methods. Second direction of the works consists in preparation of the reference book-album of possible faults and manifestations thereof. This will allow timely determining need and kind of repair actions for the purpose of prevention of deviation of parameters and direction of the MCCB mould movement.

## CONCLUSIONS

1. The need of checking correspondence of the mould movement direction to the theoretical technological axis of MCCB for the purpose of ensuring stability and safety of steel casting process and quality of produced CCB is determined.

2. Possibility of determining swinging radius of the MCCB mould by vibration parameters is theoretically substantiated. Analysis of used at metallur-

gical enterprises systems and methods for check of swinging tables is fulfilled.

3. Carried out experimental investigations confirmed efficiency of proposed method for determining radius of the arc circle (trajectory of movement of the swinging table points of the MCCB mould in longitudinal plane) and for solving tasks of diagnosing the swinging mechanism and determining reasons of a swinging radius deviation from the assigned one.

4. Further directions of investigation of the possibility of using vibrometry methods for ensuring assigned parameters and direction of the MCCB mould movement are determined.

1. Smirnov, A.N., Pilyushenko, V.P., Minaev, A.A. et al. (2002) *Processes of steel continuous casting*: Monography. Donetsk: DonNTU.
2. Mekhaev, V.P. (2003) 4th European Conference on Steel Continuous Casting. *Stal*, 7, 30–33.
3. Timokhin, O.A. (2000) Peculiarities of calculation of technological axis of MCCB and its control. *Ibid.*, 2, 16–21.
4. Tikhonovsky, V.A., Kuzminov, A.L., Shchegolev, A.P. et al. (1993) Efficiency of microprocessor control systems for equipment of MCCB. *Ibid.*, 1, 38–41.
5. Levin, P.A., Levin, M.Z. *Device for mould adjustment along the technological axis*. USSR author's cert. 1359058. Int. Cl. B22D11/04. Publ. 15.12.87.
6. Shestakov, N.I., Parshin, V.M., Nechaev, E.A. et al. *Method of alignment control between mould and supporting section in secondary cooling zone and device for its realization*. USSR author's cert. 1276435. Int. Cl. B22D11/16. Publ. 15.12.86.
7. Checker, M. (2004) *System description*. Linz: Voestalpine Mechatronics GmbH.

## TECHNOLOGY OF MANUFACTURING LIGHT-WEIGHT WELDED CYLINDERS

The technology was developed at the E.O. Paton Electric Welding Institute and is aimed at solving two priority problems, namely lowering the specific weight and increasing the operating reliability. The novelty consists in the laminated structure of the cylinder wall and a rational combination of metals with different physico-mechanical properties.

The new approach to the technology of cylinder manufacturing allows using metals with a high specific strength, and, therefore, reducing the item weight by 30 to 50 %; increasing the operating reliability by minimizing the structure imperfections associated with the welds located on the cylindrical part and the nozzle; making the technology simple and accessible for implementation under the factory conditions.

There are no foreign analogs.

Pilot production batches have been made of cylinders of small and medium volume for the working pressure of 14.7 MPa (150 kg/cm<sup>2</sup>) with the strength margin of 2.6 according to the DNAOP 0.00-1.07-94 Rules. Technical documentation for cylinders manufacture has been developed.

**Application.** Storage and transportation of pressurized gases.

Contacts: Prof. Garf E.F.  
E-mail: yupeter@ukr.net



# INVESTIGATION OF PHASE TRANSFORMATIONS IN POWDERS OF MULTI-COMPONENT AlCuFe-BASE ALLOY WITH QUASI-CRYSTALLINE STRUCTURE

Yu.S. BORISOV<sup>1</sup>, A.L. BORISOVA<sup>1</sup>, M.V. KARPETS<sup>2</sup>, **D.V. LOTSKO<sup>1</sup>**, Yu.V. MILMAN<sup>1</sup>, L.I. ADEEVA<sup>1</sup>, G.N. GORDAN<sup>1</sup> and L.K. DOROSHENKO<sup>1</sup>

<sup>1</sup>E.O. Paton Electric Welding Institute, NASU, Kiev, Ukraine

<sup>2</sup>I.N. Frantsevich Institute for Materials Science Problems, NASU, Kiev, Ukraine

Phase transformations in Al<sub>63</sub>Cu<sub>25</sub>Fe<sub>12</sub>-base alloys, alloyed by a complex of elements (titanium, chromium, silicon) at the ratios AlCuFe:TiCrSi = 95:5 85:15 and 75:25, were studied using methods of high-temperature radiography and differential thermal analysis. In system with 5 % TiCrSi formation of quasi-crystalline  $\psi$ -phase was established, while in systems with 15 and 25 % TiCrSi formation of a new  $\alpha$ -phase was registered, characterized by high hardness (about 8800 MPa), which may be interpreted as 1/1 approximant of non-equilibrium quasi-crystalline phase. At heating up to 980 and 990 °C single-phase  $\alpha$ -state was registered in two latter systems.

*Keywords:* quasi-crystals, system Al-Cu-Fe-Ti-Cr-Si, powders, phase transformations, high-temperature radiography, differential thermal analysis

Metal materials of quasi-crystalline structure are characterized by unusual properties --- low heat conductivity, high ohmic resistance, specific mechanical characteristics, low surface energy, etc., which are stipulated by peculiarities of their crystalline and electron structure. Greater part of quasi-crystalline materials relates to two- or three-component systems, among which structure and properties of alloys of the system Al-Cu-Fe with icosahedral quasi-crystalline structure were studied in greatest detail. However, for imparting to such materials higher values of service properties (resistance to oxidation, corrosion and wear, hardness and toughness, resistance to growth of grains, etc.) they are subjected to additional alloying.

In this work alloying of alloy Al<sub>63</sub>Cu<sub>25</sub>Fe<sub>12</sub> was carried out by introduction into it of titanium, chromium and silicon at ratio 60:32:8, corresponding to alloy TiCrSi with icosahedral quasi-crystalline structure. Ratios AlCuFe:TiCrSi were selected equal to 95:5, 85:15 and 75:25, because in mixing of two alloys, predisposed to formation of quasi-crystalline structures, production of new alloys with quasi-crystalline or close to it by the properties approximant structure is possible. Objects of the investigation were powders of mentioned alloys, produced by the method of the melt atomization by water\* [1].

Radiographic investigation was carried out in monochromatic CuK $\alpha$ -radiation on the DRON-UM1 diffractometer. Single crystal of graphite, installed on the diffracted beam, was used as a monochromator. Diffractograms were taken by the method of step scan-

ning within angle range  $2\theta = 10\text{--}110^\circ$ . Scanning step was 0.05°, duration of exposure at the point --- 3--9 s.

Diffractometric high-temperature investigation of specimens in situ within temperature range 20--1100 °C was performed in helium, using high-temperature attachment UVD-2000. During filming of diffractograms at high temperatures volume of the attachment was blown by helium with excessive, in comparison with atmospheric, pressure 20 kPa. Heating of a specimen up to the temperature of filming was performed at the rate 20 K/min, duration of exposure at the assigned temperature was 30 min.

For determining lattice spacing of the phases powder of semiconductor silicon was used as external standard. Lattice spacing of silicon for specific value of the filming temperature  $T$  was calculated, using the ratio proposed in [2]:

$$a(T) = a_0 \left( 1 + \sum_{i=1}^3 \alpha_i (T - T_0)^i \right)$$

where  $a_0$  is the spacing of elementary cell of silicon at  $T_0 = 293$  K (0.543047 nm);  $\alpha_i$  are the thermal coefficients of expansion of silicon ( $\alpha_1 = 1.887 \cdot 10^{-6}$  K<sup>-1</sup>;  $\alpha_2 = 1.934 \cdot 10^{-9}$  K<sup>-2</sup>;  $\alpha_3 = -4.544 \cdot 10^{-13}$  K<sup>-3</sup>). Spacing of quasi-crystalline lattice of icosahedral phase was calculated by position of three the most intensive maximums with Kahn indices ( $N, M$ ) --- (18.29), (20.32) and (52.84). Content of  $\psi$ -phase was estimated according to the calibration curve [3] by ratio of intensities of maximums of  $\psi$ -phase (18.29) and maximum (110) of  $\beta$ -phase. Mean coefficient of linear expansion,  $\alpha_{\text{mean}}$ , for the phases being investigated within temperature range  $T_0\text{--}T$  was calculated according to the ratio

\*Powders were produced by Dr. O.D. Nejkov (the I.N. Frantsevich IMSP, NASU).

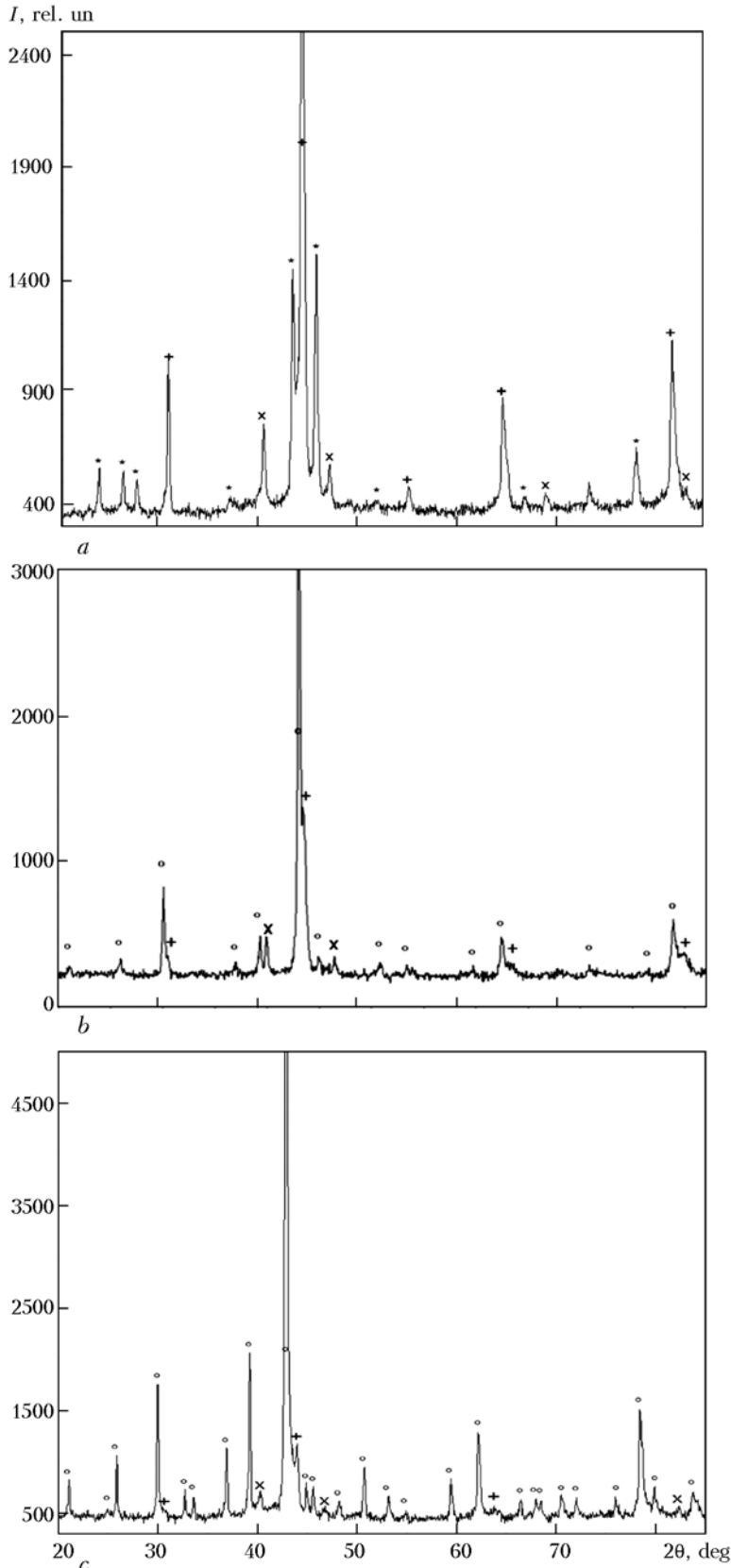


**Figure 1.** Fragments of diffractograms of powders of following composition: a — AlCuFe + 5 % TiCrSi; b — AlCuFe + 15 % TiCrSi; c — AlCuFe + 25 % TiCrSi; \* — reflections from  $\psi$ -phase; + — from  $\beta$ -phase;  $\times$  — from  $\gamma$ -phase;  $\circ$  — additional lines;  $I$  — intensity of X-ray radiation

$$\alpha_{\text{mean}} = \frac{(a' - a'_0)}{a'_0 (T - T_0)}$$

where  $a'$  and  $a'_0$  are the experimental values of identity spacing along selected crystallographic direction at temperatures  $T$  and  $T_0$ , respectively.

In case of crystal phase components, direction was selected along elementary cell axes. For icosahedral phase calculations were carried out by the value of quasi-crystalline spacing in six-dimensional space. Data processing of diffractometric experiment was performed with application of the program for full-profile analysis of X-ray spectra from the mixture of poly-crystalline phase components PowderCell 2.4\*.

Differential thermal analysis (DTA) of powders was carried out on the VDТА-8M installation in helium at constant rate of heating and cooling 80 K/min. Maximum temperature of heating was 1350 °C. As far as size of the particles does not effect character of DTA curves, only powders, having fractions 80–100  $\mu\text{m}$ , were investigated.

Diffractogram of the alloy powder with 5 wt.% TiCrSi in initial state is characterized by presence of peaks of three phase components: quasi-crystalline  $\psi$ -phase with icosahedral symmetry and lattice spacing  $\alpha_\psi = 0.6342(2)$  nm and two crystalline phases —  $\beta$ -phase, characteristic of alloys of the system Al–Cu–Fe with cubic primitive cell (lattice of CsCl type) and period  $\alpha_\beta = 0.2938(1)$  nm, and FCC-phase (we will designate it  $\gamma$ ) with parameter  $\alpha_\gamma = 0.3923(1)$  nm (Figure 1, a).

The phase, similar to  $\beta$ , exists, for example, in the Al–Ti–Cr system [4], where it is solid solution of titanium and aluminium atoms in BCC-cell of chromium ( $a = 0.3005$  nm), whereby alloying atoms are located over their positions statistically.

In this investigation  $\beta$ -phase also forms on the basis of BCC-lattice, and on its diffraction picture superstructure maximums are registered. The latter proves that in investigated  $\beta$ -phase alloying atoms (aluminium and copper) are located in BCC-cell orderly, in contrast to  $\beta$ -phase in system Al–Ti–Cr.

Registered by us  $\gamma$ -phase is very close by its value of the lattice spacing to the phase  $L_{12}$ , described in [4] (ordered location of alloying elements of titanium and

\* ftp://ftp.bam.de/Powder\_Cell//pcw23.exe



**Table 1.** Phase composition of powders AlCuFe–TiCrSi depending upon temperature of heating

Object of investigation	Temperature, °C	Phase composition, vol. %
AlCuFe + 5TiCrSi	20–800	21 $\psi$ , 63 $\beta$ , 16 $\gamma$
	900	72 $\beta$ , 28 $\gamma$
	950	$\beta$
	1000	Melting
	20*	78 $\beta$ , 22 $\gamma$
AlCuFe + 15TiCrSi	20–600	69 $\alpha$ , 16 $\beta$ , 15 $\gamma$
	800	54 $\alpha$ , 16 $\beta$ , 30 $\gamma$
	900	52 $\alpha$ , 23 $\beta$ , 25 $\gamma$
	950	63 $\alpha$ , 37 $\beta$
	980	$\alpha$
	20*	45 $\alpha$ , 55 $\beta$
AlCuFe + 25TiCrSi	20–600	88 $\alpha$ , 7 $\beta$ , 5 $\gamma$
	800	78 $\alpha$ , 5 $\beta$ , 17 $\gamma$
	860	78 $\alpha$ , 22 $\gamma$
	900	76 $\alpha$ , 24 $\gamma$
	950	75 $\alpha$ , 25 $\gamma$
	20*	27 $\alpha$ , 50 $\beta$ , 23 $\gamma$
	970	82 $\alpha$ , 18 $\gamma$
	990	$\alpha$
	20*	70 $\alpha$ , 25 $\beta$ , 5 $\gamma$

\* After cooling.

chromium in FCC-cell of aluminium with spacing  $a = 0.3951$  nm). As far as superstructure peaks are not registered in this investigation, one may assume that  $\gamma$ -phase has similar structure with  $L1_2$ -phase, but with statistical distribution of alloying elements over crystallographic positions.

High-temperature X-ray radiography of the powder of this composition showed that  $\psi$ -phase preserves till 800 °C. At a higher temperature in the specimen  $\psi \rightarrow \beta + \gamma$  phase transformation takes place, and above 900 °C  $\beta + \gamma \rightarrow \beta$ . So, at 900 °C two-phase  $\beta + \gamma$ , and at the temperature 950 °C single phase state  $\beta$  is registered in it. Heating of the specimen up to 1000 °C causes disappearance of interferences from all phases because of melting, and after cooling down to room temperature two-phase state  $\beta + \gamma$  is registered in it (Table 1).

In contrast to diffractogram of the specimen with 5 % TiCrSi, on two other specimens  $\psi$ -phase was not registered. Spacing of FCC-cell of  $\gamma$ -phase reduces as content of TiCrSi increases from the value  $a_\gamma = 0.3923(1)$  to 0.3909(1) and 0.3902(2) nm when passing over from specimen of the alloy with 5 to specimens of the alloy with 15 and 25 % TiCrSi. Content of  $\gamma$ -phase in specimens of first and second composition is, approximately, the same (about 15 vol. %), and in the specimen with 25 % TiCrSi it constitutes 5 vol. %. For  $\beta$ -phase spacing of elementary cell in initial powders acquire values  $a_\beta = 0.2938(1)$ , 0.2940(2) and 0.2910(3) nm, respectively, and volume share of  $\beta$ -phase reduces from 63 in the specimen with 5 % TiCrSi to 16 in the specimen with 15 % TiCrSi and 7 % in the specimen with 25 % TiCrSi.

On diffractograms of specimens of second and third composition in addition to lines of  $\gamma$ - and  $\beta$ -phases additional reflections were registered, which

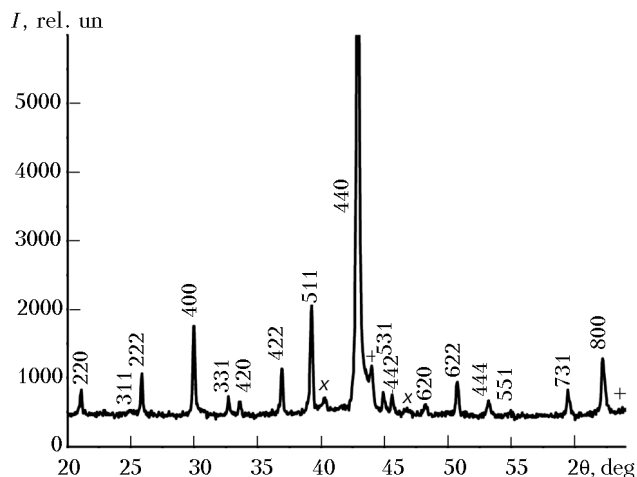


**Figure 2.** Indexing of additional diffractogram maximums from powder of 75 %  $Al_{65}Cu_{25}Fe_{12}$  + 25 %  $Ti_{60}Cr_{32}Si_8$  composition within framework of spatial group  $Fm\bar{3}m$  ( $a = 1.193$  nm): + — reflections from  $\beta$ -phase; X — from  $\gamma$ -phase

do not belong to any known in this system phase (Figure 1, b, c). Intensity of these reflections is higher in the specimen of third composition, that's why afterwards this specimen was studied in detail.

It was established that within investigated temperature range (20–990 °C) mutual ratio of intensities of additional reflections practically does not change, and angular shear of the lines follows the same functional dependence under action of thermal expansion. This proves that registered additional peaks belong to the same phase (let's designate it  $\alpha$ ). Detailed analysis of angular position of maximums of these lines allowed their indexing within the framework of a cubic cell with spacing 1.1928(2) nm (Figure 2). Analysis of conditions of extinguishing of the reflections testifies in favor of FCC elementary cell (spatial group  $Fm\bar{3}m$ ).

As one can see from presented data, the most intensive peaks of  $\alpha$ -phase are close by their position to peaks of  $\beta$ -phase. According to spacing of the elementary cell, new  $\alpha$ -phase may be considered as a result of ordered location of chemical elements within the framework of quadruple elementary cell of  $\beta$ -phase. For such description it is necessary to locate in quadruple cell 128 atoms. On the other hand, taking into account dimensions of this elementary cell  $\alpha$ -phase may be interpreted as crystalline 1/1 approximant of a certain non-equilibrium quasi-crystalline phase. Similar phases exist in systems Ti–Zr–Ni, Ti–Zr–Fe [5] and Ti–Cr–Si [6], where their formation is stipulated, in particular, by stabilizing influence of silicon. According to the Elser's ratio [7], spacing of this icosahedral phase should be 0.6124 nm.

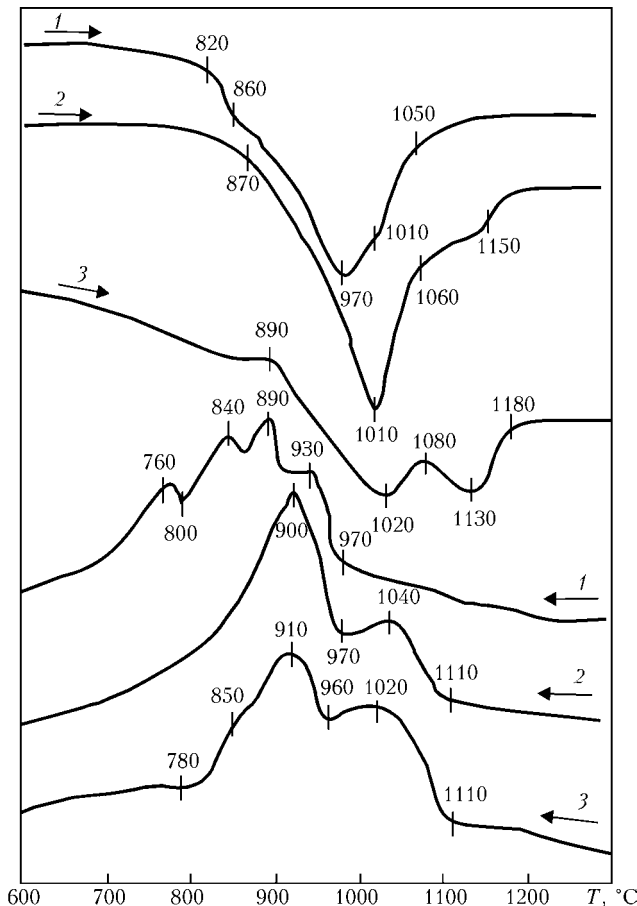
High-temperature investigation of a specimen with 25 % TiCrSi within temperature range 20–990 °C showed peculiarities of its phase composition change depending upon temperature. So,  $\beta$ -phase preserves in the specimen up to the temperature 800 °C (Table 1). Increase of temperature up to 860 °C causes disappearance of  $\beta$ -phase, whereby increase of intensity of  $\gamma$ -phase peaks in comparison with initial state

**Table 2.** Spacing values of crystal lattice ( $\alpha$ , nm) for phase components of powder of alloy 75 %  $\text{Al}_{65}\text{Cu}_{25}\text{Fe}_{12}$  + 25 %  $\text{Ti}_{60}\text{Cr}_{32}\text{Si}_8$  and coefficient of thermal expansion ( $\alpha_{\text{mean}} \cdot 10^6, \text{K}^{-1}$ ) depending upon temperature of heating

Temperature, °C	Phase					
	$\alpha$		$\beta$		$\gamma$	
	$\bar{a}$	$\alpha_{\text{mean}}$	$\bar{a}$	$\alpha_{\text{mean}}$	$\bar{a}$	$\alpha_{\text{mean}}$
20	1.1928	--	0.2910	--	0.3902	--
600	1.2036	15.6	0.2942	19.0	0.3946	19.4 (20–600 °Ñ)
800	1.2070	14.1	0.2957	25.5	0.3959	16.5 (600–800 °Ñ)
860	1.2080	13.8	--	--	0.3963	16.8 (800–860 °Ñ)
900	1.2088	16.6	--	--	0.3966	18.9 (860–900 °Ñ)
950	1.2098	16.5	--	--	0.3969	15.1 (900–950 °Ñ)
20*	1.1954	12.8	0.2962	--	0.3916	14.4 (950–20 °Ñ)
970	1.2132	15.7	--	--	0.3975	15.9 (20–970 °Ñ)
990	1.2136	16.5	--	--	--	--
20*	1.1956	15.3	0.2961	--	0.3925	--

\* After cooling.

is registered. Up to the temperature 950 °C bi-phase state  $\alpha + \gamma$  preserves, and cooling down to room temperature causes occurrence of peaks of  $\beta$ -phase with increased, in comparison with the initial one, spacing of the elementary cell (Table 2).

**Figure 3.** Differential thermal curves of heating and cooling of powders: 1 — 95 %  $\text{Al}_{63}\text{Cu}_{25}\text{Fe}_{12}$  + 5 %  $\text{Ti}_{60}\text{Cr}_{32}\text{Si}_8$ ; 2 — 85 %  $\text{Al}_{63}\text{Cu}_{25}\text{Fe}_{12}$  + 15 %  $\text{Ti}_{60}\text{Cr}_{32}\text{Si}_8$ ; 3 — 75 %  $\text{Al}_{63}\text{Cu}_{25}\text{Fe}_{12}$  + 25 %  $\text{Ti}_{60}\text{Cr}_{32}\text{Si}_8$ 

Such increase of the lattice spacing may be stipulated by diffusion redistribution of chemical elements at high temperature values. It should be noted that content of  $\beta$ -phase after cooling in furnace of the high-temperature attachment to room temperature increased up to 50 vol.%. Repeated heating of this specimen up to the temperature 970 °C causes disappearance of  $\beta$ -phase peaks and sharp reduction of intensity of  $\gamma$ -phase lines. At temperature 990 °C in the specimen practically single-phase state  $\alpha$  is registered. Subsequent cooling down of the attachment to room temperature in the furnace causes appearance of  $\beta$ - and  $\gamma$ -phase peaks, whereby amount of  $\gamma$ -phase is the same as in the initial powder (5 vol.%), and volume share of  $\beta$ -phase constitutes 25 %. Change of lattice spacing of phase components within temperature range 20–990 °C and mean coefficients of thermal expansion of phases within mentioned temperature ranges in the specimen with 25 %  $\text{TiCrSi}$  are given in Table 2.

In specimen with 15 %  $\text{TiCrSi}$  sequence of phase transformations in heating differs somewhat from considered ones, which may be connected with influence of alloying elements on temperature stability of  $\beta$ - and  $\gamma$ -phases. At the same time a common feature for specimens of second and third compositions is formation of a single-phase state — crystalline 1/1 approximant of quasi-crystalline  $\alpha$ -phase (see Table 1).

So, it was established as a result of high-temperature radiographic investigations that number of phases, their content, and lattice parameters are determined by both initial chemical composition of the alloys and phase transformations, occurring in them at high temperatures.

Additional information on phase transformations in multicomponent  $\text{AlCuFe}$ -base alloys was obtained in the investigation by DTA method (Figure 3). Character of heating curves 1–3 proves that as amount of component  $\text{TiCrSi}$  in the alloy increases, solidus tem-



perature increases from 820 to 870 °C, and liquidus temperature --- from 970 to 1020 °C.

On curve of alloy with 25 % TiCrSi, in contrast to two other curves, not one, but two endothermic effects were detected (at 1020 and 1130 °C). The most complex character of solidification curve was registered in the alloy of first composition, where presence of four exothermic peaks may be noted (at 930, 890, 840 and 760 °C). Solidification curves of second and third compositions prove two-stage solidification of alloys with close values of exothermic peaks (900, 1040 and 910, 1020 °C for second and third compositions, respectively), whereby judging by area under the curves, heat effect of low-temperature stage is higher than that of high-temperature stage for both compositions (curves 2 and 3, cooling). Certain difference between curves 2 and 3 consists in presence of bend on curve 3 near temperature 850 °C.

Metallographic analysis of produced after DTA ingots (Figure 4), their X-ray spectral microanalysis (XSMA) and X-ray diffraction phase analysis (XDPA) allowed determining chemical and phase compositions of separate structural components of alloys (Table 3), and jointly with analysis of DTA curves draw conclusion on character of phase transformations in investigated alloys under conditions of heating up to 1350 °C.

Main structural component of the alloy with 5 % TiCrSi is crystalline  $\beta$ -phase (according to XDPA data of about 80 vol.%), which in contrast to system Al-Cu-Fe is alloyed by chromium (area 1, Figure 4, a, Table 3) or titanium, chromium and silicon (area 3 in eutectics). Increased content of iron and high hardness of  $\beta$ -phase (7130±54 MPa) of area 2, in comparison with  $\beta$ -phase of system Al-Cu-Fe (Al<sub>55</sub>Cu<sub>20</sub>Fe<sub>5</sub>), may be explained by presence of inclusions in it of  $\psi$ -phase, detected in the ingot by XDPA method (see Table 3). First structural component is close by its composition to  $\lambda$ -phase of system Al-Cu-Fe (Al<sub>72</sub>Cu<sub>5</sub>Fe<sub>23</sub>), differing from it only by low content of alloying elements (titanium and chromium).

The fact that  $\lambda$ -phase was not detected in high-temperature radiography may be explained by a higher temperature of heating in investigation by DTA method (1000 and 1350 °C, respectively), while solidification of melt in system Al-Cu-Fe starts from  $\lambda$ -phase [8].

So, character of cooling curve of alloy AlCuFe + 5 % TiCrSi may be connected with progress of the following processes: precipitation of  $\lambda$ -phase crystals (in cooling down to 930 °C), formation of  $\beta$ - and  $\psi$ -phases (up to the temperature 800 °C), and solidification of eutectic (800–760 °C).

In ingots with 15 and 25 % TiCrSi main structural component, like in above described case, is  $\beta$ -phase, alloyed by titanium and chromium (areas 2 and 3, Figure 4, b, Table 3). Two other phases are  $\alpha$  and  $\gamma$ , i.e. those detected by XDPA method both in initial powder and in the specimens after cooling down from

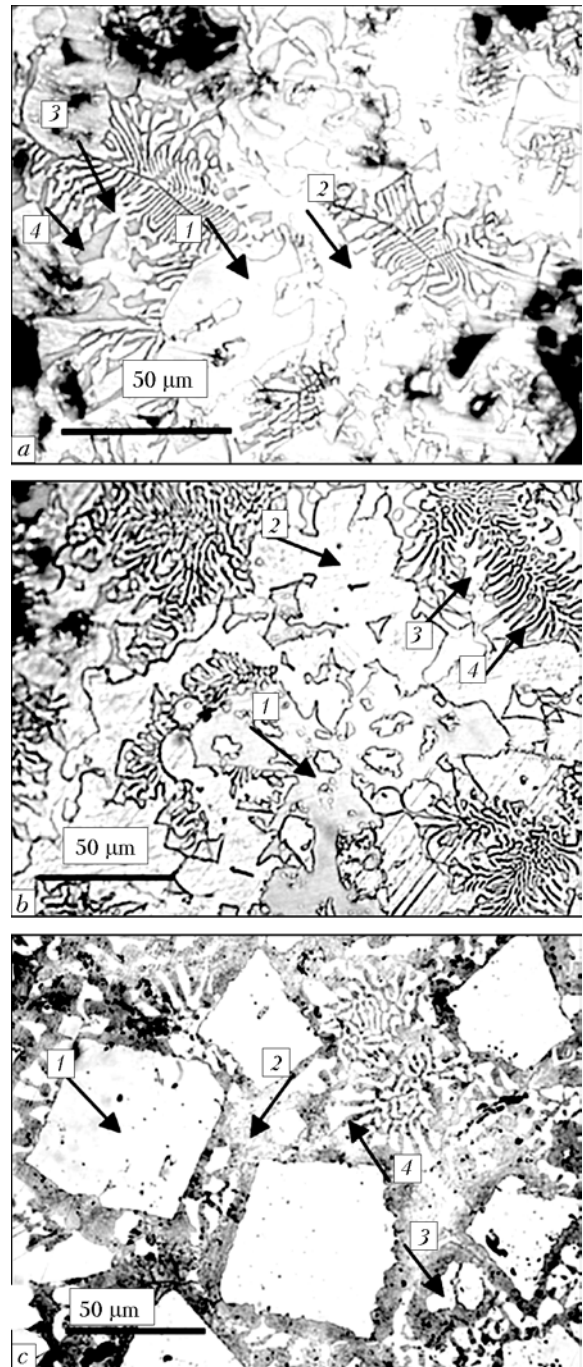


**Figure 4.** Microstructure of DTA ingot from mixture of powders: a --- 95 % Al<sub>65</sub>Cu<sub>25</sub>Fe<sub>12</sub> + 5 % Ti<sub>60</sub>Cr<sub>32</sub>Si<sub>8</sub>; b --- 85 % Al<sub>65</sub>Cu<sub>25</sub>Fe<sub>12</sub> + 15 % Ti<sub>60</sub>Cr<sub>32</sub>Si<sub>8</sub>; c --- 75 % Al<sub>65</sub>Cu<sub>25</sub>Fe<sub>12</sub> + 25 % Ti<sub>60</sub>Cr<sub>32</sub>Si<sub>8</sub>; 1–4 --- number of areas; etched

temperatures 980 and 990 °C (see Table 1). Phase  $\alpha$  contains the highest amount of silicon, which exerts stabilizing influence on its formation, and is the most high-temperature phase; it precipitates from the melt in the form of rather coarse crystals (area 1 in Figure 4, b, c); range of solidification is 1100–960 °C. Later, as temperature reduces, formation of  $\beta$ - and  $\gamma$ -phases occurs, whereby  $\beta$ -phase originates both in the form of separate grains, bordering with  $\gamma$ -phase, and in composition of  $\beta$  +  $\gamma$ -eutectic (areas 2–4, Figure 4, b, c). Content of  $\alpha$ -phase is higher in the specimen of third composition and lower in compari-

**Table 3.** Characteristics of DTA ingots, produced from powders of alloys AlCuFe + TiCrSi

DTA ingot	Area No. (Figure 4)	HV <sub>0.5</sub> , MPa	Chemical composition of structural components (XSMS data), at.%	Phase composition of ingots (XDPA data), vol.%
95AlCuFe + 50TiCrSi	1	6390 ± 640	Al <sub>71</sub> Cu <sub>5</sub> Fe <sub>21</sub> Ti <sub>2</sub> Cr	λ – 5
	2	7130 ± 54	Al <sub>57</sub> Cu <sub>32</sub> Fe <sub>9.5</sub> Cr	γ – 10
	3	5660 ± 20	Al <sub>55</sub> Cu <sub>20</sub> Fe <sub>17</sub> Ti <sub>5</sub> Cr <sub>1.5</sub> Si <sub>2</sub>	β – 80
	4	(eutectics)	Al <sub>63</sub> Cu <sub>14</sub> Fe <sub>4</sub> Ti <sub>18</sub> Cr	ψ – 5
85AlCuFe + 15TiCrSi	1	8800 ± 710	Al <sub>50</sub> Cu <sub>6</sub> Fe <sub>17</sub> Ti <sub>19</sub> Cr <sub>3</sub> Si <sub>4.5</sub>	α – 10
	2	6070 ± 690	Al <sub>53</sub> Cu <sub>29</sub> Fe <sub>10</sub> TiCr <sub>5.5</sub>	β – 75
	3	5870 ± 300	Al <sub>54</sub> Cu <sub>23</sub> Fe <sub>13</sub> Ti <sub>3</sub> Cr <sub>5.5</sub>	γ – 15
	4	(eutectics)	Al <sub>60</sub> Cu <sub>14</sub> Fe <sub>4</sub> Ti <sub>19</sub> Cr <sub>2.3</sub>	
75AlCuFe + 25TiCrSi	1	8830 ± 240	Al <sub>45</sub> Cu <sub>6</sub> Fe <sub>18</sub> Ti <sub>22</sub> Cr <sub>5</sub> Si <sub>3</sub>	α – 30
	2	4330 ± 300	Al <sub>55</sub> Cu <sub>15</sub> Fe <sub>3</sub> Ti <sub>23</sub> Cr <sub>4</sub>	β – 45
	3	5070 ± 340	Al <sub>43</sub> Cu <sub>38</sub> Fe <sub>6</sub> TiCr <sub>14</sub>	γ – 25
	4	(eutectics)	Al <sub>49</sub> Cu <sub>7</sub> Fe <sub>16</sub> Ti <sub>20</sub> Cr <sub>6</sub> Si <sub>2</sub>	

son with total content of β + γ-phases, which is in agreement with heat effects, noted on DTA curves (see Figure 3).

So, in powders of investigated alloys (mixture of quasi-crystalline alloys Al<sub>63</sub>Cu<sub>25</sub>Fe<sub>12</sub> and Ti<sub>60</sub>Cr<sub>32</sub>Si<sub>8</sub>) formation of cubic crystal 1/1 approximant of icosahedral α-phase with spacing of FCC lattice about 1.193 nm (spatial group Fm3m) was registered at ratio of the components 85:15 and 75:25, in contrast to BCC simple cubic lattices, which were previously detected in such phases. This phase appears due to stabilizing influence of silicon.

In addition, in the powders crystalline β-phase (BCC lattice of CsCl type) and γ-phase (FCC-lattice of L<sub>1</sub><sub>2</sub> type) were registered. Small amount of α-phase was registered in powders with the least content of TiCrSi (5 %). Maximum volume share of α-phase in initial powder (88 %) preserves in heating up to the temperature 600 °C at the ratio AlCuFe:TiCrSi = 75:25, and at the temperatures 980 and 990 °C in powders with 15 and 25 % TiCrSi single-phase α-state was registered. It is established that coefficient of thermal expansion of α-phase, determined by the data of high-temperature radiography (15.6·10<sup>-6</sup> K<sup>-1</sup>), is very close to coefficient of thermal expansion of non-alloyed ψ-phase (17.1·10<sup>-6</sup> K<sup>-1</sup>) [9]. In addition, α-phase is characterized by the highest hardness (8800 MPa) among other phases, detected in alloy powders of system AlCuFe–TiCrSi.

*Authors express their gratitude to Ukrainian Scientific-Technical Center for financial support of this work, carried out within the framework of project 1630.*

1. Neikov, O.D., Krajnikov, A.V., Sameljuk, A.V. et al. (2002) An experimental study of water atomization of aluminum alloys. In: *Proc. of World Congress on PM TEC* (Princeton, USA, 2002), Vol. 7.
2. Touloukian, Y.S., Kirby, R.K., Taylor R.E. et al. (1977) *Thermal expansion, nonmetallic solids, thermophysical properties of matter*. Vol. 13. New York: IFI/Plenum.
3. Sordelet, D.J., Besser, M.F., Anderson, I.E. (1996) Particle size effects on chemistry and structure of Al–Cu–Fe quasicrystalline coatings. *J. Thermal Spray Technology*, 5(2), 161–174.
4. Barabash, O.M., Milman, Yu.V., Miral, D.V. et al. (2003) Formation of periodic microstructures involving the L<sub>1</sub><sub>2</sub> phase in eutectic Al–Ti–Cr alloys. *Intermetallics*, 11, 953–962.
5. Kim, W.J., Gibbons, P.C., Kelto, K.F. et al. (1998) Structural refinement of 1/1 approximants to quasicrystals: Bergman-type W(TiZrNi) and Mackay-type M(TiZrFe). *Phys. Rev. B*, 58(5), 2578–2585.
6. Libbert, J.L., Kelton, K.F., Goldman, A.I. et al. (1994) Structural determination of a 1/1 rational approximant to the icosahedral phase in Ti–Cr–Si alloys. *Ibid.*, 49(17), 11675–11680.
7. Elser, V., Henley, C.L. (1985) Crystal and quasicrystal structures in Al–Mn–Si alloys. *Phys. Rev. Lett.*, 55, 2883–2886.
8. Adeeva, L.I., Borisova, A.L. (2002) Quasicrystalline alloys as a new prospective material for protective coatings. *Fizyka i Khimiya Tv. Tila*, 3(3), 454–465.
9. Quivy, A., Levebvre, S., Soubeyroux, J.L. et al. (1994) High-resolution time-of-flight measurements of the lattice parameter and thermal expansion of the icosahedral phase Al<sub>62</sub>Cu<sub>25.5</sub>Fe<sub>12.5</sub>. *J. Applied Crystallography*, 27(6), 1010–1014.



# BEHAVIOR OF VANADIUM IN LIQUID-PHASE MELTING OF VANADIUM-CONTAINING CONCENTRATE

V.N. KOSTYAKOV<sup>1</sup>, E.B. POLETAEV<sup>1</sup>, G.M. GRIGORENKO<sup>2</sup> and S.N. MEDVED<sup>1</sup>

<sup>1</sup>Institute of Physics and Technology of Metals and Alloys, NASU, Kiev, Ukraine

<sup>2</sup>E.O. Paton Electric Welding Institute, NASU, Kiev, Ukraine

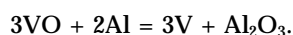
Production of ferrovandium from vanadium concentrate in the direct-current arc furnace was investigated. It is shown that molten metal represents alloy with content of vanadium from 17.7 to 23.46 %, produced at the ratio of cast iron and vanadium concentrate in the charge 1:1. Reduction of cast iron in the charge down to 25 % ensures increase of weight share of vanadium in the alloy up to 43–45 %.

*Keywords:* melting, waste, arc furnace, vanadium, direct current, alloy

Ferrovandium is produced in metallurgy from vanadium-containing feedstock, using alumo-, silico- or carbo-thermal methods [1–3].

Alumo-thermal melting is characterized by release of rather high amount of heat in consequence of reduction reaction of vanadium oxide with aluminium. This heat exceeds heat content of liquid products of the reaction, presented in [2]. That's why about 40 kg of lime are usually introduced per 100 kg of vanadium oxide V<sub>2</sub>O<sub>5</sub> for normal progress of the process of producing vanadium-aluminium master alloy [4].

Thermodynamic analysis of reduction reactions showed that limiting stage of the reduction process V<sub>2</sub>O<sub>5</sub> → V should be considered reduction of the lower oxide VO according to the reaction, presented in [2]:



Due to closeness of melting points of oxide V<sub>2</sub>O<sub>5</sub> and aluminium in their interaction, so called low-temperature reduction processes, determined by interaction of molten aluminium with solid oxides, were not registered. Similar to iron and chromium, high-temperature reduction of oxide V<sub>2</sub>O<sub>5</sub> by aluminium proceeds in the diffusion area, which means that the slowest stage are diffusion processes in the slag phase.

In silico-thermal reduction of vanadium oxide V<sub>2</sub>O<sub>5</sub> released heat is not sufficient for performance of out-of-furnace melting [2]. That's why silico-thermal ferrovandium may be produced only by the furnace method --- in electric furnaces with arc or plasma heating.

It is necessary to take into account that the lower vanadium oxides may enter into reaction with silica with formation of vanadium silicates, from which further reduction of vanadium is even more difficult [5]. So, process of vanadium reduction should be performed in presence of calcium oxide, which binds silica and prevents formation of vanadium silicates.

At Institute of Physics and Technology of Metals and Alloys, NASU, influence of the kind and amount of the reducer, technology of the charge preparation and method of conducting the melting on behavior of vanadium was studied.

Melting was performed on molten «marsh» of cast iron in direct-current arc furnace with graphite crucible. Base cast iron with content, %: 3.25 C; 4.82 Si; 0.54 Mn; 0.08 Cu; 0.06 Ti; 0.25 Cr; 0.01 Ni; 0.27 P; 0.02 S; Fe --- the rest, and vanadium concentrate, consisting of, %: 4.88 Fe<sub>2</sub>O<sub>3</sub>; 26.60 SiO<sub>2</sub>; 0.13 MnO; 0.04 Al<sub>2</sub>O<sub>3</sub>; 0.12 CaO; 63.7 V<sub>2</sub>O<sub>5</sub>; 1.22 K<sub>2</sub>O; 0.03 Cr<sub>2</sub>O<sub>3</sub>; 1.03 TiO<sub>2</sub>; 0.01 CuO; 0.08 P; 0.05 S; ferrosilicon FS65, aluminium grits and limestone, were used as the charge.

Before each melting preparation of the charge was carried out, which included weight batching of the charge components and their mixing with subsequent clotting and drying of clots in furnace at temperature 280–300 °C. In some melts clotted mixture consisted of vanadium concentrate and powder-like ferrosilicon FS65 (fraction up to 1 mm), in other melts it additionally included limestone.

In melting of the non-clotted charge first vanadium concentrate was loaded, and after its reduction --- ferrosilicon or aluminium grits in mixture with limestone.

In melting of the clotted mixture (vanadium concentrate and reducer) limestone was loaded into the furnace simultaneously with the clotted material. In some melts slag was reduced by ferrosilicon, which was introduced into the furnace together with limestone. After fulfillment of all technological operations the melt was overheated.

In Table 1 averaged results of chemical analysis of produced metal are presented.

One can see from Table 1 that a higher content of vanadium in the alloy was registered when aluminium was used as a reducer (melt No.4). Reduction of vanadium by ferrosilicon also ensures its rather high content in the alloy.

**Table 1.** Chemical composition of produced metal

Melt No.	Weight share of elements, %										
	C	Si	Mn	Fe	V	Ti	Cu	Al	Cr	P	S
1*	1.12	10.63	0.11	68.30	18.42	0.11	0.56	0.19	0.46	0.019	0.0115
2**	1.58	5.58	0.07	73.28	22.24	0.02	0.30	0.62	0.56	0.016	0.0140
3**	1.29	6.50	0.08	70.27	21.25	0.11	0.14	0.05	0.44	0.008	0.0047
4***	0.87	8.03	0.12	67.06	23.46	0.18	0.05	0.07	0.15	0.010	0.0070

\* Non-clotted mixture of vanadium concentrate, ferrosilicon and limestone.

\*\* Clotted mixture of vanadium concentrate and ferrosilicon FS65 with additional reduction of slag by ferrosilicon.

\*\*\* Non-clotted mixture of vanadium concentrate, aluminium grits and limestone.

**Table 2.** Chemical composition of slag

Melt No.	Weight share of oxide components, %											
	FeO	Cr <sub>2</sub> O <sub>3</sub>	SiO <sub>2</sub>	MnO	TiO <sub>2</sub>	CuO	V <sub>2</sub> O <sub>5</sub>	Al <sub>2</sub> O <sub>3</sub>	CaO	MgO	P	S
1	0.46	0.07	45.00	0.11	0.42	0.01	3.61	1.59	47.87	0.41	0.080	0.048
2	0.05	0.17	47.92	0.23	0.70	0.03	8.47	1.32	39.42	0.29	0.063	0.066
3	0.06	0.18	45.56	0.06	0.54	0.02	7.22	1.47	40.57	0.15	0.072	0.045
4	0.24	0.36	2.38	0.11	0.084	0.01	1.06	73.75	21.18	0.25	0.063	0.066

In all melts increased content of silicon was detected. In reduction of vanadium by aluminium increase of silicon content occurs due to reduction of the latter from slag.

Molten metal represents an alloy with 17.7–23.46 % V, produced at the ratio of cast iron and vanadium concentrate in the charge 1:1.

Reduction of weight share of cast iron in the charge down to 25 % ensures increase of vanadium concentration in the alloy up to 43–45 %.

Chemical composition of the slag is presented in Table 2.

The analysis shows that weight share of vanadium oxide in the slag constitutes from 3.61 to 8.47 % in case of vanadium reduction by silicon.

**Table 3.** Material balance of vanadium in experimental melts

Melt No.	Zone of vanadium distribution, %		
	Metal	Slag	Entrainment
1	84.4	9.2	7.3
2	78.5	21.5	--
3	82.6	17.4	--
4	92.2	2.2	5.6

**Table 4.** Balance of silicon in melts Nos. 1–3

Melt No.	Silicon consumption over periods of melting, %		Item of silicon consumption, %		
	Reduction	Diffusion deoxidizing of final slag	Reduction	Transition into metal	Melting loss
1	100	--	54.8	38.2	7.0
2	80	20	57.0	14.8	28.2
3	80	20	56.8	18.6	24.6

In reduction of vanadium by aluminium content of V<sub>2</sub>O<sub>5</sub> in the slag significantly reduces (melt No.4), which proves completeness of progress of reduction processes in melting of the concentrate.

Data of investigations allowed determining distribution of vanadium in the melting products (Table 3).

As prove data of Table 3, kind of a reducer exerts noticeable influence on distribution of vanadium in the metal and the slag. So, in melting of non-clotted vanadium concentrate from 2.2 to 9.2 % V transits into the slag, which corresponds to coefficient of its distribution in the slag and the metal --- 0.02 and 0.10.

Rather high content of vanadium was detected in the slag in remelting of the clotted mixture. This is explained by the fact that 80 % of the general volume of silicon, assigned for reduction of vanadium, were introduced into the clotted mixture, and 20 % Si were used for diffusion reduction of slag at the end of melting. However, use of a portion of the reducer for diffusion deoxidizing of the final slag is inefficient and causes just increased melting loss of silicon (Table 4).

Coefficient of silicon consumption during reduction period ( $K_{red} = \frac{G_{Si}^r}{G_{Si}^{th}}$ , where  $G_{Si}^r$  is the real con-



sumption of silicon for reduction,  $G_{Si}^{th}$  is the theoretically necessary silicon) in melt No.1 was 1.6, and in melts Nos. 2 and 3 --- 1.4.

Data obtained show that kind of the reducer noticeably effects energy parameters of the melting. So, in silico-thermal reduction of vanadium (in melts Nos. 1-3) main power consumption is connected with the reduction period (65-70 % of total power consumption in a melt), and specific power consumption equals 4.1-4.5 kW·h/kg.

Reduction of vanadium by aluminium enables decrease of power consumption during reduction period down to 35 % per a melt and decrease of specific power consumption down to 1.22 kW·h/kg.

## CONCLUSIONS

1. Carried out investigations showed that kind of the reducer effects behavior of vanadium and power con-

sumption in a melt. The highest degree of vanadium reduction is achieved when aluminium is used as a reducer.

2. Power consumption in a melt significantly decreases in case of vanadium reduction by aluminium.

3. Efficiency of alumo- and silico-thermal melts may be estimated only on the basis of comparison of technical-economic indices of a melt.

1. Durrer, R., Folkert, G. (1976) *Metallurgy of ferroalloys*. Moscow: Metallurgiya.
2. Lyakishev, N.P., Slotvinsky-Sidan, N.P., Pliner, Yu.L. et al. (1983) *Vanadium in ferrous metallurgy*. Moscow: Metallurgizdat.
3. Gasik, M.I., Lyakishev, N.P., Emlin, B.I. (1988) *Theory and technology of manufacture of ferroalloys*. Moscow: Metallurgiya.
4. Lyakishev, N.P., Pliner, Yu.L., Ignatenko, G.F. et al. (1978) *Alumothermics*. Moscow: Metallurgiya.
5. Ryss, M.A. (1975) *Manufacture of ferroalloys*. Moscow: Metallurgiya.

## SYSTEM VEDN-1 FOR HIGH-VELOCITY ELECTRIC-ARC SPRAYING OF COATINGS



The system comprises electric arc metalliser, wire feed mechanism and power supply. The equipment is mobile and can operate both in manual and mechanised modes. Compared with traditional electric arc equipment, the system with the spraying unit of a new design provides increase in the velocity of a high-temperature jet, possibility of formation of contracted gas plume, increased density and low oxidation degree of coatings, as well as high strength of adhesion to the substrate:

### Specifications of system VEDN-1

Operating current, A .....	50-400
Operating arc voltage, V .....	17-40
Wire feed speed, m/min .....	2-12
Working pressure of compressed air, MPa (kgf/cm <sup>2</sup> ) .....	0.5-0.7 (5-7)
Compressed air flow rate, m <sup>3</sup> /h .....	90-120
Productivity, kg/h:	
aluminium or its alloys .....	12.5
zinc .....	40.0
Weight of electric arc metalliser (gun), kg .....	1.5
Material utilisation factor .....	0.75

The equipment is intended for deposition of wear- and corrosion-resistant, as well as special coatings, repair of worn out machine parts by spraying of electrically conducting materials made in the form of wire 1.6-2.2 mm in diameter. Thickness of the deposited coatings ranges from 0.05 to 5 mm. Compressed air is used as a working gas. A wide range of wires of aluminium, zinc, copper, bronze, brass, steel, as well as composite and flux-cored wires are applied for coating.

Prof. Borisov Yu.S.  
E-mail: borisov@pwi.ru.kiev.ua

# INDEX OF ARTICLES FOR AEM'2006, Nos. 1--4

On welding, metals science and metallurgy in the scientist heritage or on present status and future of special electrometallurgy: Towards the 90 birthday anniversary of Prof. B.I. Medovar (Paton B.E., Medovar L.B., Saenko V.Ya., Tsykulenko A.K., Fedorovsky B.B., Us V.I. and Shevchenko N.T.)

## Electrometallurgy of steel and ferroalloys

Behavior of vanadium in liquid-phase melting of vanadium-containing concentrate (Kostyakov V.N., Poletaev E.B., Grigorenko G.M. and Medved S.N.)

Innovation technological processes of electric furnace ferrometallurgy refining by progressive industrial methods. Part 1. Thermodynamic properties of nickel-base systems and binary compounds (Novikov N.V., Kapran I.I., Sokolov K.D., Gasik M.I. and Ovcharuk A.N.)

Innovation technological processes of electric furnace ferrometallurgy refining by progressive industrial methods. Part 2. Thermodynamic investigations of processes and technology of ladle desulfuration of electric furnace ferrometallurgy by sodium carbonate (Novikov N.V., Kapran I.I., Sokolov K.D., Gasik M.I. and Ovcharuk A.N.)

Innovation technological processes of electric furnace ferrometallurgy refining by progressive industrial methods. Part 3. Processes and technology for refining ferrometallurgy in acid and basic oxygen converters (Novikov N.V., Kapran I.I., Sokolov K.D., Gasik M.I. and Ovcharuk A.N.)

Peculiarities of producing intermediate product for manufacturing especially low-carbon steel in electric arc furnace (Saviuk A.N., Derevyanchenko I.V., Kucherenko O.L., Projdak Yu.S., Stovpchenko A.P., Kamkina L.V. and Grishchenko Yu.N.)

The Danieli metallurgical equipment (Sojfer V.M.)

## Electron beam processes

Composite materials on base of copper and molybdenum, condensed from vapor phase, for electric contacts. Structure, properties, technology. Part 2. Fundamentals of electron beam technology for producing materials for electric contacts (Grechanyuk N.I., Osokin V.A., Grechanyuk I.N., Kucherenko P.P., Minakova R.V., Golovkova M.E. and Kopylova G.E.)

Deposition of coatings, containing refractory elements, by electron beam evaporation using «flash» method (Yakovchuk K.Yu., Skryabinsky V.V. and Krushinskaya L.A.)

Electron beam melting of uncrushed spongy titanium blocks (Trigub N.P., Akhonin S.V., Zhuk G.V., Telin V.V. and Davydov S.V.)

Investigation of heat exchange processes in mould of electron beam installation (Nakonechny N.F., Fyodorov V.N. and Shchekin-Krotov V.A.)

Investigation of process of manufacturing hot-rolled and cold-formed pipes from cast non-deformed pipe billet of titanium alloy VT1-0 produced by method of electron beam melting (Trigub N.P., Zhuk G.V., Chepinsky A.A., Tarasov K.K., Kurilenko P.V., Antipieva N.V. and Kopylova N.E.)

Structure and mechanical properties of dispersion-strengthened titanium-base materials deposited from gas phase (Nerodenko L.M., Onoprienko E.V. and Movchan B.A.)

Structure and properties of thick MgO condensates produced by electron beam evaporation (Stelmakh Ya.A., Melnichenko T.V. and Movchan B.A.)

## Electroslag technology

Application of modifying for improving properties of annular billets from nitrogen-containing stainless steels produced by method of centrifugal electroslag casting (Eryomin E.N.)

Centrifugal electroslag casting of tractor bushings of turning hinge (Eryomin E.N. and Zherebtsov S.N.)

Metal nitriding from gas phase in ESR (Lakomsky V.V., Pomarin Yu.M., Ryabtsev A.D. and Grigorenko G.M.)

On transportation of nitrogen through molten slag (Lakomsky V.V., Pomarin Yu.M., Grigorenko G.M. and Orlovsky V.Yu.)

Peculiarities of bimetal material quality estimation (Saenko V.Ya., Medovar L.B., Fedorovsky B.B., Shevchenko N.T., Yarosh V.M., Zhukov V.V., Zhuravel V.M., Zajtsev V.A., Kozin R.V. and Remizov A.G.)

## Energy and resource saving

Application of steam-plasma process for pyrolysis of organic wastes including medical and other hazardous ones (Petrov S.V., Marinsky G.S., Chernets A.V., Korzhik V.N. and Mazunin V.M.)

Economic efficiency of railway wheel profile renovation by surfacing of worn treads (Matveev V.V.)

Mathematical modeling of heat processes in casting of cast iron by magnetodynamic meter-mixer (Goryuk M.S., Tarasevich N.I., Dubodelov V.I., Pogorsky V.K. and Rybitsky A.I.)

On temperature dependence of thermoanthracite electric resistance (Lakomsky V.I. and Kutuzov S.V.)

Power consumption of liquid-phase reduction melting process (Kostyakov V.N., Grigorenko G.M., Poletaev E.B., Medved S.N. and Shevchuk E.A.)

Present state and ways of improving technology of titanium alloy granule metallurgy for the purpose of increasing properties and reliability of gas-turbine engine components (Polkin I.S., Demchenkov G.G. and Snegiryova L.A.)

To issue on specific electric resistance of thermoanthracite (Petrov B.F. and Lakomsky V.I.)

## General problems of metallurgy

Determination of swinging radius of the MCCB mould (Sidorov V.A. and Sotnikov A.L.)

Diffusion titanizing of tungsten-free hard alloys TN20 and KKhN15 (Khizhnyak V.G., Pomarin Yu.M. and Tereshchenko P.A.)

Effect of alloying on composition, structure and properties of powders of alloy AlCuFe, containing quasi-crystalline phase (Borisova A.L., Borisov Yu.S., Adeeva L.I.,

Tunik A.Yu., Karpets M.V. and Doroshenko L.K.)

Investigation of phase transformations in powders of multi-component AlCuFe–base alloy with quasi-crystalline structure (Borisov Yu.S., Borisova A.L., Karpets M.V., Lotsko D.V., Milman Yu.V., Adeeva L.I., Gordan G.N. and Doroshenko L.K.)

Investigation of structure and mechanical properties of Ti–7.2Al–2.9Mo–2.7W–3Nb–2.3Zr–0.4Si alloy (Firstov S.A., Zamkov V.N., Brodnikovskiy N.P., Topolsky V.F., Kotko A.V., Samelyuk A.V. and Golovash A.V.)

Short-term strength and microstructure of brazed joints of alloy VJL12U produced using boron-containing brazing alloy with addition of silicon (Malashenko I.S., Kurenkova V.V., Belyavin A.F. and Trokhimchenko V.V.)

Short-term strength of brazed joints of nickel alloy VJL12U at temperatures 20 and 950 °C (Kurenkova V.V., Malashenko I.S., Trokhimchenko V.V., Chervyakova L.V. and Rabinovich A.A.)

Strength and physical metallurgy of brazed joints of cast nickel alloy ChS70 VI (Malashenko I.S., Kurenkova V.V., Belyavin A.F., Chervyakova L.V. and Shelkovej A.N.)

#### Information

Developed at PWI

Theses for a scientific degree

#### New materials

New functional material: oxide cathode of welding electric arc. Part 1 (Lakomsky V.I.)

New functional material: oxide cathode of welding electric arc. Part 2 (Lakomsky V.I.)

#### Plasma-arc technology

Application of plasma-arc remelting of technogenic waste in movable horizontal mould for producing quality ferroalloys and master alloys (Koleda V.N., Shapovalov V.A., Torkhov G.F. and Aksinichenko A.V.)

Behavior of phosphorus in liquid-phase reduction melting (Kostyakov V.N., Poletaev E.B., Grigorenko G.M., Medved S.N. and Shevchuk E.A.)

4 Experimental investigation of erosion of copper water-cooled anodes (Shapovalov V.A., Melnik G.A., Vislobokov O.M., Tsykulenko K.A., Prikhodko M.S. and Zhirov D.M.)

2 Geometric shape and erosion resistance of copper water-cooled anode of arc heat source (Shapovalov V.A., Vislobokov O.M., Melnik G.A. and Tsykulenko K.A.)

4 Kinetics of nitrogen absorption by molten highly reactive metals in arc and plasma melting (Grigorenko G.M., Pomarin Yu.M., Orlovsky V.Yu. and Lakomsky V.V.)

3 Peculiarities of technology for producing strips with amorphous structure by spinning method with application of plasma heating (Shapovalov V.A., Torkhov G.F., Nikitenko Yu.A. and Karusevich O.V.)

1 Plasma liquid-phase reduction of iron from its oxides using gaseous reducers (Zhadkevich M.L., Shapovalov V.A., Melnik G.A., Zhirov D.M., Zhdanovsky A.A., Tsykulenko K.A. and Prikhodko M.S.)

#### Vacuum-induction melting

1 Influence of manganese on properties of lanthanum-alloyed chromium alloys (Rudoj A.P., Zhuchenko L.P., Melnik V.Kh. and Portnov A.P.)

2 Melting of silicon in vertical induction crucible-free zonal melting (Chervony I.F., Shvets E.Ya. and Egorov S.G.)

#### Index of articles for AEM'2006

4 List of authors

## LIST OF AUTHORS

**A**deeva L.I. No.2, 4  
Akhonin S.V. No.4  
Aksinichenko A.V. No.4  
Antipieva N.V. No.3

**B**elyavin A.F. No.1, 4  
Borisov Yu.S. No.2, 4  
Borisova A.L. No.2, 4  
Brodnikovskiy N.P. No.2

**C**hepinsky A.A. No.3  
Chernets A.V. No.2  
Chervony I.F. No.3  
Chervyakova L.V. No.1, 3

**D**avydov S.V. No.4  
Demchenkov G.G. No.1  
Derevyanchenko I.V. No.3  
Doroshenko L.K. No.2, 4  
Dubodelov V.I. No.1

**E**gorov S.G. No.3  
Eryomin E.N. No.2, 3

**F**edorovsky B.B. No.1, 2  
Firstov S.A. No.2  
Fyodorov V.N. No.4

**G**asik M.I. No.1, 2, 3  
Golovash A.V. No.2  
Golovkova M.E. No.2  
Gordan G.N. No.4  
Goryuk M.S. No.1  
Grechanyuk I.N. No.2  
Grechanyuk N.I. No.2  
Grigorenko G.M. No.3(4), 4(2)  
Grishchenko Yu.N. No.3

**K**amkina L.V. No.3  
Kapran I.I. No.1, 2, 3  
Karpets M.V. No.2, 4  
Karusevich O.V. No.1  
Khizhnyak V.G. No.3  
Koleda V.N. No.4  
Kopylova G.E. No.2  
Kopylova N.E. No.3  
Korzhih V.N. No.2  
Kostyakov V.N. No.3(2), 4  
Kotko A.V. No.2

Kozin R.V. No.1  
Krushinskaya L.A. No.1  
Kucherenko O.L. No.3  
Kucherenko P.P. No.2  
Kurenkova V.V. No.1, 3, 4  
Kurilenko P.V. No.3  
Kutuzov S.V. No.1

**L**akomsky V.I. No.1(2), 2(2), 3(2), 4  
Lotsko D.V. No.4

**M**alashenko I.S. No.1, 3, 4  
Marinsky G.S. No.2  
Matveev V.V. No.2  
Mazunin V.M. No.2  
Medovar L.B. No.1, 2  
Medved S.N. No.3(2), 4  
Melnichenko T.V. No.3  
Melnik G.A. No.1, 2, 4  
Melnik V.Kh. No.1  
Milman Yu.V. No.4  
Minakova R.V. No.2  
Movchan B.A. No.3, 4

**N**akonechny N.F. No.4  
Nerodenko L.M. No.4  
Nikitenko Yu.A. No.1  
Novikov N.V. No.1, 2, 3

**O**noprienko E.V. No.4  
Orlovsky V.Yu. No.3(2)  
Osokin V.A. No.2  
Ovcharuk A.N. No.1, 2, 3

**P**aton B.E. No.2(2)  
Petrov B.F. No.2  
Petrov S.V. No.2  
Pogorsky V.K. No.1  
Poletaev E.B. No.3(2), 4  
Polkin I.S. No.1  
Pomarin Yu.M. No.3(3), 4  
Portnov A.P. No.1  
Prikhodko M.S. No.1, 2  
Projdak Yu.S. No.3

**R**abinovich A.A. No.3  
Remizov A.G. No.1  
Rudoj A.P. No.1  
Ryabtsev A.D. No.4  
Rybitsky A.I. No.1

**S**aenko V.Ya. No.1, 2  
Samelyuk A.V. No.2  
Saviuk A.N. No.3  
Shapovalov V.A. No.1(2), 2, 4(2)  
Shchekin-Krotov V.A. No.4  
Shelkovej A.N. No.1  
Shevchenko N.T. No.1, 2  
Shevchuk E.A. No.3(2)  
Shvets E.Ya. No.3  
Sidorov V.A. No.4  
Skryabinsky V.V. No.1  
Snegiryova L.A. No.1  
Sojfer V.M. No.2  
Sokolov K.D. No.1, 2, 3  
Sotnikov A.L. No.4  
Stelmakh Ya.A. No.3  
Stovpchenko A.P. No.3

**T**arasevich N.I. No.1  
Tarasov K.K. No.3  
Telin V.V. No.4  
Tereshchenko P.A. No.3  
Topolsky V.F. No.2  
Torkhov G.F. No.1, 4  
Trigub N.P. No.3, 4  
Trokhimchenko V.V. No.3, 4  
Tsykulenko A.K. No.2  
Tsykulenko K.A. No.1, 2, 4  
Tunik A.Yu. No.2

**U**s V.I. No.2

**V**islubokov O.M. No.1, 4

**Y**akovchuk K.Yu. No.1  
Yarosh V.M. No.1

**Z**ajtsev V.A. No.1  
Zamkov V.N. No.2  
Zhadkevich M.L. No.2  
Zhdanovsky A.A. No.2  
Zherebtsov S.N. No.2  
Zhirov D.M. No.1, 2  
Zhuchenko L.P. No.1  
Zhuk G.V. No.3, 4  
Zhukov V.V. No.1  
Zhuravel V.M. No.1